1

Principles of Limit State Design

1.1 Structural Design Philosophies

While in service, structures are likely to be subjected to various types of loads (or actions) and load effects (or action effects) due to operational and environmental conditions that are usually normal but are sometimes extreme or even accidental. The mission of the structural designer is to design a structure that can withstand the operational and environmental requirements designated throughout its expected lifetime.

The load effects or maximum load-carrying capacities or limit states of a structure are affected by a variety of factors that essentially involve a great deal of uncertainty, which include the following:

- Geometric factors associated with structural characteristics, buckling, large deformation, crushing, or folding
- Material factors associated with chemical composition, mechanical properties, yielding or plasticity, or fracture
- Fabrication related initial imperfections, such as initial distortion, welding induced residual stress, or softening
- Temperature factors, such as low temperatures associated with operation in cold waters or low-temperature cargo and high temperatures due to fire and explosions
- Dynamic or impact factors (e.g., strain rate sensitivity or inertia effect) associated with freak waves and impact pressure actions that arise from sloshing, slamming, or green water; overpressure actions that arise from explosion; and impact from collisions, grounding, or dropped objects
- Age related degradation factors, such as corrosion or fatigue cracking
- Accident induced damage factors, such as local denting, collision damage, grounding damage, fire damage, or explosion damage
- Human factors related to unusual operations (e.g., ship's operational speed compared with maximum permitted speed or acceleration, ship's heading, or loading or unloading conditions)

Uncertainties can comprise two groups: inherent uncertainties and modeling uncertainties. Inherent uncertainties are caused by natural variabilities in environmental actions and material properties, and modeling uncertainties arise from inaccuracy in engineering modeling associated with the evaluation and control of loads, load effects

Ultimate Limit State Analysis and Design of Plated Structures, Second Edition. Jeom Kee Paik. © 2018 John Wiley & Sons Ltd. Published 2018 by John Wiley & Sons Ltd.

0003369274.3D 1 24/1/2018 10:47:52 AM

2

(e.g., stress, deformation), load-carrying capacities, or limit states and from variations in building and operational procedures. In design, a structure is thus required to have an adequate margin of safety against service requirements because of such inherent and modeling uncertainties.

A "demand" is analogous to load, and a "capacity" is analogous to the strength necessary to resist that load, both measured consistently (e.g., as stress, deformation, resistive or applied load or moment, or energy either lost or absorbed). In this regard, a performance function G of a structure can be given as follows:

$$G = C_{d} - D_{d} \tag{1.1a}$$

where C_d represents the "design" capacity and D_d represents the "design" demand. The terminology "design" implies that both demand and capacity are determined by accounting for the inherent and modeling uncertainties.

Because both C_d and D_d in Equation (1.1a) are a function of the basic variables, $X = (x_1, x_2, ..., x_i, ..., x_n)$, the performance function G can be rewritten as follows:

$$G = G(X) = G(x_1, x_2, ..., x_i, ..., x_n)$$
(1.1b)

When G(X) > 0, the structure is in the desired state. When $G(X) \le 0$, the structure is in the undesired state. In industry practice, the performance function of a structure is sometimes defined in an opposite manner to Equation (1.1a) as follows:

$$G^* = D_d - C_d \tag{1.2}$$

where G^* is the performance function of a structure. In this case, the structure is in the desired state when $G^* < 0$, and it is in the undesired state when $G^* \ge 0$. Figure 1.1 illustrates the two performance functions associated with the desired and undesired states.

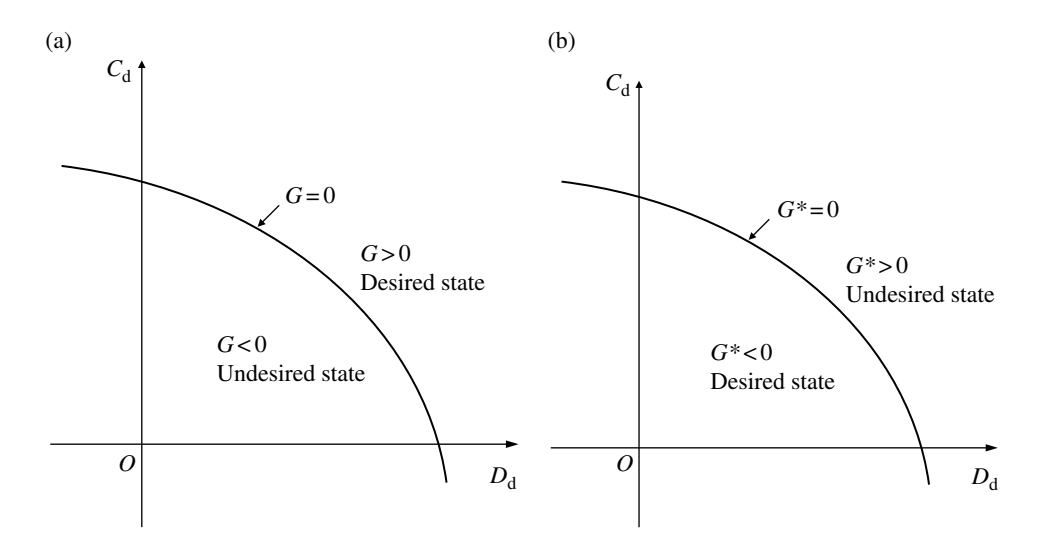


Figure 1.1 The performance functions associated with the desired and undesired states: (a) a performance function G, Equation (1.1a); (b) a performance function G^* , Equation (1.2).

0003369274.3D 2 24/1/2018 10:47:52 AM

Reliability-Based Design Format

The reliability-based design format usually involves the following tasks:

- 1) Definition of a target reliability
- 2) Identification of all unfavorable failure modes of the structure
- 3) Formulation of the limit state (performance) function for each failure mode identified in item (2)
- 4) Identification of the probabilistic characteristics (mean, variance, probability density distribution) of the random variables in the limit state function
- 5) Calculation of the reliability against the limit state with respect to each failure mode of the structure
- 6) Evaluation of the predicted reliability whether or not it is greater than the target reliability
- 7) Redesign of the structure otherwise
- 8) Evaluation of the reliability analysis results with respect to a parametric sensitivity consideration

Each of the basic variables in the reliability-based design format is dealt with in a probabilistic manner as a random parameter, where each random variable must be characterized by the corresponding probability density function that has a mean value and standard deviation. If the first-order approximation is adopted, the performance function G(X) can be rewritten by the Taylor series expansion as follows:

$$G(X) \cong G(\mu_{x1}, \mu_{x2}, ..., \mu_{xi}, ..., \mu_{xn}) + \sum_{i=1}^{n} \left(\frac{\partial G}{\partial x_i}\right)_{\bar{x}} (x_i - \mu_{xi})$$
 (1.3)

where μ_{xi} is the mean value of the variable x_i , \bar{x} is the mean value of the basic variables = $(\mu_{x1}, \mu_{x2}, ..., \mu_{xi}, ..., \mu_{xn})$, and $(\partial G/\partial x_i)_{\bar{x}}$ is the partial differentiation of G(X) with respect

The mean value of the performance function G(X) is then given by

$$\mu_{G} = G(\mu_{x1}, \mu_{x2}, ..., \mu_{xi}, ..., \mu_{xn}) \tag{1.4}$$

where μ_G represents the mean value of the performance function G(X).

The standard deviation of the performance function G(X) is calculated by

$$\sigma_{G} = \left[\sum_{i=1}^{n} \left(\frac{\partial G}{\partial x_{i}} \right)_{\bar{x}}^{2} \sigma_{xi}^{2} + 2 \sum_{i>j} \left(\frac{\partial G}{\partial x_{i}} \right)_{\bar{x}} \left(\frac{\partial G}{\partial x_{j}} \right)_{\bar{x}} \operatorname{covar}(x_{i}, x_{j}) \right]^{1/2}$$
(1.5a)

where σ_G is the standard deviation of G(X), σ_{x_i} is the standard deviation of the variable x_i , $\operatorname{covar}(x_i, x_j) = E\left[(x_i - \mu_{x_i})(x_j - \mu_{x_j})\right]$ is the covariation of x_i and x_j , and E[] is the mean value of [].

When the basic variables $X = (x_1, x_2, ..., x_i, ..., x_n)$ are independent of each other, $covar(x_i, x_i) = 0$. In this case, Equation (1.5a) is simplified to

$$\sigma_{G} = \left[\sum_{i=1}^{n} \left(\frac{\partial G}{\partial x_{i}} \right)_{\bar{x}}^{2} \sigma_{xi}^{2} \right]^{1/2}$$
(1.5b)

0003369274.3D 3 24/1/2018 10:47:53 AM If the so-called first-order second-moment method (Benjamin & Cornell 1970) is adopted, the reliability index for this case can be determined as follows:

$$\beta = \frac{\mu_{\rm G}}{\sigma_{\rm G}} \tag{1.6}$$

where β represents the reliability index.

For a simpler case with a performance function G(X) of two parameters, for example, capacity C and demand D, that are considered to be statistically independent, the reliability index β can be calculated as follows:

$$\mu_{G} = \mu_{C} - \mu_{D} \tag{1.7a}$$

$$\sigma_{\rm G} = \sqrt{\left(\sigma_{\rm C}\right)^2 + \left(\sigma_{\rm D}\right)^2} \tag{1.7b}$$

$$\beta = \frac{\mu_{\rm C} - \mu_{\rm D}}{\sqrt{(\sigma_{\rm C})^2 + (\sigma_{\rm D})^2}} = \frac{\mu_{\rm C}/\mu_{\rm D} - 1}{\sqrt{(\mu_{\rm C}/\mu_{\rm D})^2 (\eta_{\rm C})^2 + (\eta_{\rm D})^2}}$$
(1.7c)

where μ_C or μ_D are the mean values of C or D, σ_C or σ_D are the standard deviations of C or D, and η_C or η_D are the coefficients of variation (i.e., the standard deviation divided by the mean value) of C or D.

To achieve a successful design, the reliability index should be greater than a target reliability index:

$$\beta \ge \beta_{\mathrm{T}} \tag{1.8}$$

where $\beta_{\rm T}$ is the target reliability.

The target reliability or the required level of structural reliability may vary from one industry to another depending on various factors such as the type of failure, the seriousness of its consequence, or public and media sensitivity. Appropriate values of target reliability are not readily available and are usually determined by surveys or by examinations of the statistics on failures although the fundamental difference between a risk assessment and a reliability analysis needs to be acknowledged when interpreting such results. The methods to select the target safeties and reliabilities may be categorized into the following three groups (Paik & Frieze 2001):

- "Guesstimation": A "reasonable" value as recommended by a regulatory body or professionals on the basis of successful prior experience. This method may be employed for the new types of structure for which statistical database on failures does not exist.
- Calibration of design rules: The level of reliability is estimated by calibrating a new
 design rule to an existing successful one. This method is normally used for the revisions of existing design rules.
- Economic value analysis: The target reliability is selected to minimize total expected costs during the service life of the structure.

For elaborate descriptions in reliability analysis, interested readers may refer to Benjamin and Cornell (1970), Nowak and Collins (2000), Melchers (1999a), and Modarres et al. (2016), among others.

0003369274.3D 4 24/1/2018 10:47:53 AM

Partial Safety Factor-Based Design Format

In the partial safety factor-based design format, the design capacity or demand is defined by considering the corresponding partial safety factors that are associated with the inherent and modeling uncertainties. A characteristic or nominal value of capacity Ck or demand D_k is determined as the mean value of the corresponding random variable. A design capacity C_d or demand D_d is, however, defined to suit a specified percentage of the area below the probability curve for the corresponding random variable. For instance, a design strength or capacity $C_{\rm d}$ can be defined for a lower bound or 95% exceedance value, whereas a design load or demand D_d can be defined for an upper bound or a 5% exceedance value, as shown in Figure 1.2. In this regard, the design capacity or demand is defined as follows:

$$C_{\rm d} = \frac{C_{\rm k}}{\gamma_{\rm C}} \tag{1.9a}$$

$$D_{\rm d} = \gamma_{\rm D} D_{\rm k} \tag{1.9b}$$

where C_k is the characteristic (or nominal) value of capacity or μ_C in Equation (1.7a), D_k is the characteristic (or nominal) value of demand or μ_D in Equation (1.7a), γ_C is the partial safety factor associated with capacity, and γ_D is the partial safety factor associated with demand. Because the partial safety factors must be greater than 1.0, it is obvious that the characteristic value of capacity C_k is reduced and the characteristic value of demand D_k is amplified to determine their design values, C_d or D_d .

The measure of structural adequacy η can be determined as follows:

$$\eta = \frac{C_{\rm d}}{D_{\rm d}} = \frac{1}{\gamma_{\rm C} \gamma_{\rm D}} \frac{C_{\rm k}}{D_{\rm k}} \tag{1.10}$$

To achieve a successful design, the measure of structural adequacy η must be greater than 1.0 by a sufficient margin as follows:

$$\eta = \frac{C_{\rm d}}{D_{\rm d}} = \frac{1}{\gamma_{\rm C} \gamma_{\rm D}} \frac{C_{\rm k}}{D_{\rm k}} > 1 \tag{1.11}$$

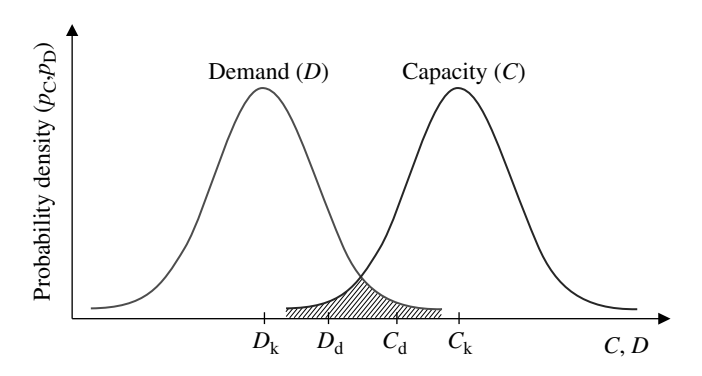


Figure 1.2 Probability density distributions of capacity and demand.

0003369274.3D 5 24/1/2018 10:47:53 AM

1.1.3 Failure Probability-Based Design Format

Whatever the level of uncertainty, every structure may have some probability of failure, which is the possibility of a load or demand exceeding its limit value or capacity. The probability of failure P_f for a particular type of failure in association with the performance function G, Equation (1.1), or G^* , Equation (1.2), is defined as follows:

Probability of failure
$$P_f = \text{prob}(G \le 0) = \text{prob}(G^* \ge 0) = \text{prob}(C_d \le D_d)$$
 (1.12a)

The safety of a structure is the converse, which is the probability that it will not fail, namely,

Safety =
$$\text{prob}(G > 0) = \text{prob}(G^* < 0) = \text{prob}(C_d > D_d) = 1 - P_f$$
 (1.12b)

The probability of failure can generally be calculated as follows:

$$P_{f} = \int_{G \le 0} p_{x}(X) dx = \int_{G^{*} \ge 0} p_{x}^{*}(X) dx$$
 (1.13)

where $p_x(X)$ and $p_x^*(X)$ are the joint probability density functions of the random variables, $X = (x_1, x_2, ..., x_i, ..., x_n)$, associated with demand and capacity, and G(X) or $G^*(X)$ is the limit state (performance) function defined such that negative or positive values imply failure, respectively.

Since G(X) or $G^*(X)$ is usually a complicated nonlinear function, it is not straightforward to perform the direct integration of Equation (1.13) associated with the joint probability density function, $p_x(X)$ or $p_x^*(X)$. Therefore, Equation (1.13) is often solved with approximate procedures, where the limit state (performance) function G(X) or $G^*(X)$ is approximated at the design point by either a tangent hyperplane or hyperparabola, which simplifies the mathematics related to the calculation of failure probability. The first type of approximation with the tangent hyperplane is called the first-order reliability method (FORM), and the second type with the hyperparabola is called the second-order reliability method (SORM). Such methods facilitate the rapid calculation of the probability of failure by widely available standard software packages. In addition to the individual probability distributions of the random variables involved, the correlation between the "A" and "B" parameters can also be readily accounted for in such calculations.

Considering the probability density distributions of capacity and demand, as illustrated in Figure 1.2, the probability of a particular type of failure can be calculated as follows:

$$P_{\rm f} = \int_0^\infty \left[\int_0^y p_{\rm C}(x) dx \right] p_{\rm D}(y) dy \tag{1.14}$$

where $p_C(x)$ is the probability density function of capacity associated with a variable x and $p_D(y)$ is the probability density function of demand associated with a variable y.

Although the mean value of capacity C_k is much greater than the mean value of demand D_k , there is still some possibility that the capacity is less than the demand. It is usually challenging to compute Equation (1.14), but it is interesting to note that the shaded area of the overlap in Figure 1.2 indicates an approximation of the probability of failure P_f . To achieve a successful design, the probability of failure should be minimized to a sufficiently low value.

0003369274.3D 6 24/1/2018 10:47:53 AM

1.1.4 Risk-Based Design Format

The risk-based design format usually involves the following five tasks: (i) hazard identification, (ii) risk calculation, (iii) establishment of a set of potential risk control options, (iv) cost—benefit analysis for the risk control options, and (v) decision making. In engineering community, risk is defined as a product of the frequency of the hazard and the level of consequence as follows:

$$R = F \times C \tag{1.15}$$

where R is the risk, F is the frequency of the hazard, and C is the level of consequence. The frequency of the hazard represents the likelihood that the hazard will occur, and the level of consequence represents the impact or severity of consequence, indicating how bad the consequences would be if the hazard did occur in terms of casualties, property damage, and environmental pollution. The frequency of a hazard is usually measured by the number of occurrences per unit time (e.g., per year). The level of consequence is sometimes measured on a monetary basis (e.g., repair costs for accidental damage or insurance costs for pollution).

The characterization of the frequency and the consequences is required for risk assessment. Qualitative risk assessment techniques use simple methods that do not require numerical computations, but quantitative risk assessment requires more refined methods associated with numerical and experimental investigations. It is of course much more desirable to apply the quantitative risk assessment methods for more precise calculations of the risks in association with casualties, property damage, and environmental pollution.

According to Equation (1.15), it is obvious that one may need to reduce F or C or both to reduce risks. To achieve a successful design, fabrication, or operation, the risk should be minimized to an "as low as reasonably practicable (ALARP)" level. Undertaking activities to control risks is risk management, which involves risk control options. Costbenefit analysis is undertaken to make a ranking between a set of potential risk control options, and a single or multiple options should be applied to best control the risks to meet the ALARP level. Risk assessment and management are recognized as the best tools for decision making in association with robust design, building, operation, or decommissioning of structures.

1.2 Allowable Stress Design Versus Limit State Design

Limit state design differs from the traditional allowable stress design. In the allowable stress design, the focus is on keeping the stresses from the design loads under a certain working stress level, which is usually based on successful similar experience. In industry practice, regulatory bodies or classification societies usually specify the value of the allowable stress as some fraction of the mechanical properties of materials (e.g., yield strength). The criterion of the allowable stress design is typically given by

$$\sigma < \sigma_{\rm a}$$
 (1.16)

where σ is the working stress and σ_a is the allowable stress.

0003369274.3D 7 24/1/2018 10:47:53 AM

In contrast to the allowable stress design, the limit state design is based on explicit consideration of the various conditions under which the structure may cease to fulfill its intended function. For these conditions, the applicable capacity or strength is estimated and used during design as a limit for such behavior.

For this purpose, a structure's load-carrying capacity is normally evaluated with simplified design formulations or more refined computations such as nonlinear elastic—plastic large-deformation finite element analyses with appropriate modeling related to geometric or material properties, initial imperfections, boundary conditions, load application, and finite element mesh sizes, as appropriate.

During the past several decades, the emphasis on structural design has moved from the allowable stress design to the limit state design because the latter approach makes possible a rigorously designed, yet economical, structure that directly takes into consideration the various relevant modes of failure.

A limit state is formally defined by the description of a condition for which a particular structural member or an entire structure would fail to perform the function designated beforehand. From the viewpoint of structural design, four types of limit states are relevant for structures:

- The serviceability limit state (SLS)
- The ultimate limit state (ULS)
- The fatigue limit state (FLS)
- The accidental limit state (ALS)

The SLS represents failure states for normal operations due to deterioration from routine functioning. SLS considerations in design may address the following:

- Local damage that reduces the structure's durability or affects the efficiency of structural elements
- Unacceptable deformations that affect the efficient use of structural elements or the functioning of equipment that relies on them
- Excessive vibration or noise that can cause discomfort to people or affect the proper functioning of equipment
- Deformations and deflections that may spoil the structure's aesthetic appearance

The ULS (also called ultimate strength) represents the collapse of the structure due to a loss of structural stiffness and strength. Such loss of capacity may be related to:

- A loss of equilibrium, of a part or of the entire structure, which is often considered as a rigid body (e.g., overturning or capsizing)
- Attainment of the maximum resistance of structural regions, members, or connections by gross yielding or fracture
- Instability, of a part or of the entire structure, from buckling and plastic collapse of plating, stiffened panels, and support members

The FLS represents the occurrence of fatigue cracking of structural details due to stress concentration and damage accumulation or crack growth under repeated loading.

The ALS represents excessive structural damage from accidents, such as collisions, grounding, explosion, and fire, that affect the safety of the structure, the environment, and personnel.

0003369274.3D 8 24/1/2018 10:47:53 AM

The partial safety factor-based criterion of the limit state design for a particular type of limit state is typically given from Equation (1.11) as follows:

$$C_{\rm d} > D_{\rm d} \quad \text{or} \quad \frac{C_{\rm k}}{\gamma_C} > \gamma_{\rm D} D_{\rm k}$$
 (1.17)

It is important to emphasize that in the limit state design, these various types of limit states may be designed against different safety levels, with the actual safety level to be attained for a particular type of limit state being an indirect and implicit function of its perceived consequences and the ease of recovery from that state to be incorporated in design. Within the context of Equation (1.17), useful guidelines for determination of the partial safety factors related to a structure's limit state design may be found in ECCS (1982), BS 5950 (1985), ENV 1993-1 (1992a, 1992b), ISO 2394 (1998), and NORSOK (2004), among others.

1.2.1 Serviceability Limit State Design

The structural design criteria used for the SLS design of structures are normally based on the limits of deflections or vibration for normal use. In reality, the excessive deformation of a structure may also be associated with excessive vibration or noise, and thus certain interrelationships may exist among the design criteria being defined and used separately for convenience.

The SLS criteria are normally defined by the operator of a structure or by established practice, with the primary aim being efficient and economical in-service performance without excessive routine maintenance or downtime. The acceptable limits necessarily depend on the type, mission, and arrangement of structures. Furthermore, in defining such limits, experts in other disciplines, such as machinery design, must also be consulted. As an example, the limiting values of vertical deflections for beams in structures as shown in Figure 1.3 are indicated in Table 1.1.

In Table 1.1, L is the span of the beam between supports. For cantilever beams, L may be taken as twice the projecting length of the cantilever. δ_{\max} is the maximum deflection, which is given by $\delta_{\max} = \delta_1 + \delta_2 - \delta_0$, where δ_0 is the pre-camber, δ_1 is the variation of the deflection of the beam due to permanent loads immediately after loading, and δ_2 is the variation of the deflection of the beam due to variable loading plus any subsequent variant deflections due to permanent loads.

For plate elements, criteria based on elastic buckling control are often used for SLS design, in some cases to prevent such an occurrence entirely and in other cases to allow

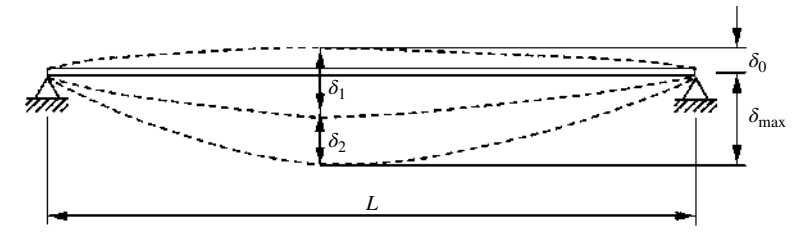


Figure 1.3 Nomenclature: lateral deflections of a beam.

0003369274.3D 9 24/1/2018 10:47:53 AM

10

Table 1.1 Serviceability limit values for vertical deflections of beams.

Condition	Limit for δ_{max}	Limit for δ_2
Deck beams	L/200	L/300
Deck beams that support plaster or other brittle finish or non-flexible partitions	L/250	L/350

elastic buckling to a known and controlled degree. Elastic plate buckling and its related effects, such as relatively large lateral deflections, must be prevented if such effects are likely to be detrimental. However, because a plate may have some reserve strength beyond elastic buckling until its ultimate strength is reached, allowing elastic buckling in a controlled manner can in some cases lead to a more economical structure. In Chapters 3 and 5 of this book, the use of such elastic buckling strength-based SLS design methods for plates and stiffened panels is described.

1.2.2 Ultimate Limit State Design

The structural design criteria to prevent the ULS are based on plastic collapse or ultimate strength. The simplified ULS design of many types of structures has tended to rely on estimates of the buckling strength of the components, usually from their elastic buckling strength adjusted by a simple plasticity correction, which is represented by point A in Figure 1.4. In such a design scheme based on the strength at point A, the structural designer does not use detailed information on the post-buckling behavior of the component members and their interactions. The true ultimate strength represented by point B in Figure 1.4 may be higher, although one can never be sure of this because the actual ultimate strength is not being directly evaluated.

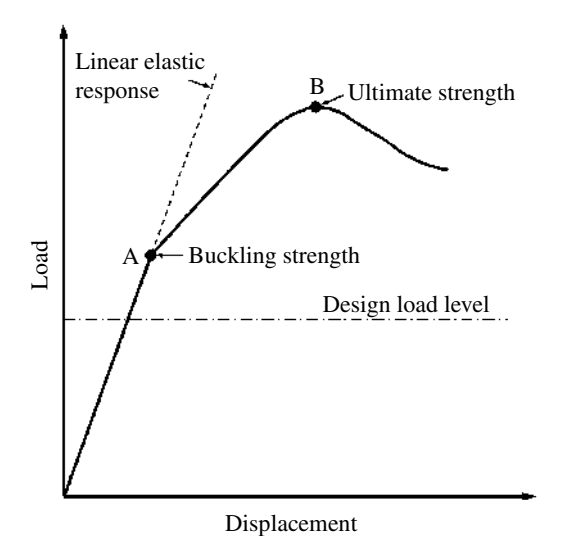


Figure 1.4 Structural design considerations based on the ultimate limit state.

0003369274.3D 10 24/1/2018 10:47:54 AM

In any event, as long as the strength level associated with point B remains unknown (as it is with traditional allowable stress design or linear elastic design methods), it is difficult to determine the real safety margin. Hence, more recently, the design of structures such as those of ships, offshore platforms, box girder bridges, and box girder cranes has tended to be based on the ultimate strength.

The safety margin of a structure can be evaluated by comparison of its ultimate strength with the extreme applied loads (or load effects, such as stress) as depicted in Figure 1.4. To obtain an economic yet safe structure, the ultimate strength and the design load must be assessed accurately. The structural designer may even desire to estimate the ultimate strength for not only the intact structure but also the structures with existing or in-service damage (e.g., corrosion wastage, fatigue cracking, or local denting damage) or even accident induced damage (e.g., due to collision, grounding, dropped object, fire, or explosion) to assess their damage tolerance and survivability.

The ULS design criterion can also be expressed by Equation (1.17). The characteristic measure of design capacity C_d in Equation (1.17) is in this case the ultimate strength, whereas D_d is the related load or demand measure. For ULS design, the partial safety factor γ_C is sometimes taken as $\gamma_C = 1.15$ for ships and offshore structures (NORSOK 2004).

It is important to note that any failure in a structure must ideally occur in a ductile manner rather than a brittle manner; the avoidance of brittle failure will lead to a structure that does not collapse suddenly, because ductility allows the structure to redistribute internal stresses and thus absorb greater amounts of energy before global failure. Adequate ductility in the design of a structure is facilitated by:

- Meeting the requisite material toughness requirements
- Avoiding failure initiation situations with a combination of high stress concentration and undetected weld defects in the structural details
- Designing structural details and connections to allow a certain amount of plastic deformation, that is, avoiding "hot spots"
- Arranging the members in such a manner that a sudden decrease in the structural capacity would not occur as a result of abrupt transitions or member failure

This book is primarily concerned with ULS design methods for structural members and systems composed of such ductile members, although other types of limit states are also described to some extent.

1.2.3 Fatigue Limit State Design

The FLS design is carried out to ensure that the structure has an adequate fatigue life. The predicted fatigue life can also be a basis for planning efficient inspection programs during the structure's operation. The design fatigue life for structural components is normally based on the structure service life required by the operator or by other responsible body such as a class society. For ship structures, the fatigue life is often considered to be 25 years or longer. The shorter the design fatigue life, or the greater the required reliability, the smaller the inspection intervals should be to assure an operation free from crack problems.

The FLS design and analysis should in principle be undertaken for every suspected location of fatigue cracking, which includes welded joints and local areas of stress concentration.

0003369274.3D 11 24/1/2018 10:47:54 AM

The structural design criteria for the FLS are usually based on the structure's cumulative fatigue damage under repeated fluctuation of loading, as measured by the Palmgren–Miner cumulative damage rule. A particular value of the Miner sum (e.g., unity) is taken to be synonymous with the formation or initiation of a crack. The structure is designed so that when it is analyzed for fatigue, a reduced target Miner sum results, implying that cracks will not form with a given degree of certainty.

The fatigue damage at a crack initiation site is affected by many factors, such as the stress ranges experienced during load cycles, the local stress concentration characteristics, and the number of stress range cycles. Two types of the FLS design approach are typically considered for structures:

- The S-N curve approach (S = fluctuating stress, N = associated number of cycles)
- The fracture mechanics approach

In the S-N curve approach, the Palmgren–Miner cumulative damage rule is applied together with the relevant S-N curve. This application normally follows three steps: (i) definition of the histogram of cyclic stress ranges, (ii) selection of the relevant S-N curve, and (iii) calculation of the cumulative fatigue damage.

One of the most important factors in fatigue design is the characteristic stress to be used both in defining the S-N curve (the capacity) and in the stress analysis (with the fluctuating local fatigue stresses being the demand on the structure). Four types of methods have been suggested on this basis:

- The nominal stress method
- The hot spot stress method
- The notch stress method
- The notch strain method

The nominal stress method uses the nominal stresses in the field far from the stress concentration area, together with S–N curves that must include implicitly the effects of both structural geometry and the weld. In the nominal stress method, therefore, the S–N curve should be selected for structural details depending on the detail type and weld geometry involved. Many S–N curves for various types of weld and geometry are generally needed and are available. When a limited number of standard S–N curves are used, any structural detail considered must be assigned to one of those categories, which requires a certain amount of judgment.

The hot spot stress method uses a well-defined hot spot stress in the stress concentration area to account for the effect of structural geometry alone, and the weld effect is incorporated into the S-N curve. This is currently a very popular approach, but certain practical difficulties must be conceded. The most basic of these pertains to the concept of hot spot stress itself, which is more appropriate for surface cracks than for imbedded cracks. Difficulties can also arise in the consistent definition of hot spot stresses across a range of weld and structural geometries and in the estimation of the hot spot structural stress needed for application of the technology in regions of stress concentration. For instance, attention should be paid to extrapolation of the stress to the weld toe for calculation of the stress concentration factor, and the need for appropriate selection of a relevant S-N curve from those for different weld types is still significant.

The notch stress method uses the stresses at the notch calculated by accounting for the effects of both structural geometry and the weld, whereas the *S*–*N* curve is developed to

0003369274.3D 12 24/1/2018 10:47:54 AM

represent the fatigue properties of either the base material, the material in the heat-affected zone (HAZ), or the weld material, as appropriate. A significant advantage of the notch stress method is that it can address the specific weld toe geometry in the calculation of fatigue damage. A related difficulty is that the relevant parameters (e.g., the weld toe angle) in the case of the actual structure must be known with some confidence.

The notch strain method uses the strains at the notch when the low-cycle fatigue is predominant, because the working stresses in this case sometimes likely approach the material yield stress, and thus the stress-based approaches are less appropriate.

The fracture mechanics approach considers that one or more premised cracks of a small dimension exist in the structure and predicts the fatigue damage during the process of crack propagation, including any coalescence and breakthrough, and the subsequent fracture. In this approach to design, a major task is to preestablish the relevant crack growth equations or "laws." The crack growth rate is often expressed as a function of only the stress intensity factor range at the crack tip, on the assumption that the yielded area around the crack tip is relatively small. In reality, the crack propagation behavior is affected by many other parameters (e.g., mean stresses, load sequence, crack retardation, crack closure, crack growth threshold, and stress intensity range) in addition to the stress intensity factor range.

The structural fracture mechanics is dealt with in Chapter 9, and the *S*–*N* curve approach using nominal stresses is herein briefly described under the assumption of the linear cumulative damage rule, that is, the Palmgren–Miner rule. In the fatigue damage assessment of welded structural details, of primary concern are the ranges of the cyclic maximum and minimum stresses rather than the mean stresses, as shown in Figure 1.5, because of the usual presence of residual mean stresses near the yield magnitude. This tends to make the entire stress range damaging. The situation in non-welded cases is, of course, different, and, in such cases, the mean stresses can be important.

For practical FLS design using the nominal stress-based approach, the relevant S–N curves must be developed for various types of weld joints. To do this, fatigue tests are carried out for various types of specimens that are subjected to cyclic stress ranges of a uniform amplitude. As indicated in Figure 1.5, the maximum and minimum stresses

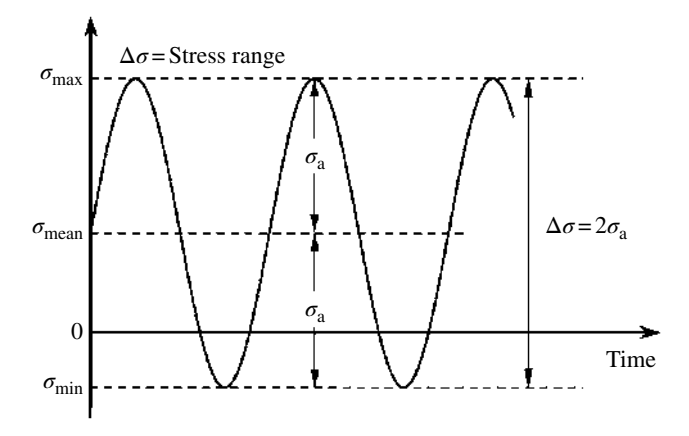


Figure 1.5 Cyclic stress range versus time.

0003369274.3D 13 24/1/2018 10:47:54 AM

are denoted by $\sigma_{\rm max}$ and $\sigma_{\rm min}$, respectively. In such tests, the effect of the mean stress, $\sigma_{\rm mean} = (\sigma_{\rm max} + \sigma_{\rm min})/2$, on fatigue damage can be quantified, which is necessary for non-welded cases. For convenience, the fatigue tests for specimens that incorporate non-welded geometries are usually carried out at either $\sigma_{\rm min} = 0$ or $\sigma_{\rm max} = -\sigma_{\rm min}$ with a constant stress range, that is, $\Delta \sigma = \sigma_{\rm max} - \sigma_{\rm min} = 2\sigma_{\rm a}$, where $\sigma_{\rm a}$ is the stress amplitude.

The number of stress cycles, $N_{\rm I}$ or $N_{\rm F}$, with the former representing the crack initiation life, that is, until a crack initiates, and the latter representing the fracture life, such as until a small-scale test specimen is separated into two pieces, is obtained on the basis of the fatigue test results. With a series of such tests for a variety of stress ranges, $\Delta\sigma$, the S-N curves for the particular structural details may typically be plotted as shown in Figure 1.6. The curves for design are usually expressible by curve fitting the test results plotted on a log–log scale, namely,

$$\log N = \log a - 2s - m \log \Delta \sigma \tag{1.18a}$$

$$N(\Delta\sigma)^m = A \tag{1.18b}$$

where $\Delta \sigma$ is the stress range, N is the number of stress cycles with constant stress range, $\Delta \sigma$, until failure, m is the negative inverse slope of the S-N curve, $\log A = \log a - 2s$, a is the life intercept of the mean S-N curve, and s is the standard deviation of $\log N$.

For the FLS design criterion based on the S-N curve approach, Equation (1.17) may be rewritten in the nondimensional form when the distribution of a long-term stress range is given by a relevant stress histogram in terms of a number of constant amplitude stress range blocks, $\Delta \sigma_i$, each with a number of stress fluctuations, n_i , as follows:

$$D = \sum_{i=1}^{B} \frac{n_i}{N_i} = \frac{1}{A} \sum_{i=1}^{B} n_i (\Delta \sigma_i)^m \le D_{cr}$$
 (1.19)

where D is the accumulated fatigue damage, B is the number of stress blocks, n_i is the number of stress cycles in stress block i, N_i is the number of cycles until failure at the ith constant amplitude stress range block, $\Delta \sigma_i$, and D_{cr} is the target cumulative fatigue damage for design.

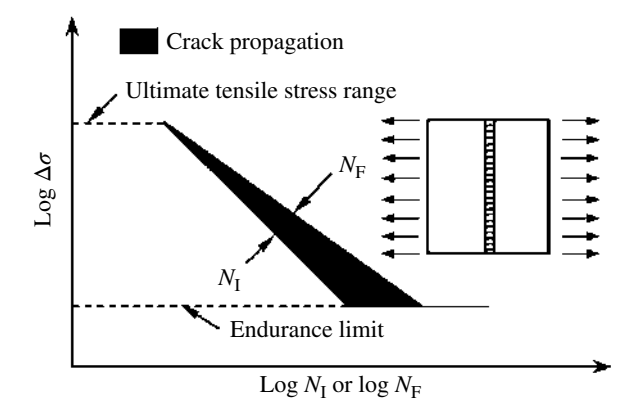


Figure 1.6 Typical S–N curves from constant amplitude tests.

0003369274.3D 14 24/1/2018 10:47:55 AM

To achieve greater fatigue durability in a structure, it is important to minimize stress concentrations, potential flaws (e.g., misalignment, poor materials), and structural degradation, including corrosion and fatigue effects. Fatigue design is interrelated with the maintenance regime to be used. In some cases, it may be more economical in design to allow the possibility of a certain level of fatigue damage, as long as the structure can continue to function after the fatigue symptoms are detected until repairs can be made. In other cases, fatigue damage may not be allowed to occur, if it is inconvenient to inspect the structure or interrupt production. The former approach may thus be applied as long as regular inspections and related maintenance are possible, whereas the latter concept is obviously more relevant if there are likely to be difficulties associated with inspections and thus a high likelihood of undetected fatigue damage.

Fatigue is sometimes classified into high-cycle fatigue and low-cycle fatigue. High-cycle fatigue indicates that a structure has a long fatigue life due to a small stress range, whereas low-cycle fatigue indicates that a structure has a short fatigue life due to a large stress range. The two are sometimes distinguished by the fatigue cycle of 10⁴.

In Chapter 9, structural fracture mechanics and the ultimate strength of plate panels associated with fatigue cracking damage are described. For elaborate descriptions in fatigue damage analysis methods, interested readers may refer to Schijve (2009), Nussbaumer et al. (2011), and Lotsberg (2016), among others.

1.2.4 Accidental Limit State Design

The primary aim of the ALS design for structures may be characterized by the following three broad objectives:

- To avoid loss of life in the structure or the surrounding area
- To avoid pollution of the environment
- To minimize loss of property or financial exposure

In the ALS design, it is necessary to achieve a design in which the structure's main safety functions are not impaired during any accidental event or within a certain time after the accident. The structural design criteria for the ALS are based on limiting accidental consequences such as structural damage and environmental pollution.

Because the structural damage characteristics and behavior of damaged structures depend on the type of accidents, it is not straightforward to establish universally applicable structural design criteria for the ALS. Typically, for a given type of structure, the design of accidental scenarios and associated performance criteria must be decided on the basis of risk assessment.

In the case of ships or offshore platforms, possible accidental events that may need to be considered for the ALS include collisions, grounding, dropped objects, significant hydrodynamic impact (e.g., sloshing, slamming, or green water) that leads to buckling or structural damage, excessive loads from human error, berthing or dry docking, fires or internal gas explosions in oil tanks or machinery spaces, and underwater or atmospheric explosions. In land-based structures, the accidental scenarios may include fire, explosion, foundation movements, or related structural damage from earthquakes.

In selecting the design target ALS performance levels for such events, the approach is normally to tolerate a certain level of damage consistent with a greater aim such as

0003369274.3D 15 24/1/2018 10:47:55 AM

survivability or minimized consequences; to do otherwise would result in an uneconomical structure.

The main safety functions of a structure that should not be compromised during any accident event or within a certain time after the accident include:

- Usability of escape ways
- · Integrity of shelter areas and control spaces
- Global load-bearing capacity
- Integrity of the environment

Therefore, the ALS design criteria should be formulated so that the main safety functions mentioned previously will work successfully and the following points are considered to adequate levels:

- Energy dissipation related to structural crashworthiness
- Capacity of local strength members or structures
- Capacity of the global structure
- Allowable tensile strains to avoid tearing or rupture
- Endurance of fire protection

For the ALS design, the structure's integrity will typically be checked in two steps. In the first step, the structural performance will be assessed against design accident events, and post-accident effects such as damage to the environment are evaluated in the second step.

In the case of accidents to ships, for instance, the primary concern of the ALS design is to maintain the watertightness of the ship's compartments, the containment of dangerous or pollutant cargoes (e.g., chemicals, bulk oil, liquefied gas), and the integrity of the reactor compartments of nuclear-powered ships. To continue normal operations for the structure's mission, it is also important to maintain the integrity and residual strength of damaged structures at a certain level immediately after the accident occurs.

The different types of accident events normally require different methods to analyze the structure's resistance. For the ALS design criteria under predominantly impactoriented loading, Equation (1.17) may typically be rewritten using energy dissipationrelated criteria adopted with the view that the safety of the structure or the environment is not lost:

$$E_{\mathbf{k}}\gamma_{\mathbf{k}} < \frac{E_{\mathbf{a}}}{\gamma_{\mathbf{a}}} \tag{1.20}$$

where E_k is the kinetic energy lost during the accident, E_a is the available energy absorption capability until critical damage occurs, and γ_k and γ_a are partial safety factors related to kinetic energy loss and energy absorption capability, respectively.

The structure's dissipated energy during the accident may usually be calculated by integrating the area below the load—displacement curve of the structure under accidental loading, as shown in Figure 1.7. In Chapter 10, an elaborate description for the structural impact mechanics and the residual ultimate strength of plate panels with accident induced damage such as local denting is presented.

0003369274.3D 16 24/1/2018 10:47:55 AM

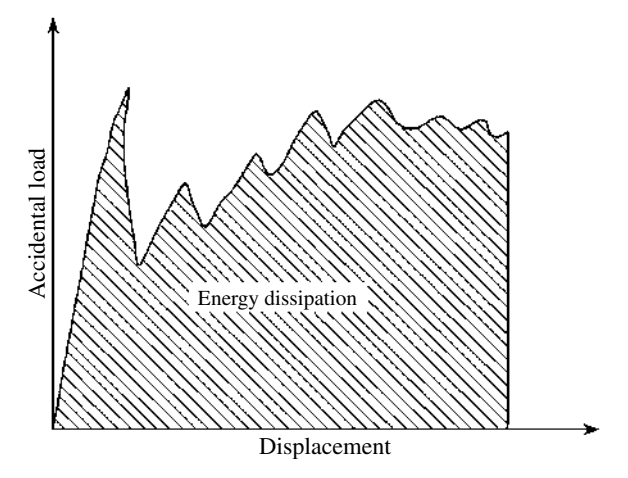


Figure 1.7 Energy absorption of the structure under accidental loading.

1.3 Mechanical Properties of Structural Materials

For materials of plated structures, steels or aluminum alloys are typically used. The specific gravity of aluminum alloys is about one-third that of steels, and thus aluminum alloys are primarily used in weight-critical structures. Aluminum alloys also have merits with their good resistance to corrosion by seawater and with an easier processing of extrusion, leading to the availability in a wide variety of section forms. However, the elastic modulus of aluminum alloys is only one-third that of steels, which is an apparent disadvantage of aluminum alloys.

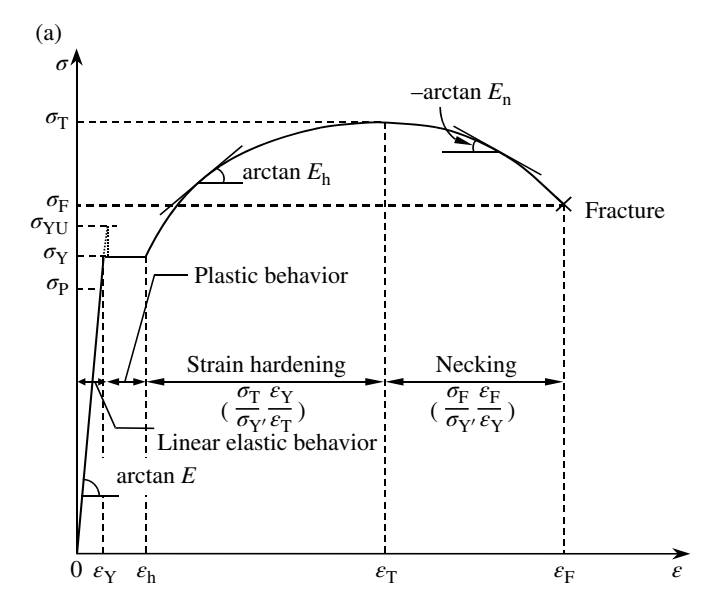
In structural analysis and design, it is essential to define the material properties associated with the targeted structural systems. In industry practice, nominal values of material properties are often used in the analysis and design of a structure. When harsh environmental or operational conditions are of primary concern, however, the mechanical properties of the materials must be accurately quantified by considering the effects of such conditions. Because testing is only a method to quantify material properties, numerous test databases have been developed in the literature (e.g., Callister 1997); some are limited to specific conditions, and others are based on old materials that are no longer in use.

Modern material-manufacturing technologies have greatly advanced the material properties featured in old test databases, and today's structural systems are often exposed to the harsher environmental and operational conditions associated with their functional requirements. Thus, test databases for these volatile material properties should be continuously developed to meet such requirements (Paik et al. 2017).

1.3.1 Characterization of Material Properties

The mechanical properties of structural materials are characterized by testing predesignated specimens under monotonic tensile loading. Figure 1.8 shows an idealized

0003369274.3D 17 24/1/2018 10:47:55 AM



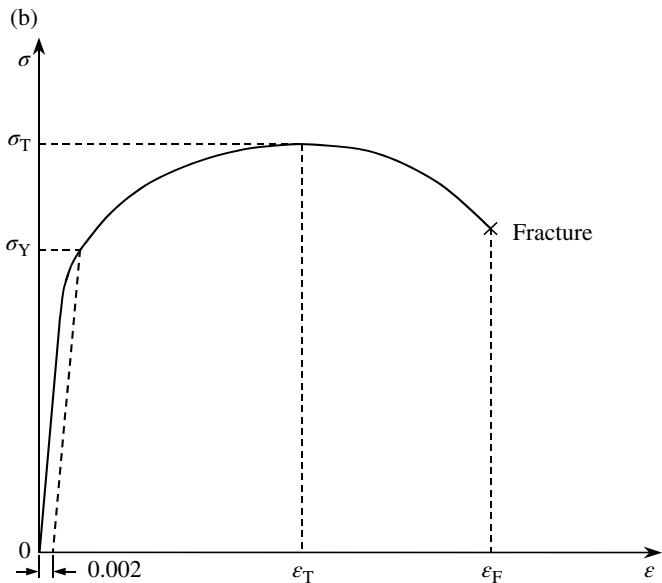


Figure 1.8 Schematic of engineering stress–engineering strain relationship for (a) ductile materials and (b) specially treated ductile materials.

engineering stress—engineering strain curve for structural metals. The material properties can be characterized using the following parameters:

- Young's modulus (or modulus of elasticity), E
- Poisson's ratio, ν
- Proportional limit, $\sigma_{\rm P}$

0003369274.3D 18 24/1/2018 10:47:55 AM

- Upper yield point, σ_{YU}
- Lower yield point, σ_{YL} ($\approx \sigma_{Y}$)
- Yield strength, $\sigma_{\rm Y}$
- Yield strain, $\varepsilon_{\rm Y}$
- Strain-hardening strain, $\varepsilon_{\rm h}$
- Strain-hardening tangent modulus, E_b
- Ultimate tensile strength, $\sigma_{\rm T}$
- Ultimate tensile strain, ε_{T}
- Necking tangent modulus, E_n
- Necking stress at fracture (total breaking), $\sigma_{\rm F}$
- Fracture (total breaking) strain, $\varepsilon_{\rm F}$

1.3.1.1 Young's Modulus, E

The initial relationship between stress and strain is linear elastic, wherein the material recovers perfectly upon unloading. The slope of the linear portion of the stress-strain relationship in the elastic regime is defined as the modulus of elasticity, E (also called Young's modulus). Table 1.2 indicates typical values of Young's moduli for selected metals and metal alloys at room temperature. Young's modulus of aluminum alloys is about one-third that of steel.

1.3.1.2 Poisson's Ratio, v

Poisson's ratio is defined as the ratio of the transverse strain to the longitudinal strain of a material under tensile load in the elastic regime. Table 1.2 indicates typical values of Poisson's ratio for selected metals and metal alloys at room temperature.

1.3.1.3 Elastic Shear Modulus, G

The mechanical properties of materials under shear are usually defined using principles of structural mechanics rather than by testing. The elastic shear modulus is expressed by a function of Young's modulus, E, and Poisson's ratio, v, as follows:

$$G = \frac{E}{2(1+\nu)} \tag{1.21}$$

Table 1.2 Typical values of Young's moduli and Poisson's ratios for selected metals and metal alloys at room temperature.

Material	E (GPa)	v
Aluminum alloy	70	0.33
Copper	110	0.34
Steel	205.8	0.3
Titanium	104–116	0.34

0003369274.3D 19 24/1/2018 10:47:56 AM

1.3.1.4 Proportional Limit, σ_P

The maximum stress in the elastic regime, that is, immediately before initial yielding, is termed the proportional limit, σ_P .

1.3.1.5 Yield Strength, σ_{Y} , and Yield Strain, ε_{Y}

Strictly speaking, structural materials without special treatment (e.g., quenching, tempering) may have upper and lower yield points, as illustrated in Figure 1.8a. The lower yield point typically has an extended plateau in the stress–strain curve, which is approximated by the yield strength $\sigma_{\rm Y}$ and the corresponding yield strain, $\varepsilon_{\rm Y} = \sigma_{\rm Y}/E$.

The mechanical properties of structural materials vary with the amount of work and heat treatment applied during the rolling process. Typically, plates that receive more work have a higher yield strength than plates that do not. The yield strength of metals is usually increased by special treatment.

Figure 1.8b illustrates an idealized engineering stress—engineering strain curve of specially treated metals or metal alloys in which neither upper nor lower yield points appear until the ultimate tensile strength is reached. In this case, the yield strength is commonly defined as the stress at the intersection of the stress—strain curve and a straight line through an offset point strain, $(\sigma,\varepsilon)=(0,0.002)$, that is, the proof stress at 0.2% strain, that is, with $\varepsilon=0.002$, which is parallel to the linear portion of the stress—strain curve in the elastic regime.

It is important to realize that a material's yield strength is significantly affected by operational and environmental conditions, such as temperatures and loading speed (or strain rates), among others. For structural design purposes, regulatory bodies or classification societies identify the "minimum" requirements for the mechanical properties and the chemical composition of materials. For example, the International Association of Classification Societies (IACS) specify the minimum requirements of the yield strength, ultimate tensile strength, and fracture strain (elongation) of rolled or extruded aluminum alloys for marine applications, as indicated in Tables 1.3 and 1.4 (IACS 2014). Interested readers may also refer to Sielski (2007, 2008).

1.3.1.6 Strain-Hardening Tangent Modulus, E_h , and Strain-Hardening Strain, ε_h

Beyond the yield stress or strain, the metal flows plastically without appreciable changes in stress until the strain-hardening strain ε_h is reached. The slope of the stress–strain curve in the strain-hardening regime is defined as the strain-hardening tangent modulus E_h , which may not be constant, but rather dependent on different conditions.

Strain hardening may also be characterized as the ratio of the ultimate tensile stress σ_T to the yield stress σ_Y or as the ratio of the ultimate tensile stress ε_T to the yield strain ε_Y . The stress σ beyond the yield strength of the elastic-plastic material with strain hardening is often expressed at a certain level of plastic strain as follows:

$$\sigma = \sigma_{\rm Y} + \frac{EE_{\rm h}}{E - E_{\rm h}} \varepsilon_{\rm p} \tag{1.22}$$

where $\varepsilon_{\rm p}$ is the effective plastic strain.

1.3.1.7 Ultimate Tensile Strength, σ_T

When strain exceeds the strain-hardening strain, ε_h , the stress increases above the yield stress, σ_Y , because of strain hardening, and this behavior can continue until the ultimate

0003369274.3D 20 24/1/2018 10:47:56 AM

Table 1.3 Minimum requirements of the mechanical properties for rolled aluminum alloys (IACS 2014).

	Temper	Thickness t (mm)	$\sigma_{ m Y}$ (MPa)	σ_{T} (MPa)	$arepsilon_{F}$ (%)	
Grade					<i>t</i> ≤ 12.5mm	<i>t</i> > 12.5 mm
5083	О	$3 \le t \le 50$	125	275-350	16	14
	H111	$3 \le t \le 50$	125	275-350	16	14
	H112	$3 \le t \le 50$	125	275	12	10
	H116	$3 \le t \le 50$	215	305	10	10
	H321	$3 \le t \le 50$	215-295	305-385	12	10
5383	O	$3 \le t \le 50$	145	290	_	17
	H111	$3 \le t \le 50$	145	290	_	17
	H116	$3 \le t \le 50$	220	305	10	10
	H321	$3 \le t \le 50$	220	305	10	10
5059	O	$3 \le t \le 50$	160	330	24	24
	H111	$3 \le t \le 50$	160	330	24	24
	H116	$3 \le t \le 20$	270	370	10	10
		$20 < t \le 50$	260	360	_	10
	H321	$3 \le t \le 20$	270	370	10	10
		$20 < t \le 50$	260	360	_	10
5086	O	$3 \le t \le 50$	95	240-305	16	14
	H111	$3 \le t \le 50$	95	240-305	16	14
	H112	$3 \le t \le 12.5$	125	250	8	_
		$12.5 < t \le 50$	105	240	_	9
	H116	$3 \le t \le 50$	195	275	$10^{1)}$	9
5754	O	$3 \le t \le 50$	80	190-240	18	17
	H111	$3 \le t \le 50$	80	190-240	18	17
5456	O	$3 \le t \le 6.3$	130-205	290-365	16	_
		$6.3 < t \le 50$	125-205	285-360	16	14
	H116	$3 \le t \le 30$	230	315	10	10
		$30 < t \le 40$	215	305	_	10
		$40 < t \le 50$	200	285	_	10
	H321	$3 \le t \le 12.5$	230-315	315-405	12	_
		$12.5 < t \le 40$	215-305	305-385	_	10
		$40 < t \le 50$	200-295	285-370	_	10

Notes:

0003369274.3D 21 24/1/2018 10:47:56 AM

a) 8% for $t \le 6.3$ mm.

b) The mechanical properties for the O and H111 tempers are the same, but they are separated to encourage dual certification as these tempers represent different processing.

Table 1.4 Minimum requirements of the mechanical properties for extruded aluminum alloys (IACS 2014).

Grade	Temper	Thickness t (mm)	$\sigma_{ m Y}$ (MPa)	σ_{T} (MPa)	ε _F (%)	
					<i>t</i> ≤ 12.5 mm	t > 12.5 mm
5083	О	$3 \le t \le 50$	110	270-350	14	12
	H111	$3 \le t \le 50$	165	275	12	10
	H112	$3 \le t \le 50$	110	270	12	10
5383	O	$3 \le t \le 50$	145	290	17	17
	H111	$3 \le t \le 50$	145	290	17	17
	H112	$3 \le t \le 50$	190	310	_	13
5059	H112	$3 \le t \le 50$	200	330	_	10
5086	O	$3 \le t \le 50$	95	240-315	14	12
	H111	$3 \le t \le 50$	145	250	12	10
	H112	$3 \le t \le 50$	95	240	12	10
6005A	T5	$3 \le t \le 50$	215	260	9	8
	T6	$3 \le t \le 10$	215	260	8	6
		$10 < t \le 50$	200	250	8	6
6061	T6	$3 \le t \le 50$	240	260	10	8
6082	T5	$3 \le t \le 50$	230	270	8	6
	T6	$3 \le t \le 5$	250	290	6	_
		$5 < t \le 50$	260	310	10	_

tensile strength (also simply termed tensile strength), σ_T , is reached. The value of σ_T is obtained by the maximum axial tensile load divided by the original cross-sectional area of the test specimen. Tables 1.3 and 1.4 indicate the minimum requirements of the ultimate tensile strength for rolled or extruded aluminum alloys.

1.3.1.8 Necking Tangent Modulus, E_n

With further increase in strain, a large local reduction of the cross section occurs, which is termed necking or strain softening. The internal engineering stress decreases in the necking regime. The slope of the engineering stress—engineering strain curve in the necking regime is sometimes defined as the necking tangent modulus, $E_{\rm n}$. Necking may also be characterized as the ratio of the fracture stress $\sigma_{\rm F}$ to the ultimate tensile stress $\sigma_{\rm T}$ or as the ratio of the fracture strain $\varepsilon_{\rm F}$ to the ultimate tensile strain $\varepsilon_{\rm T}$.

1.3.1.9 Fracture Strain, $\varepsilon_{\rm F}$, and Fracture Stress, $\sigma_{\rm F}$

Fracture takes place when the strain reaches the fracture strain (elongation or total breaking strain), ε_F . The fracture stress σ_F is defined as the stress at fracture in the necking regime. Fracture strain is also significantly affected by operational and environmental conditions, such as temperatures and loading speed (or strain rates), among other factors.

0003369274.3D 22 24/1/2018 10:47:56 AM

Tables 1.3 and 1.4 indicate the minimum requirements of the fracture strain for rolled or extruded aluminum alloys.

Elastic-Perfectly Plastic Material Model

Figure 1.9 shows the illustrative effects of strain hardening on the elastic-plastic largedeflection behavior (i.e., average stress-average strain curve) of a steel rectangular plate under uniaxial compressive loads in the longitudinal direction, as obtained by the nonlinear finite element analysis. The characteristics of the strain hardening are varied as shown in Figure 1.9a in the analysis. The plate is simply supported at all four edges, keeping them straight. It is evident that the strain-hardening effect can cause the plate ultimate strength to be greater than that obtained by neglecting it.

For the ULS assessment of structures made of ductile materials, an elastic-perfectly plastic material model, as shown in Figure 1.10, that is, one without strain hardening or necking, is often applied because strains are usually not significant. This material model may lead to a pessimistic estimation of the characteristic value of capacity. For the ALS assessment, however, the true stress—true strain relation with strain-hardening and necking effects should be considered because large plastic strains are usually involved.

Characterization of the Engineering Stress-Engineering Strain Relationship

When the details of the relationship between engineering stress σ versus engineering strain ε are unavailable, but such fundamental parameters as the elastic modulus E and the yield strength $\sigma_{\rm Y}$ are known, the relationship between engineering stress and engineering strain can often be approximated using the Ramberg-Osgood equation, which was originally proposed for aluminum alloys (Ramberg & Osgood 1943), as follows:

$$\varepsilon = \frac{\sigma}{F} + \left(\frac{\sigma}{R}\right)^n \tag{1.23}$$

where E is the elastic modulus at the origin of the stress versus strain curve, ε is the engineering strain, σ is the engineering stress, and B and n are constants to be determined by experiments.

Equation (1.23) is often simplified as follows (Mazzolani 1985):

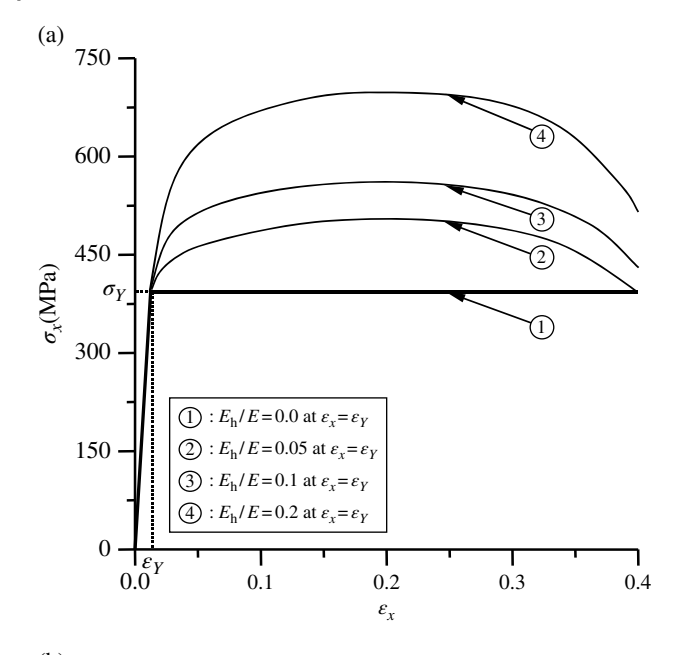
$$\varepsilon = \frac{\sigma}{E} + 0.002 \left(\frac{\sigma}{\sigma_{0.2}}\right)^n \tag{1.24a}$$

where $\sigma_{0.2}$ is the proof stress at 0.2% strain, that is, with $\varepsilon = 0.002$, which is usually taken as material yield stress σ_Y , that is, $\sigma_{0.2} = \sigma_Y$, as shown in Figure 1.11. Exponent n is given as a function of $\sigma_{0,2}$ and $\sigma_{0,1}$ as follows:

$$n = \frac{\ln 2}{\ln(\sigma_{0.2}/\sigma_{0.1})} \tag{1.24b}$$

where $\sigma_{0.1}$ is the proof stress at 0.1% strain, with $\varepsilon = 0.001$.

0003369274.3D 23 24/1/2018 10:47:56 AM



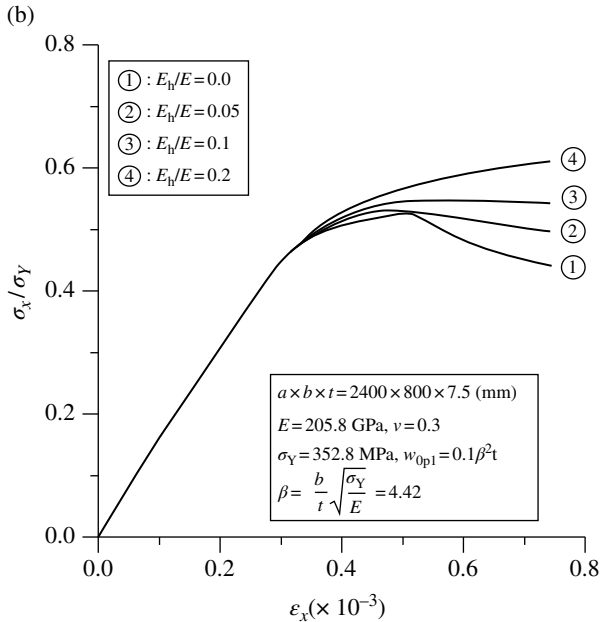


Figure 1.9 The effect of strain hardening on the ultimate strength of a steel plate under axial compression: (a) the engineering stress—engineering strain curves varying the strain-hardening characteristics; (b) a thin plate; (c) a thick plate (w_{0pl} , buckling mode initial deflection of the plate).

0003369274.3D 24 24/1/2018 10:47:56 AM

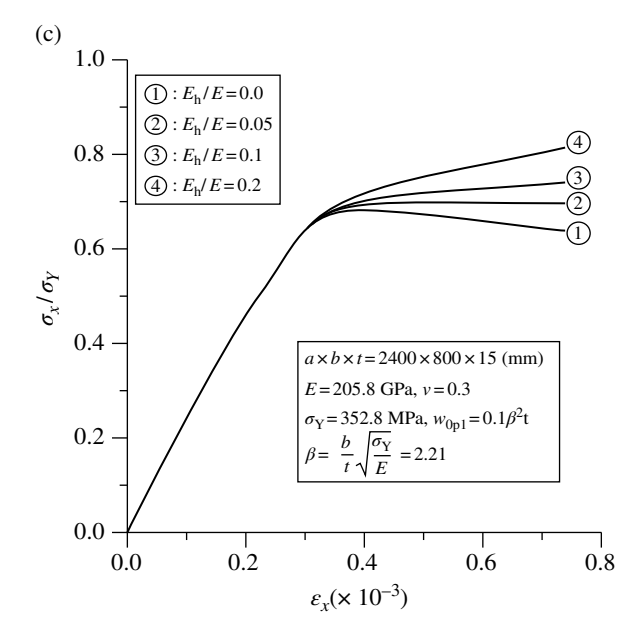


Figure 1.9 (Continued)

When the Ramberg-Osgood law is used, one practical difficulty is the determination of $\sigma_{0.1}$, in addition to *E* and $\sigma_{0,2}$ ($\approx \sigma_{\rm Y}$). Without considering the strainhardening effect, if the ratio $\sigma_{0,2}/\sigma_{0,1}$ approaches 1 (or $\sigma_{0.1} = \sigma_{0.2}$), the exponent becomes infinity, that is, $n = \infty$. This behavior corresponds to the elastic perfectly plastic model of material, as illustrated in Figure 1.10, which can be expressed by

$$\varepsilon = \frac{\sigma}{E} + 0.002 \left(\frac{\sigma}{\sigma_{0.2}}\right)^{\infty} \tag{1.25}$$

For aluminum alloys, Steinhardt (1971) proposed an approximate method for determining exponent *n* without the value of $\sigma_{0,1}$ being known as follows:

$$0.1n = \sigma_{0.2} (N/mm^2)$$
 or $n = 10\sigma_{0.2}$ (1.26)

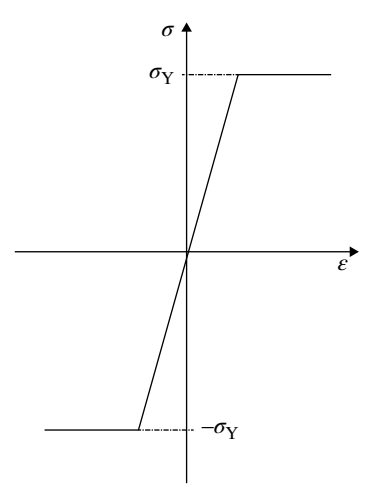


Figure 1.10 The elastic-perfectly plastic model of material.

1.3.4 Characterization of the True Stress-True Strain Relationship

For structural materials, the engineering stress-engineering strain relationship can be converted to the true stress-true strain relationship as follows:

$$\sigma_{\text{true}} = \sigma(1 + \varepsilon), \quad \varepsilon_{\text{true}} = \ln(1 + \varepsilon)$$
 (1.27)

where $\sigma_{\rm true}$ is the true stress, $\varepsilon_{\rm true}$ is the true strain, σ is the engineering stress, and ε is the engineering strain.

0003369274.3D 25 24/1/2018 10:47:56 AM

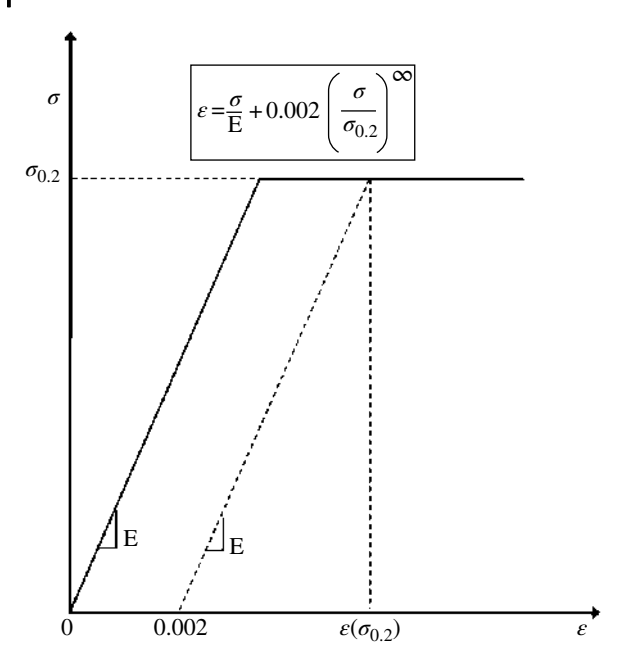


Figure 1.11 The Ramberg-Osgood law with the elastic-perfectly plastic model of material.

Figure 1.12 shows the engineering stress—engineering strain curve versus the true stress—true strain curve for mild steel and the aluminum alloy 5383-H116. It is recognized that Equation (1.27) tends to overestimate the strain-hardening and necking (strain-softening) effects. To resolve this issue, Paik (2007a, 2007b) suggested that Equation (1.27) be modified by the introduction of a knockdown factor that is a function of the engineering strain as follows:

$$\sigma_{\text{true}} = f(\varepsilon)\sigma(1+\varepsilon), \quad \varepsilon_{\text{true}} = \ln(1+\varepsilon)$$

$$f(\varepsilon) = \begin{cases} \frac{C_1 - 1}{\ln(1+\varepsilon_T)} \ln(1+\varepsilon) + 1 & \text{for } 0 < \varepsilon \le \varepsilon_T \\ \frac{C_2 - C_1}{\ln(1+\varepsilon_F) - \ln(1+\varepsilon_T)} \ln(1+\varepsilon) + C_1 - \frac{(C_2 - C_1) \ln(1+\varepsilon_T)}{\ln(1+\varepsilon_F) - \ln(1+\varepsilon_T)} & \text{for } \varepsilon_T < \varepsilon \le \varepsilon_F \end{cases}$$

$$(1.28a)$$

where $f(\varepsilon)$ is the knockdown factor as a function of the engineering strain, $\varepsilon_{\rm F}$ is the material's fracture strain (elongation), $\varepsilon_{\rm T}$ is the strain at the ultimate tensile stress, and C_1 and C_2 are the test constants affected by material type and plate thickness, among other factors.

Although the knockdown factor is governed by the characteristics of the material type and plate thickness, the test constants may be given as C_1 = 0.9 and C_2 = 0.85 for mild and high-tensile steel (Paik 2007a, 2007b). Figure 1.13 compares the original true stress—true strain curve versus the modified (knocked-down) true stress—true strain curve of mild steel and the aluminum alloy 5383-H116, where the constants C_1 = 0.9 and C_2 = 0.85 are applied for both mild steel and the aluminum alloy.

0003369274.3D 26 24/1/2018 10:47:57 AM

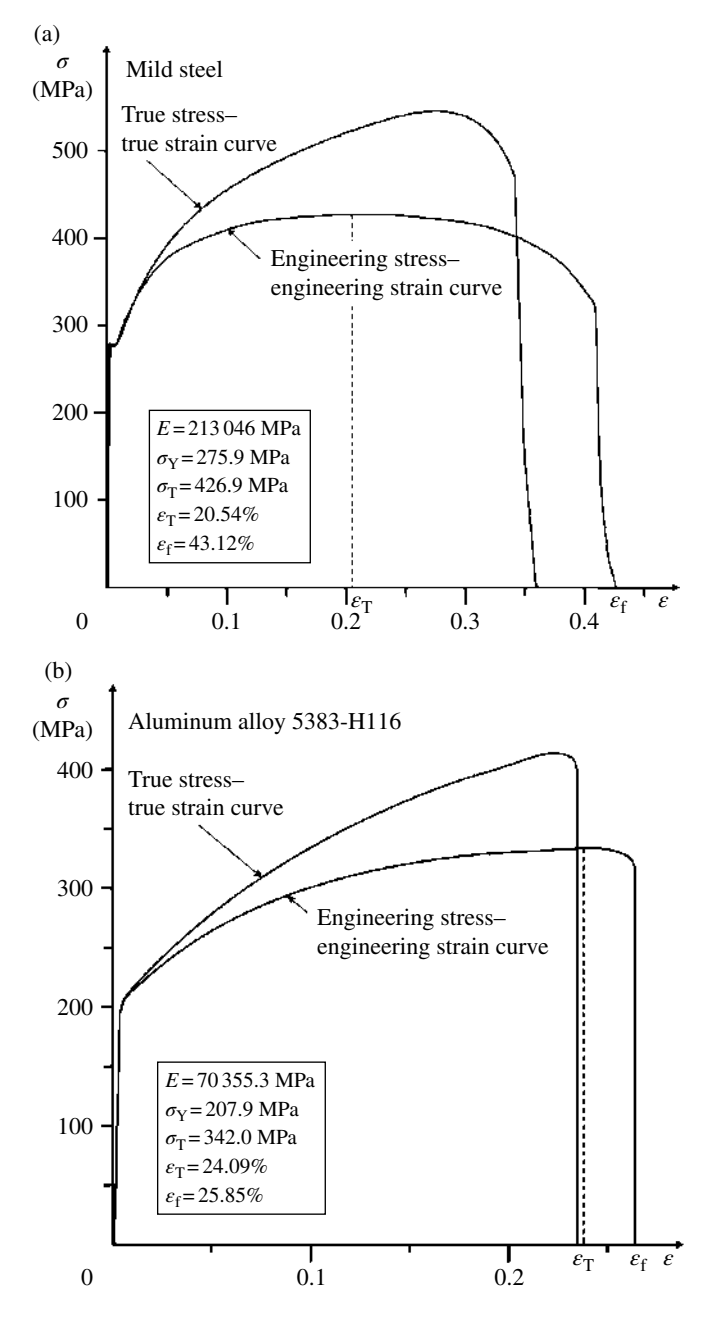


Figure 1.12 Engineering stress-engineering strain curve versus true stress-true strain curve for materials: (a) mild steel; (b) aluminum alloy 5383-H116.

24/1/2018 10:47:57 AM 0003369274.3D 27

Figure 1.13 The original true stress–true strain curve versus the modified true stress–true strain curve for materials: (a) mild steel; (b) aluminum alloy 5383-H116.

0003369274.3D 28 24/1/2018 10:47:58 AM

1.3.5 **Effect of Strain Rates**

A material's mechanical properties are significantly affected by loading speed or strain rates $\dot{\varepsilon}$, which can be determined in an approximate fashion by assuming that the initial speed V_0 of the dynamic loads is linearly reduced to zero until the loading is finished, with average displacement δ , namely,

$$\dot{\varepsilon} = \frac{V_0}{2\delta} \tag{1.29}$$

In structural crashworthiness and/or impact response analysis, strain rate sensitivity plays an important role. Therefore, material modeling in terms of the dynamic yield strength and dynamic fracture strain must be considered. Figure 1.14 shows the engineering stress-engineering strain curves with varying strain rates obtained from experiments with mild steel (Grade A) and aluminum alloy 5083-O at room temperature, respectively (Paik et al. 2017).

As described in Section 10.3.2, the dynamic yield strength is often determined from the following Cowper-Symonds equation (Cowper & Symonds 1957):

$$\sigma_{\rm Yd} = \left\{ 1 + \left(\frac{\dot{\varepsilon}}{C}\right)^{1/q} \right\} \sigma_{\rm Y} \tag{1.30a}$$

where $\sigma_{\rm Y}$ is the static yield stress, $\sigma_{\rm Yd}$ is the dynamic yield stress, $\dot{\varepsilon}$ is the strain rate (1/s), and C and q are test constants, which may be taken as C = 40.4/s, q = 5 for mild steel, C = 3200/s, q = 5 for high-tensile steel, and C = 6500/s, q = 4 for aluminum alloys (Paik & Thayamballi 2007, Jones 2012, Paik et al. 2017).

The dynamic fracture strain is taken as the inverse of the Cowper-Symonds equation for the dynamic yield strength as follows:

$$\varepsilon_{\rm Fd} = \left\{ 1 + \left(\frac{\dot{\varepsilon}}{C}\right)^{1/q} \right\}^{-1} \varepsilon_{\rm F} \tag{1.30b}$$

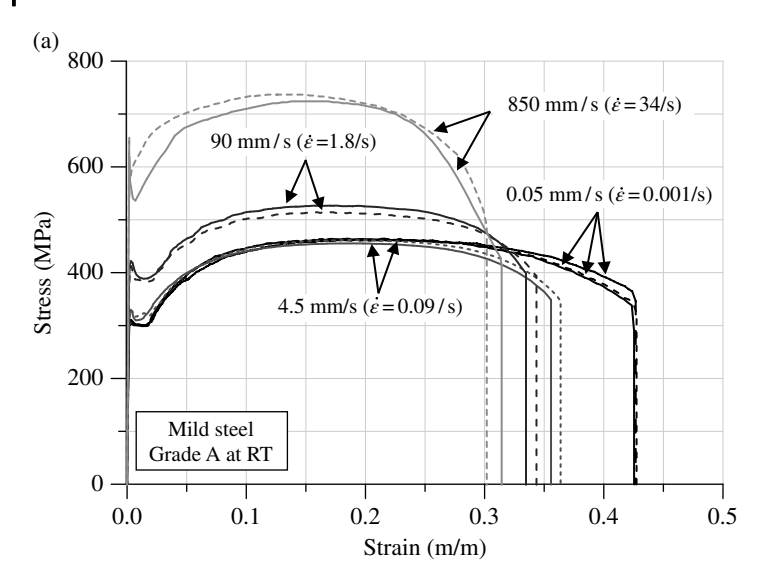
where $\varepsilon_{\rm F}$ is the static fracture strain and $\varepsilon_{\rm Fd}$ is the dynamic fracture strain. It is noted that the test constants C and q for the dynamic fracture strain are different from those for the dynamic yield strength as described in Section 10.3.3.

Figures 1.15 and 1.16 show the effects of strain rates combined with cold temperatures on the yield strength or fracture strain obtained from experiments for mild steel, hightensile steel, and aluminum alloy 5083-O, obtained from the experiments by Paik et al. (2017).

Effect of Elevated Temperatures

A material's mechanical properties are significantly decreased with elevated temperatures from operational and environmental conditions or accidents such as fires because the material's properties are associated with its thermal characteristics. Figure 1.17a shows the specific heat of steel, which varies with elevated temperature. The reduction factors of the proportional limit, Young's modulus, and yield strength for steel are indicated in Table 1.5 according to the ECCS Eurocode design manuals (Franssen & Real 2010).

0003369274.3D 29 24/1/2018 10:47:58 AM



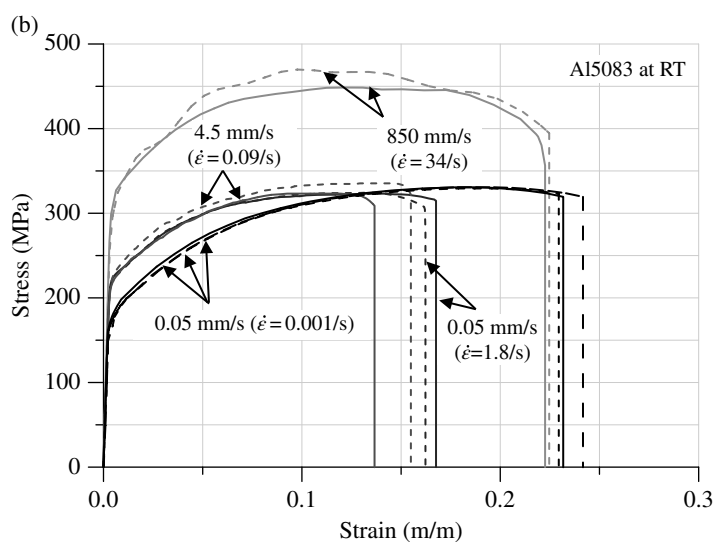


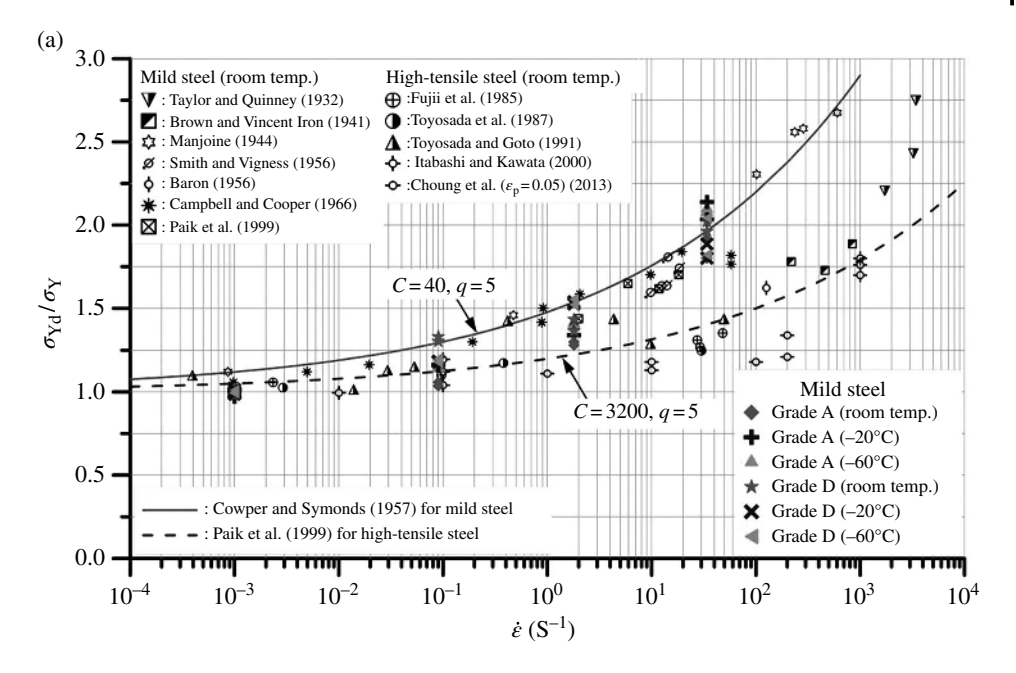
Figure 1.14 Engineering stress—engineering strain curves with different strain rates at room temperature (RT): (a) for mild steel (Grade A); (b) aluminum alloy 5083-O (Paik et al. 2017).

Figure 1.17b plots Table 1.5, showing that the mechanical properties of steel significantly decrease at temperatures above 400° C.

1.3.7 Effect of Cold Temperatures

The mechanical properties of materials are significantly affected by cold temperatures, which may be caused by operational conditions due to liquefied petroleum or natural gas

0003369274.3D 30 24/1/2018 10:47:58 AM



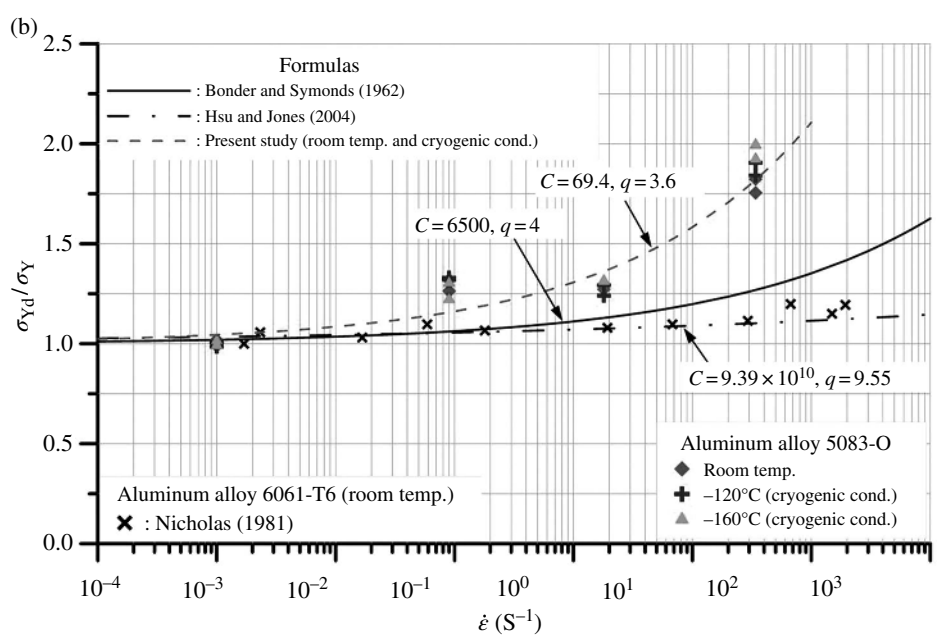
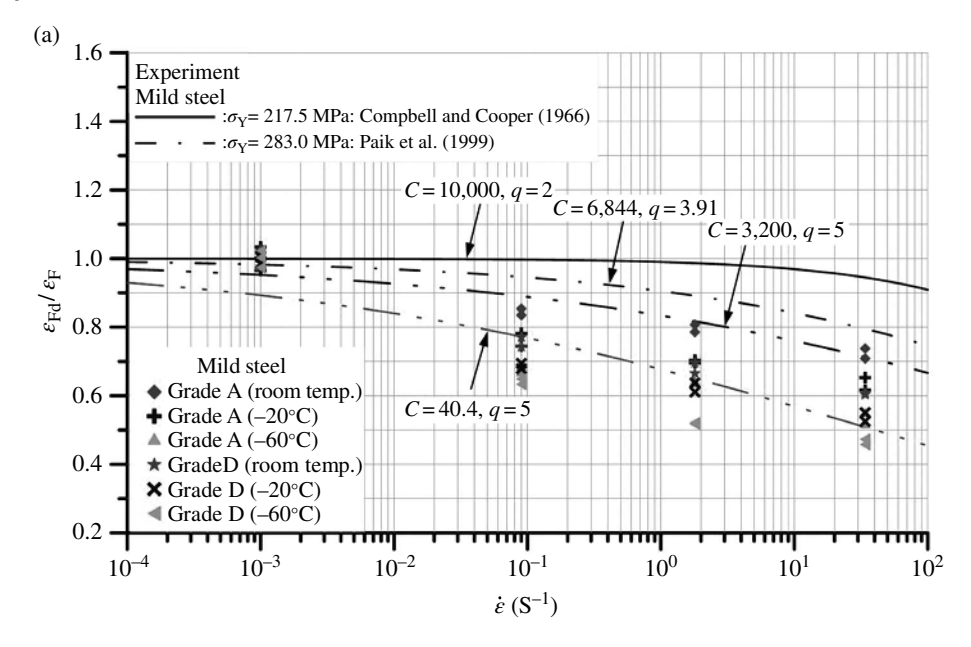


Figure 1.15 Effect of strain rates and cold temperatures on yield strength of materials: (a) mild steel and high-tensile steel; (b) aluminum alloy 5083-O. (Cited references are from Paik et al. 2017.)

0003369274.3D 31 24/1/2018 10:47:59 AM



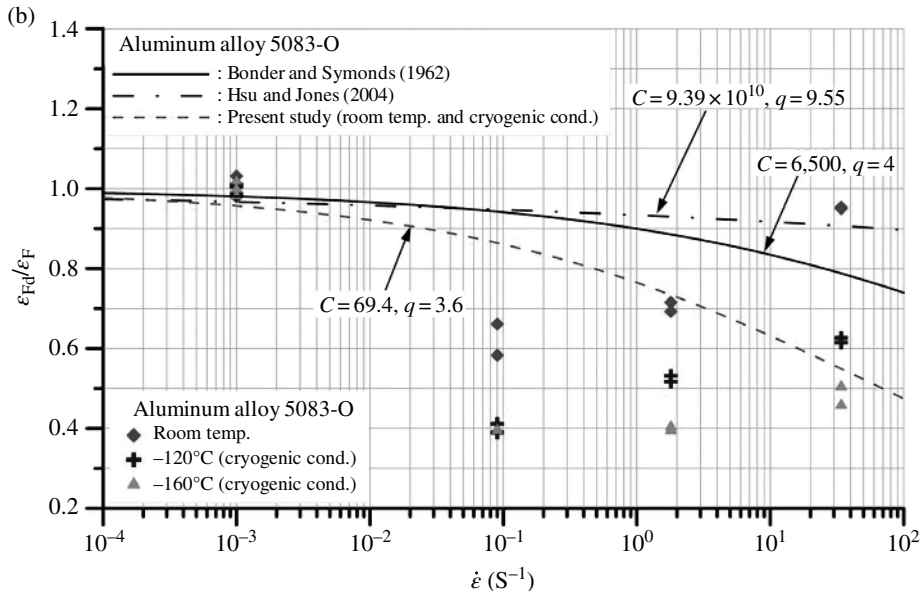


Figure 1.16 Effect of strain rates and cold temperatures on fracture strain of materials: (a) mild steel and high-tensile steel; (b) aluminum alloy 5083-O. (Cited references are from Paik et al. 2017.)

cargoes and by environmental conditions due to Arctic operations. Figures 1.18 and 1.19 show the combined effects of cold temperatures and strain rates on the yield strength or fracture strain of mild steel (Grade A) and aluminum alloy 5083-O, obtained from the experiments by Paik et al. (2017).

0003369274.3D 32 24/1/2018 10:48:00 AM

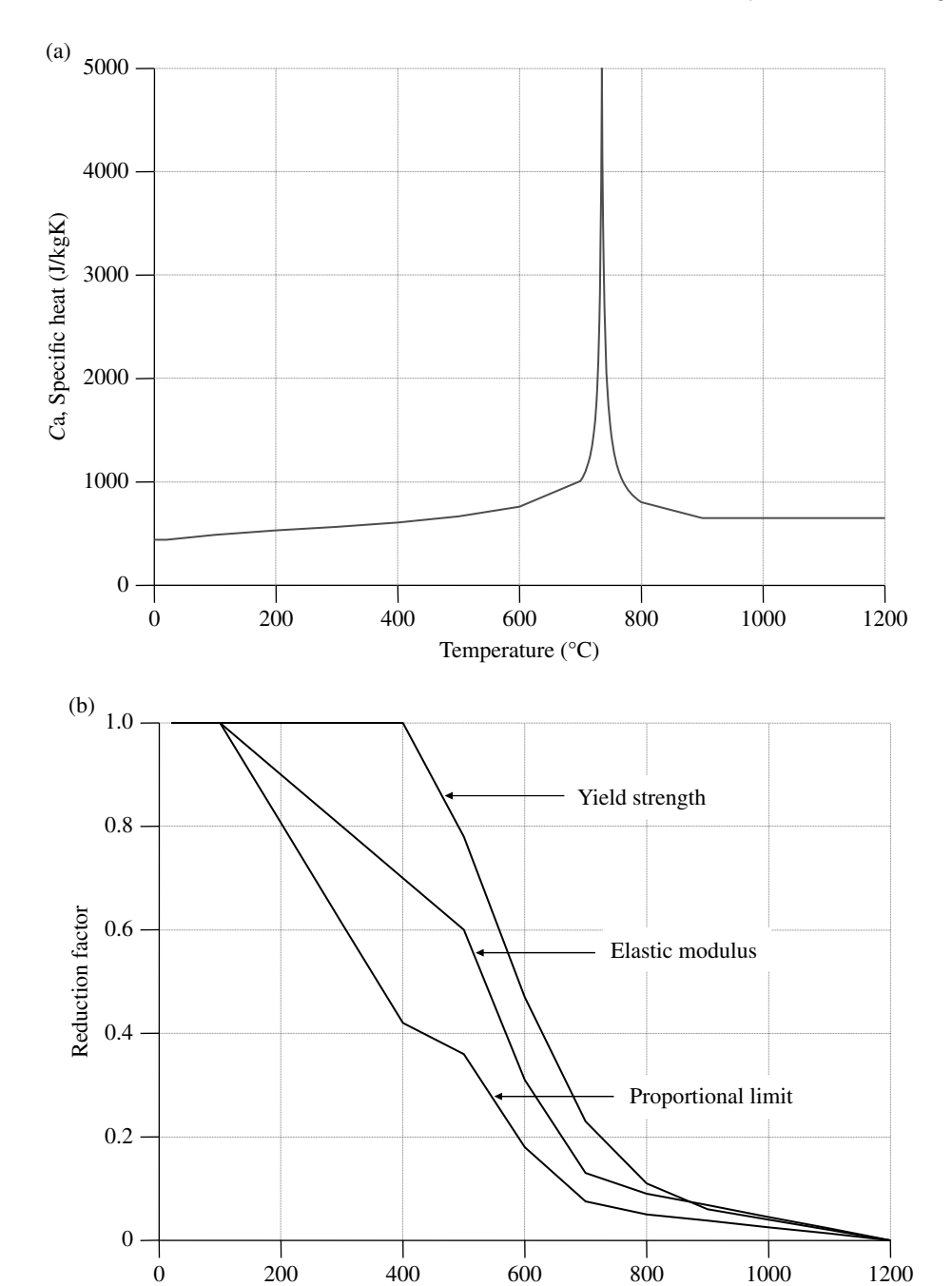


Figure 1.17 Effects of elevated temperature on properties of steel: (a) specific heat (ECCS 1982); (b) mechanical properties.

Temperature ($^{\circ}$ C)

0003369274.3D 33 24/1/2018 10:48:01 AM

Table 1.5 Reduction factors of mechanical properties for carbon steels at elevated temperatures.

	Reduction factors at temperature relative to value of σ_Y , σ_P , or E at 20°C			
Steel temperature (°C)	σ_{Y}	$\sigma_{ extsf{P}}$	E	
20	1.000	1.0000	1.0000	
100	1.000	1.0000	1.0000	
200	1.000	0.8070	0.9000	
300	1.000	0.6130	0.8000	
400	1.000	0.4200	0.7000	
500	0.780	0.3600	0.6000	
600	0.470	0.1800	0.3100	
700	0.230	0.0750	0.1300	
800	0.110	0.0505	0.0900	
900	0.060	0.0375	0.0675	
1000	0.040	0.0250	0.0450	
1100	0.020	0.0125	0.0225	
1200	0.000	0.0000	0.0000	

Note: For intermediate values of the steel temperature, a linear interpolation may be used.

1.3.8 Yield Condition Under Multiple Stress Components

For a one-dimensional strength member under uniaxial tensile or compressive loading, the yield strength determined from a uniaxial tension test can be used to check the state of yielding, with the essential question to be answered being simply whether the axial stress reaches the yield strength.

A plate element that is the principal strength member of a steel- or aluminum-plated structure is likely to be subjected to a combination of biaxial tension/compression and shear stress, which can usually be considered to be in a plane stress state (as contrasted to a state of plane strain).

For an isotropic two-dimensional structural member for which the dimension in one direction is much smaller than those in the other two directions, and with three in-plane stress components (i.e., two normal stresses, σ_x , σ_y , and shear stress, τ_{xy}) or, equivalently, two principal stress components (i.e., σ_1 , σ_2), three types of yield criteria are usually adopted as follows:

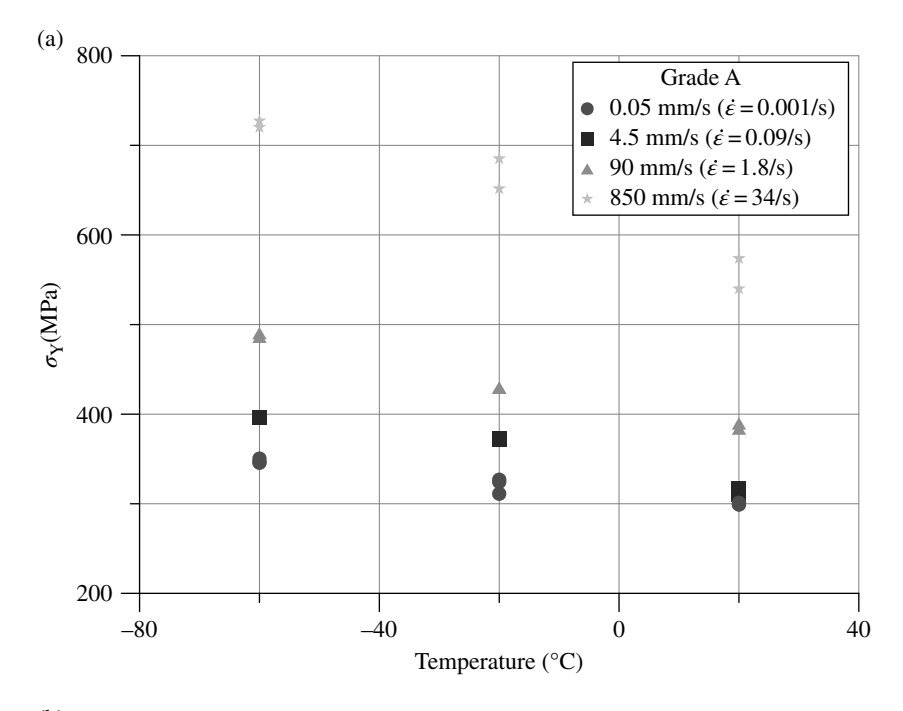
1) Maximum principal stress-based criterion: The material yields if the maximum absolute value of the two principal stresses reaches a critical value, namely,

$$\max(|\sigma_1|, |\sigma_2|) = \sigma_Y \tag{1.31a}$$

2) Maximum shear stress-based criterion (also called the Tresca criterion): The material yields if the maximum shear stress, τ_{max} , reaches a critical value, namely,

$$\tau_{\text{max}} = \left| \frac{\sigma_1 - \sigma_2}{2} \right| = \frac{\sigma_Y}{2} \tag{1.31b}$$

0003369274.3D 34 24/1/2018 10:48:02 AM



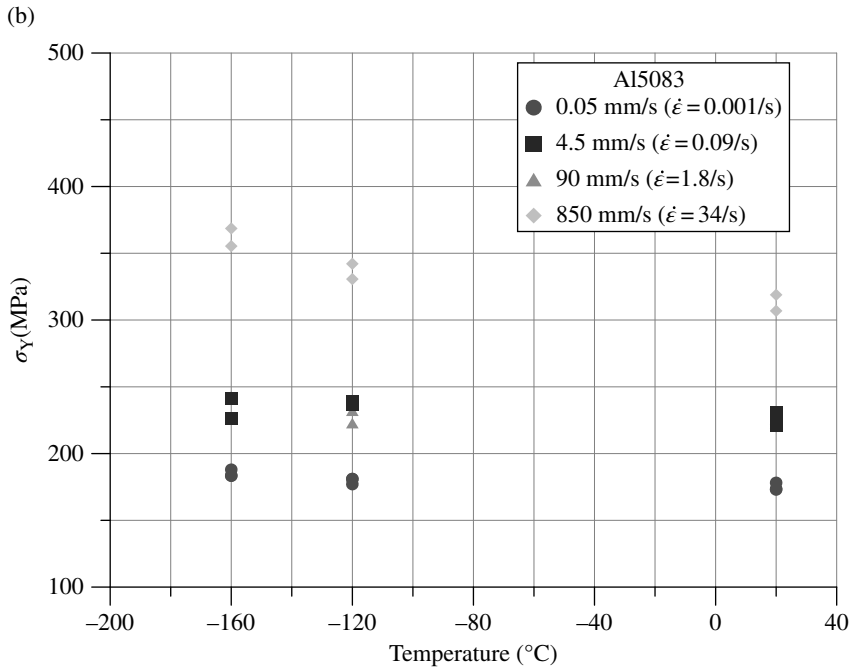
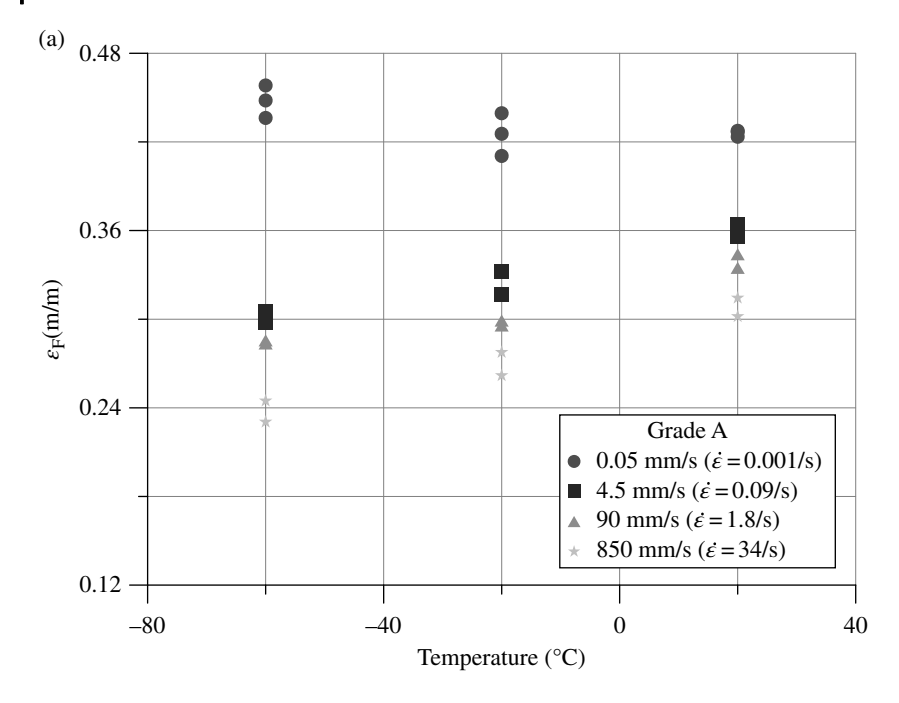


Figure 1.18 Effect of cold temperatures and strain rates on yield strength of materials: (a) mild steel (Grade A); (b) aluminum alloy 5083-O (Paik et al. 2017).

0003369274.3D 35 24/1/2018 10:48:02 AM



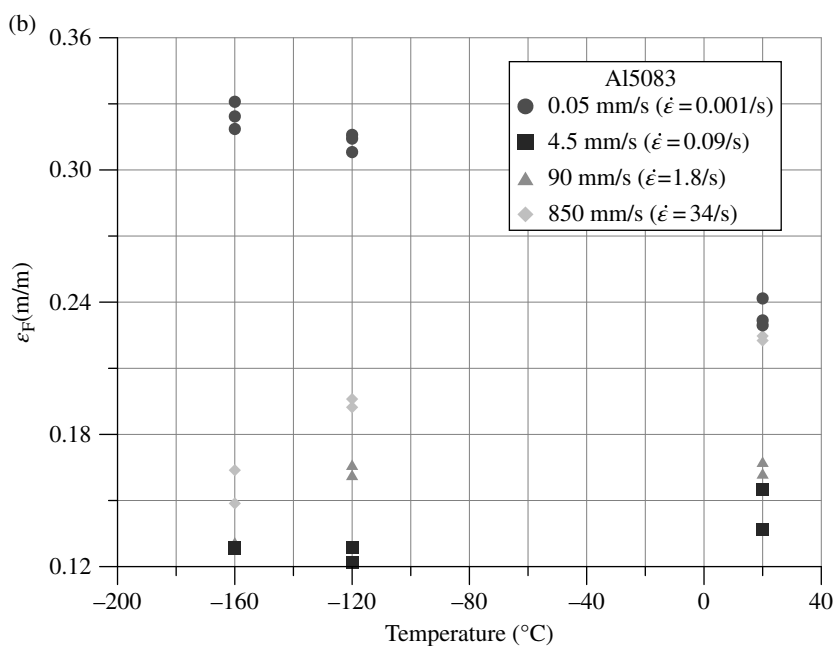


Figure 1.19 Effect of cold temperatures and strain rates on fracture strain of materials: (a) mild steel (Grade A); (b) aluminum alloy 5083-O (Paik et al. 2017).

0003369274.3D 36 24/1/2018 10:48:02 AM

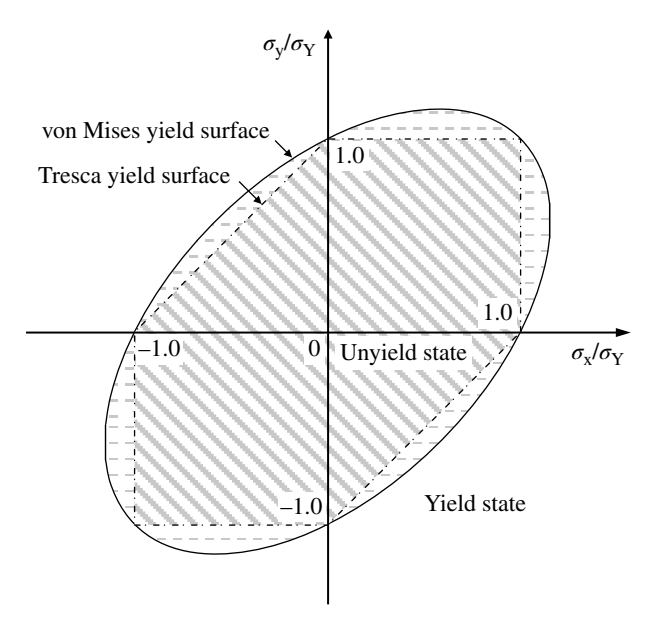


Figure 1.20 The von Mises and Tresca yield surfaces associated with two normal stress components.

3) Strain energy-based criterion (also called the Mises-Hencky or Huber-Hencky-Mises or von Mises criterion): The material yields if the strain energy due to geometric changes reaches a critical value, which corresponds to that at which the equivalent stress, $\sigma_{\rm eq}$, reaches the yield strength, $\sigma_{\rm Y}$, as determined from the uniaxial tension test as follows:

$$\sigma_{\rm eq} = \sqrt{\sigma_x^2 - \sigma_x \sigma_y + \sigma_y^2 + 3\tau_{xy}^2} = \sigma_{\rm Y} \tag{1.31c}$$

where $\sigma_{\rm Y}$ is the yield strength of material.

It is recognized that the first yield condition, Equation (1.31a), is relevant for a brittle material and that the last two conditions, Equations (1.31b) and (1.31c), are more appropriate for a ductile material, although the von Mises condition, Equation (1.31c), is more popular for the analysis of plated structures. Figure 1.20 illustrates the von Mises and Tresca yield surfaces associated with two normal stress components, σ_x and σ_y . The shear yield stress, τ_Y , under pure shear can be determined by solving the von Mises condition, Equation (1.31c), with regard to τ_{xy} when $\sigma_x = \sigma_y = 0$, with the result as follows:

$$\tau_{\rm Y} = \frac{\sigma_{\rm Y}}{\sqrt{3}} \tag{1.31d}$$

The Bauschinger Effect: Cyclic Loading

During operation, structural members are likely to be subjected to load cyclic effects, as shown in Figure 1.21. If a material that has been plastically strained in tension is unloaded and then strained in compression, the stress-strain curve for the compression loading

0003369274.3D 37 24/1/2018 10:48:02 AM

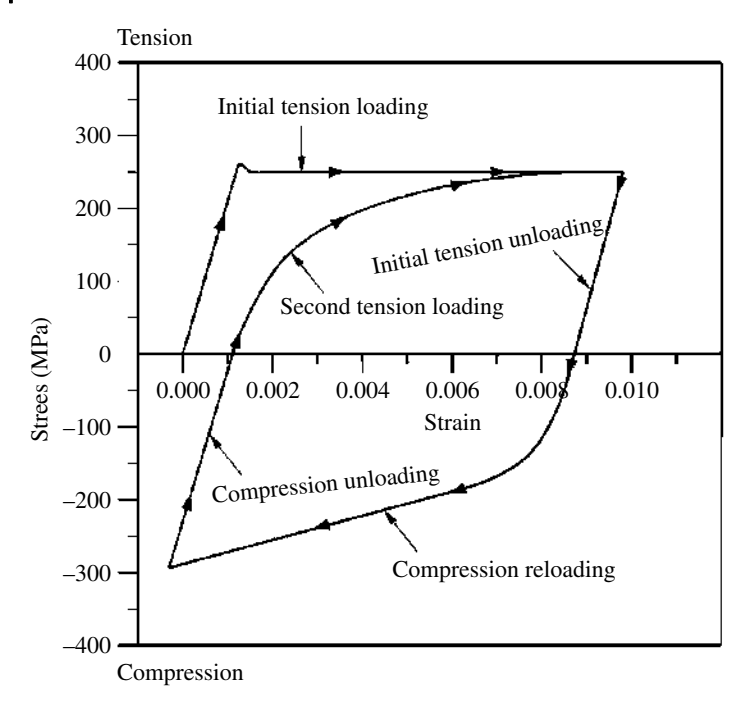


Figure 1.21 The Bauschinger effect in metals.

deviates from a linear relationship at stresses well below the yielding point of the virgin material, but it returns to the point of maximum stress and strain for the first tension loading cycle. The same effect is observed for the opposite loading cycle, that is, compression before tension. In this case, the modulus of elasticity is reduced, as shown by the shape of the stress–strain curve in Figure 1.21. This phenomenon is typically termed the Bauschinger effect (Brockenbrough & Johnston 1981). When stiffness is of primary concern, for example, in the evaluation of buckling or deflection, the Bauschinger effect may be of interest.

Within an acceptable level of accuracy, however, the mechanical properties of a particular type of steel or aluminum alloy as determined by uniaxial tension testing are also approximately accepted as being valid for the same type of the material under uniaxial compression.

1.3.10 Limits of Cold Forming

Cold forming is an efficient technique to form structural shapes, for example, a curved plate. However, it is important to realize that excessive strain during cold forming can exhaust ductility and cause cracking. Hence the strain in cold forming the structural shapes must be limited, not only to prevent cracking but also to prevent buckling collapse of structural elements subject to compressive loads. The cold-forming-induced strain is usually controlled by requiring the ratio of the bending radius to the plate thickness to be large, in the range of 5-10.

0003369274.3D 38 24/1/2018 10:48:03 AM

1.3.11 Lamellar Tearing

In most cases of plated structures, the behavior in the length and breadth of the plates related to load effects is of primary concern. The behavior in the wall thickness direction is normally not of interest. In heavy, welded structures, particularly in joints or connections with thick plates and heavy structural shapes, however, crack-type separation or delamination can take place in the wall thickness direction beneath the surface of plates or at weld toes. This failure is typically caused by large through-thickness strain, which is sometimes associated with weld metal shrinkage in highly restrained joints. This phenomenon is termed lamellar tearing. Careful selection of weld details, filler metal, and welding procedure and the use of steels with controlled through-thickness properties (e.g., the so-called Z grade steels) can be effective to control this failure mode.

1.4 Strength Member Types for Plated Structures

The geometric configuration of a steel- or aluminum-plated structure is determined primarily on the basis of the function of the particular structure. Figure 1.22 shows a basic part of a typical plated structure. A major difference between plated and framed structures is that the principal strength members of the former type of structure are plate panels together with support members, whereas those of the latter typically consist of truss or beam members for which the dimension in the axial direction is usually much greater than those in the other two directions.

Typical examples of plated structures are ships, ship-shaped offshore platforms, box girder bridges, and box girder cranes. Basic types of structural members that usually make up plated structures are as follows:

- Plate panels: Plating, stiffened panel, corrugated panel
- Small support members: Stiffener, beam, column, beam-column
- Strong main support members: Plate girder, frame, floor, bulkhead, box girder

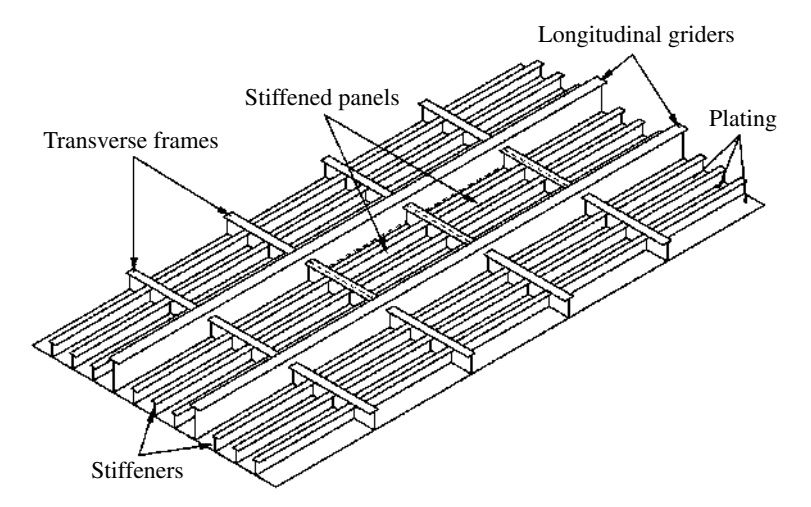


Figure 1.22 Typical plated structure.

0003369274.3D 39 24/1/2018 10:48:03 AM

To improve the stiffness and strength of plate panels, increasing the stiffener dimensions is usually more efficient than simply increasing the plate thickness, and thus the plate panel is usually reinforced by beam members (stiffeners) in the longitudinal or transverse direction. Figure 1.23a shows typical beam members used to stiffen the plating. A self-stiffened plate, such as the corrugated panel shown in Figure 1.23b, may also be used in some cases.

When the stiffened panels are likely to be subjected to lateral loads or out-of-plane bending or just require lateral support, they are supported by stronger beam members. Figure 1.23c shows typical strong main support members used to build plated structures. For ships and offshore structures, plate girders composed of deep webs and wide flanges are typically used for main support members. The deep web of a plate girder is often stiffened vertically and/or horizontally. Box-type support members that consist of plate panels are used for construction of land-based steel bridges or cranes. Diaphragms or transverse floors or transverse bulkheads are arranged at relevant spaces in the box girder.

Although plating primarily sustains in-plane loads, support members resist out-of-plane (lateral) loads and bending. A plate panel between stiffeners is called "plating," and plating with stiffeners is termed a "stiffened panel." A cross-stiffened panel is termed a "grillage," which in concept is essentially a set of intersecting beam members. When a one-dimensional strength member is predominantly subjected to axial compression, it is called a "column," whereas it is termed a "beam" when subjected to lateral loads or

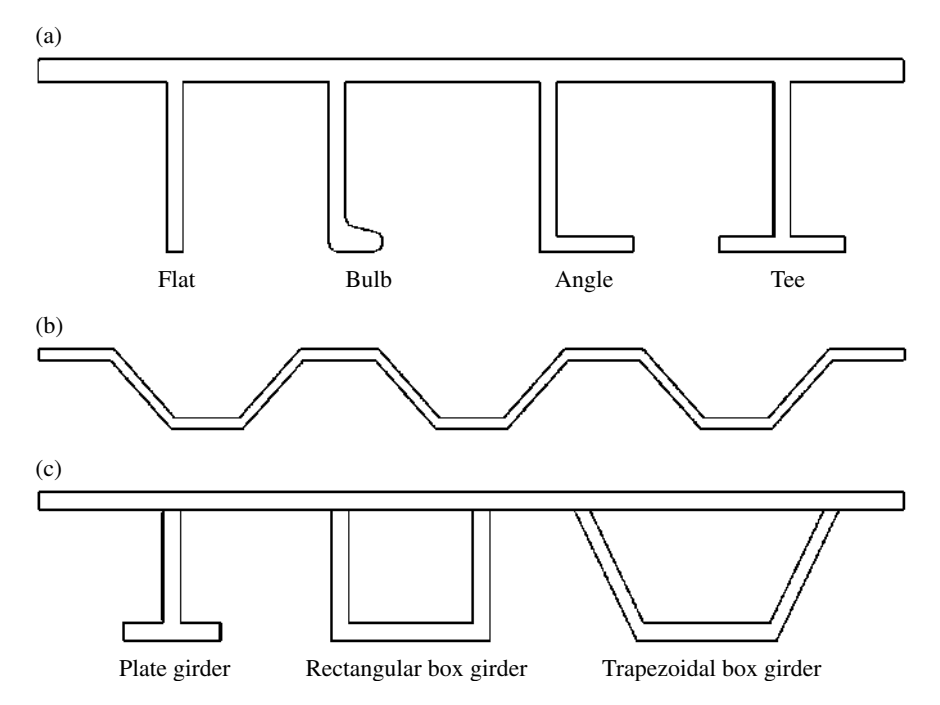


Figure 1.23 (a) Various types of beam members (stiffeners); (b) a self-stiffened plate-corrugated panel; (c) various types of strong main support members.

0003369274.3D 40 24/1/2018 10:48:03 AM

bending. A one-dimensional strength member under combined axial compression and bending is called a "beam–column." When the strength member is subjected to combined bending and axial tension, it is called a "tension-beam."

Strong main support members are normally called "(longitudinal) girders" when they are located in the primary loading direction (i.e., the longitudinal direction in a box girder or a ship hull girder), whereas they are sometimes called "(transverse) frames" or main support members when they are located in a direction orthogonal to the primary load direction (i.e., in the transverse direction in a box girder or a ship hull girder).

For strength analysis of plated structures, stiffeners or some support members together with their associated plating are often modeled as beams, columns, or beam—columns, as described in Chapter 2.

1.5 Types of Loads

The terminology related to the classification of applied loads for ships and offshore structures is similar to that used for land-based structures. The types of loads to which plated structures or strength members are likely to be subjected may be categorized into the following four groups:

- Dead loads
- · Operational or service (live) loads
- Environmental loads
- Accidental loads

Dead loads (also called permanent loads) are time-independent, gravity-dominated service loads. Examples of dead loads are the weight of structures or permanent items that remain in place throughout the life of the structure. Dead loads are typically static and can usually be determined accurately even if the weight of some of the items may in some cases be unknown until the structural design has been completed.

Operational or service loads are typically live loads by nature with gravity and/or thermal loads that vary in magnitude and location during the normal operation of the structure. Operational loads can be quasistatic, dynamic, or even impulsive in loading speed. Examples of operational loads are the weight of people, furniture, movable equipment, wheel loads from vehicles or cargoes, and stored consumable goods. In marine structures, pressure loads due to water and cargoes and thermal loads due to cargoes (e.g., liquefied petroleum gas, liquefied natural gas) are also examples of operational loads. In the design of land-based box girder bridges, highway vehicle loading is usually separately classified under highway live loads. Although some live loads (e.g., persons and furniture) are practically permanent and static, others (e.g., box girder cranes and various types of machinery) are highly time dependent and dynamic. Because the magnitude, location, and density of live load items are generally unknown in a particular case, the determination of operational loads for design purposes is not straightforward. For this reason, regulatory bodies sometimes prescribe design service loads based on experience and proven practice.

0003369274.3D 41 24/1/2018 10:48:04 AM

Environmental loads are actions related to wind, current, waves, snow, and earthquake. Most environmental loads are time dependent and repeated in some fashion, that is, cyclic. Environmental loads can thus be quasistatic, dynamic, or even impulsive in loading speed. The determination of design environmental loads is often specified by regulatory bodies or classification society rules, typically using the concept of a mean return period. The design loads of snow or wind, for instance, may be specified based on a return period of 100 years or longer, indicating that extreme snowfall or wind velocity that is expected to occur once in 100 years is used in the design.

Accidental loads are actions that arise from accidents such as collision, grounding, fire, explosion, or dropped objects. Accidental loads typically have a dynamic or impact effect on structural behavior with large strains. Guidelines to predict and account for accidental loads are more meager because of the unknown nature of accidents. However, it is important to treat such loads in design, particularly when novel types of structures are involved, about which experience may be lacking. This often happens in the offshore field, where several new types of structures have been introduced in recent decades. Experimental databases in a full-scale prototype or at least large-scale models are highly required to characterize and quantify the nonlinear mechanics of structures exposed to accidental conditions, as scaling laws to convert small-scale model test results to the actual full-scale structure are not always available.

The maxima of the various types of loads mentioned previously are not always applied simultaneously, but more than one type of load normally may coexist and interact. Therefore, the structural design must account for the effects of phasing for definition of the combined loads. Usually, this involves the consideration of multiple load combinations for design, each representing a load at its extreme value together with the accompanying values of other loads. The guidelines for relevant combinations of loads to be considered in design are usually specified by regulatory bodies or classification societies for particular types of structures.

1.6 Basic Types of Structural Failure

This book is concerned with the fundamentals and practical procedures for the ULS analysis and design of steel- and aluminum-plated structures. One primary task in ULS design is to determine the level of imposed loads that cause the structural failure of individual members and the overall structure. Therefore, it is crucial to better understand what types of structural failure can primarily occur. The failure of plated structures made of ductile materials is normally related to one or both of the following nonlinear types of behavior:

- Geometric nonlinearity associated with buckling or large deflection
- Material nonlinearity due to yielding or plastic deformation

For structural members, many basic types of failure are considered, the more important of which include:

- Buckling or instability
- Plasticity in local regions
- Fatigue cracking related to cyclic loading

0003369274.3D 42 24/1/2018 10:48:04 AM

- Ductile or brittle fracture, given fatigue cracking or preexisting defects
- Excessive deformations

The basic failure types mentioned previously do not always occur simultaneously, but more than one phenomenon may in principle be involved until the structure reaches the ULS. For convenience, the basic types of structural failure noted previously are sometimes described and treated separately.

As the external loads increase, the most highly stressed region inside a structural member will yield first, resulting in local plastic deformation, which decreases the member stiffness. With a further increase in the load, local plastic deformation will increase and/or occur at several different regions. The stiffness of the member with large local plastic regions becomes quite low, and the displacements increase rapidly, eventually becoming so large that the member is considered to have failed.

Buckling or instability can occur in any structural member that is predominantly subjected to load sets that result in compressive effects in the structure. In buckling-related design, two types of buckling are considered, bifurcation and non-bifurcation. The former type is seen for an ideal perfect member without initial imperfections, and the latter typically occurs in an actual member with some initial imperfections. For instance, a straight elastic column has an alternative equilibrium position at a critical axial compressive load that causes a bent shape to suddenly occur at a certain value of the applied load. This threshold load, which separates into two different equilibrium conditions, is called a bifurcation load.

An initially deflected column or beam—column induces bending from the beginning of the loading contrary to the straight column, and the lateral deflection increases progressively. The member stiffness is reduced by considerable deflection and local yielding, and it eventually becomes zero at a peak load. The deflection of the member with very low or zero stiffness becomes so great that the member is considered to have collapsed. In this case, an obvious sudden buckling point does not appear until the member collapses; this type of failure is called non-bifurcation instability or limit-load buckling (Galambos 1988).

Due to repeated fluctuation of loading, fatigue cracking can initiate and propagate in the structure's stress concentration areas. Fracture is a type of structural failure caused by the rapid extension of cracks. Three types of fracture are relevant, brittle fracture, rupture, and ductile fracture. Brittle fracture normally takes place at a very small strain in materials with a low toughness or below a certain temperature, when the material's ultimate tensile strength diminishes sharply. For materials with a very high toughness, rupture occurs at a very large strain by necking of the member, typically at room temperature or higher. Ductile fracture is an intermediate fracture mode between brittle fracture and rupture. In steels or aluminum alloys, the tendency to fracture is related not only to the temperature but also to the rate at which loading is applied. The higher the loading rate, the greater the tendency toward brittle fracture.

1.7 Fabrication Related Initial Imperfections

Welded metal structures always have initial imperfections in the form of initial distortions, residual stresses, or softening in the weld fusion zone or HAZ. Because such fabrication related initial imperfections may affect the structural properties and

0003369274.3D 43 24/1/2018 10:48:04 AM

load-carrying capacities of structures, they must be dealt with as parameters of influence in structural analysis and design.

1.7.1 Mechanism of Initial Imperfections

When local heating is input to structural material, the heated part will expand, but because of adjacent cold parts, it will be subjected to compressive stress and distortion. When the heated part cools, it will locally shrink rather than revert to its initial shape and will thus be subjected to tensile stress. The strength of welded aluminum alloys in the HAZ is reduced by softening phenomenon in that melting temperature is reduced by improving fluidity, while it is recognized that the material strength in the softened zone is recovered by natural aging over a period of time (Lancaster 2003).

Experimental studies to examine the mechanism of initial imperfections have been undertaken in the literature with direct measurements of welding induced initial imperfections: Masubuchi (1980), Smith et al. (1988), Ueda (1999), and Paik and Yi (2016) for initial distortions of steel-plated structures; Paik et al. (2006), Paik (2007c, 2008), and Paik et al. (2008, 2012) for initial distortions of aluminum-plated structures; Masubuchi (1980), Smith et al. (1988), Cheng et al. (1996), Ueda (1999), Kenno et al. (2010, 2017), and Paik and Yi (2016) for residual stresses of steel-plated structures; and Paik et al. (2006), Paik (2008), and Paik et al. (2008, 2012) for residual stresses and softening of aluminum-plated structures, among others.

Based on the insights available in the literature, it is recognized that various types of welding induced distortions are relevant, as shown in Figure 1.24. In practice for the evaluation of structural capacity, both angular change and longitudinal bending distortion are of greater concern, as shown in Figure 1.24e, whereas the shrinkage in the longitudinal or transverse directions may often be neglected. Also, residual stress distributions in welded structural members represent the tensile residual stresses that develop in the HAZ and the compressive residual stresses that must then also exist to achieve self-equilibrium in the plane of the structural member, as shown in Figure 1.25. In welded aluminum structures with extruded stiffeners, residual stresses are developed as those shown in Figure 1.26. The breadth of the softened zone in welded aluminum structures almost equals that of the HAZ, as shown in Figure 1.27.

Figure 1.28 shows experimental and finite element method investigations of welding induced initial distortions and residual stresses in full-scale welded steel-stiffened plate structure models, obtained by Paik and Yi (2016) using modern technologies of the fabrication and measurements. Figure 1.29 shows experimental investigations of welding induced initial distortions and residual stresses in full-scale fusion-welded aluminum-stiffened plate structure models, obtained by Paik (2008).

1.7.2 Initial Distortion Modeling

Figure 1.30 shows some typical initial deflection shapes of welded one-dimensional members and their possible idealizations. For practical design purposes, the initial deflection shape of a welded one-dimensional member may be idealized as the dotted

0003369274.3D 44 24/1/2018 10:48:04 AM

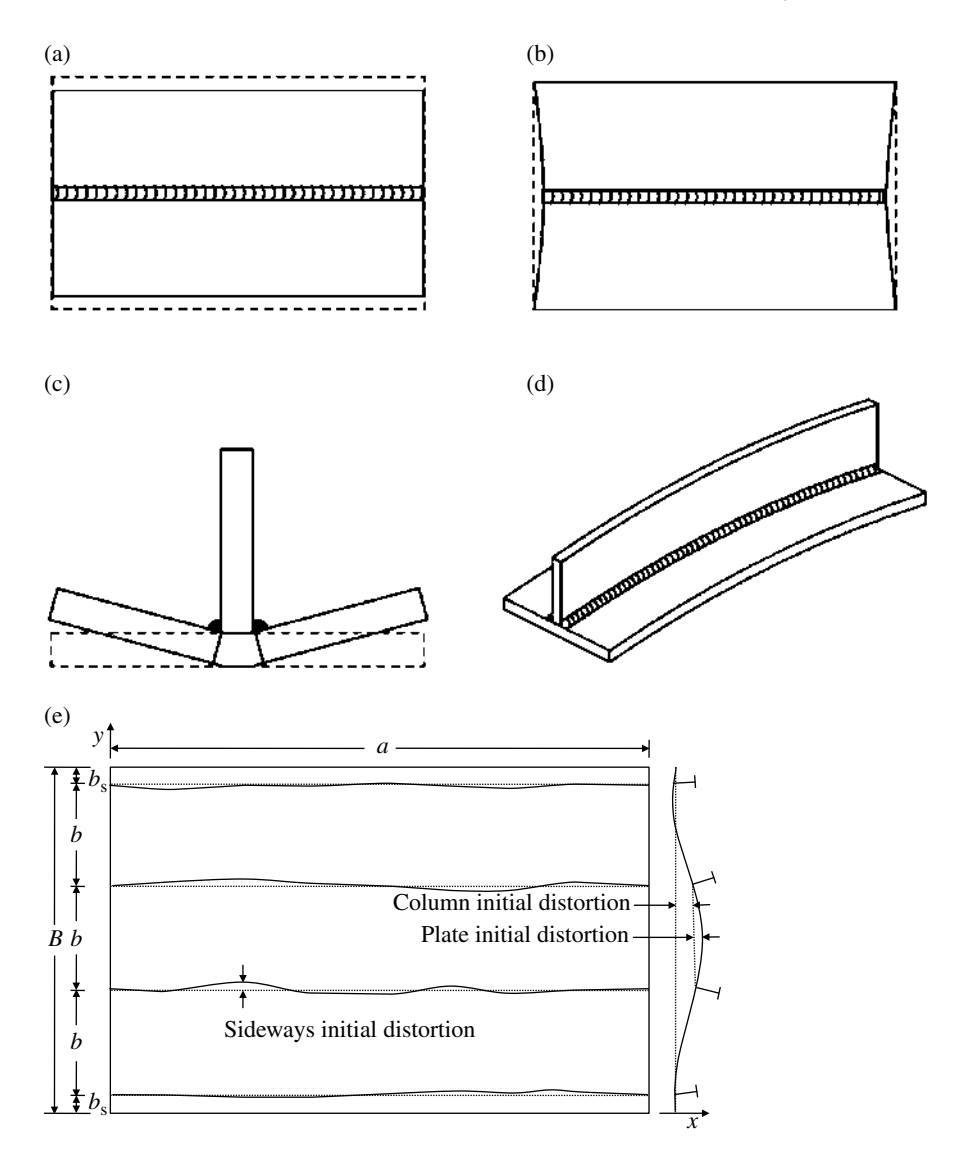


Figure 1.24 Types of welding induced initial distortions in a stiffened plate structure: (a) transverse shrinkage; (b) longitudinal shrinkage; (c) angular change; (d) longitudinal bending distortion; (e) three typical distortions.

line in Figure 1.30, which can be expressed approximately in mathematical form as follows:

$$w_0 = \delta_0 \sin \frac{\pi x}{L} \tag{1.32}$$

where w_0 is the initial deflection function; δ_0 is the initial deflection amplitude, which is often taken as 0.0015L for a practical strength calculation at an "average" level of imperfections; and L is the member length between supports.

0003369274.3D 45 24/1/2018 10:48:04 AM

46 Ultimate Limit State Analysis and Design of Plated Structures

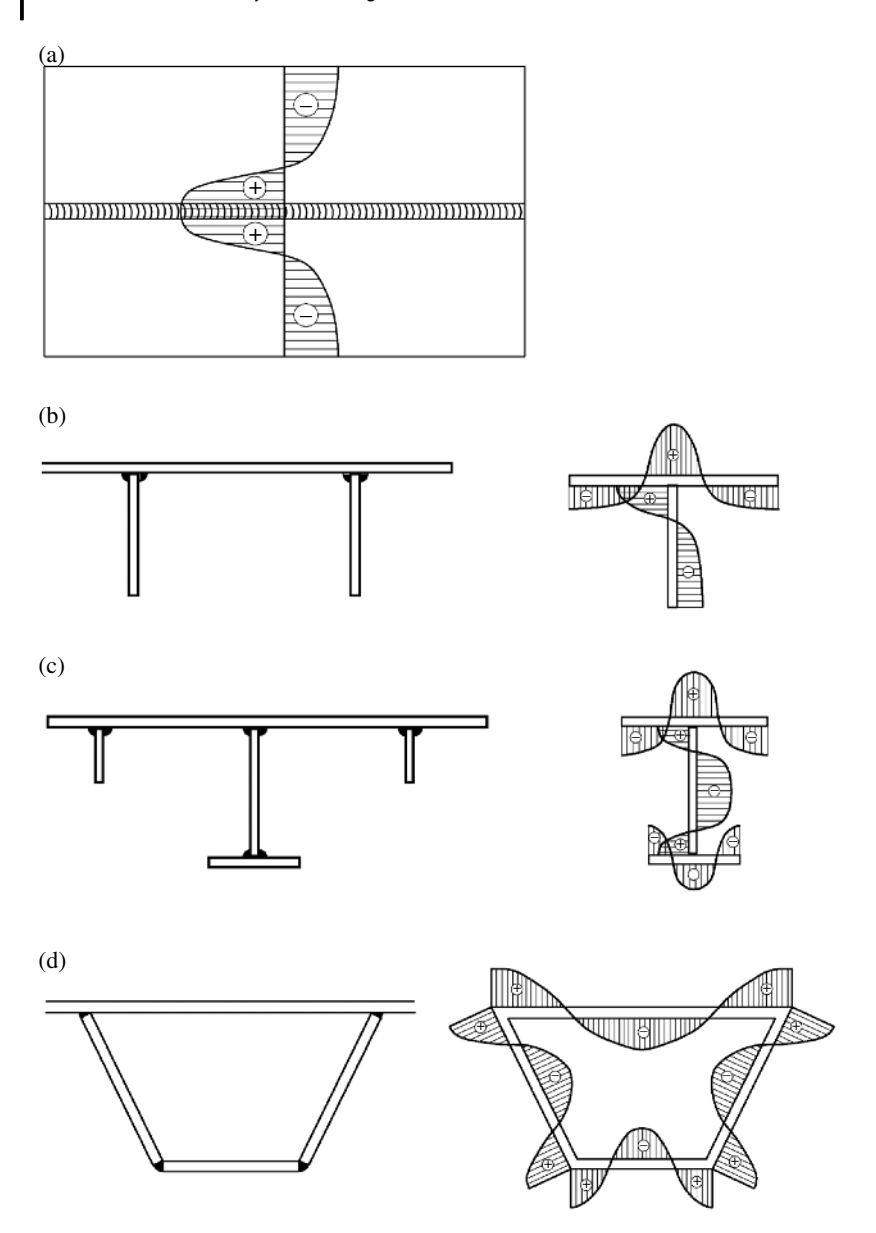


Figure 1.25 Distribution of the welding induced residual stresses in a stiffened plate structure: (a) buttwelded plate; (b) welded stiffened panel; (c) welded plate girder; (d) welded box section.

For welded stiffened plate structures, three types of initial distortions are relevant to welded metal-stiffened plate structures, as illustrated in Figure 1.31:

- \bullet The initial deflection $w_{0\mathrm{pl}}$ of the plating between the support members
- ullet The column-type initial deflection w_{0c} of the support members
- The sideways initial deflection w_{0s} of the support members

0003369274.3D 46 24/1/2018 10:48:04 AM

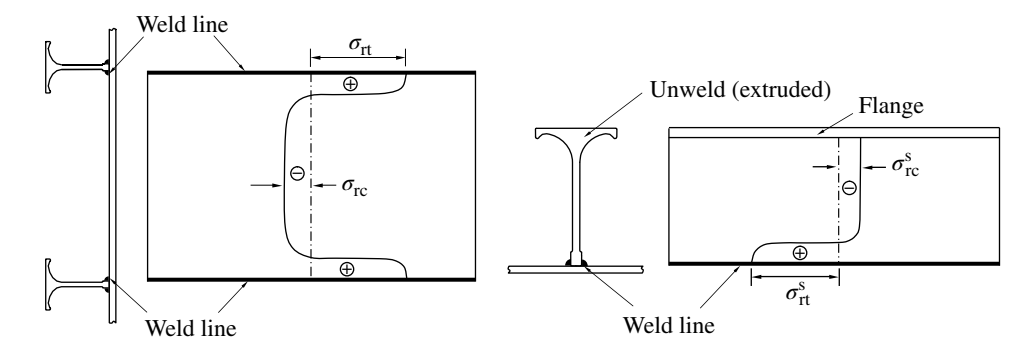


Figure 1.26 Distribution of the welding induced residual stresses in an aluminum plate welded at two edges and a stiffener web welded at one edge (+, tension, –, compression; left, plating, right, extruded stiffener web) (Paik et al. 2012, Hughes & Paik 2013).

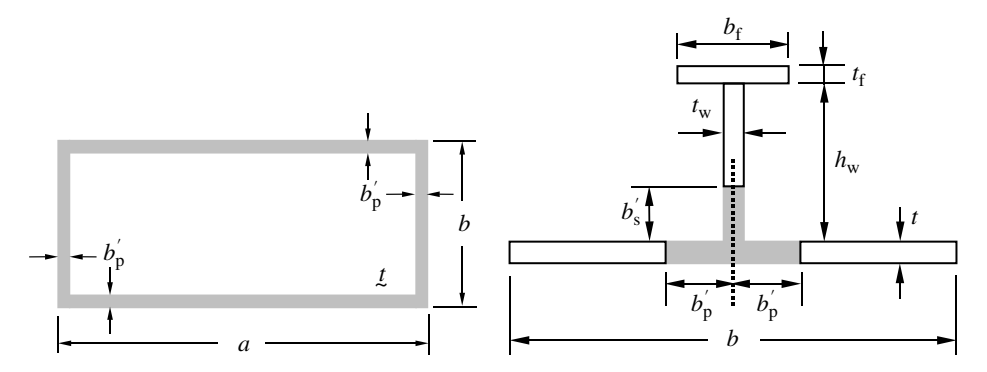


Figure 1.27 Breadths of the softening zones inside an aluminum plate welded at four edges and its counterpart in the extruded stiffener attachment to the plating (Hughes & Paik 2013).

The magnitude and shape of each type of initial distortion play important roles in buckling collapse behavior, and thus a better understanding of the actual imperfection configurations in the target structures is necessary (Paik et al. 2004). In fact, it is desirable to obtain precise information about the initial distortions of the target structure before structural modeling even begins. Considering the significant amount of uncertainty involved in fabrication related initial imperfections, existing measurements of the initial distortions in welded metal structures are often useful for the development of representative models.

1.7.2.1 Plate Initial Deflection

The shape of welding induced initial deflections for thin plates after support members are attached by welding is quite complex. The initial deflection of plating between stiffeners can be expressed as a Fourier series function as follows:

$$\frac{w_0}{w_{0pl}} = \sum_{i=1}^{M} \sum_{j=1}^{N} B_{0ij} \sin \frac{i\pi x}{a} \sin \frac{j\pi y}{b}$$
 (1.33)

0003369274.3D 47 24/1/2018 10:48:05 AM







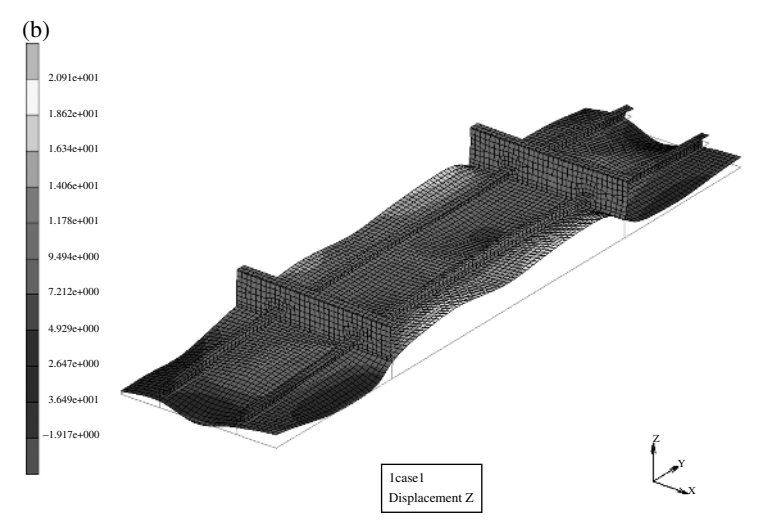
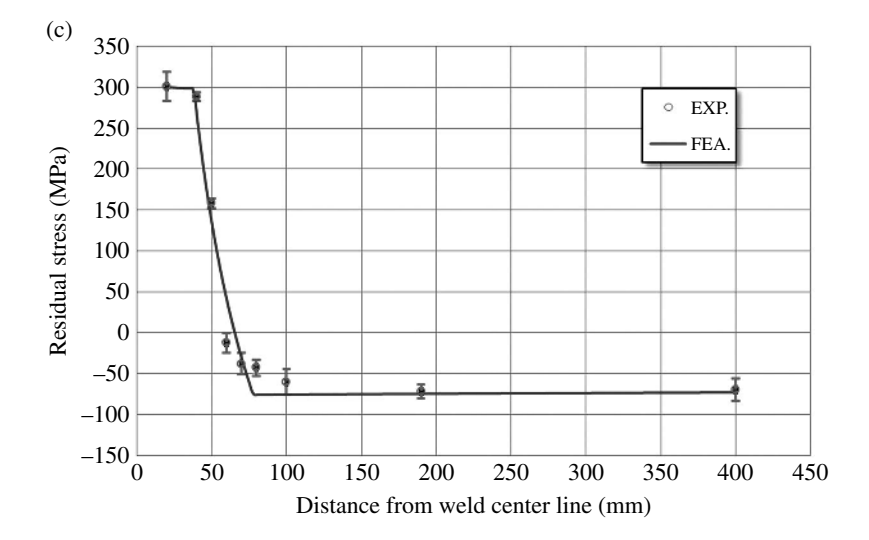


Figure 1.28 (a) Full-scale testing of initial imperfections in steel-stiffened plate structure models: (a) left: fabrication by auto flux-cored arc welding; right: three-dimensional scanning measurement of initial distortions; below: nondestructive measuring technique of welding induced residual stresses; (b) measurement of the welding induced initial distortions; (c) measurement and finite element method prediction of the welding induced residual stresses in the longitudinal stiffener direction; (d) measurement and finite element method prediction of the welding induced residual stresses in the transverse frame direction (Paik & Yi 2016).

0003369274.3D 48 24/1/2018 10:48:05 AM



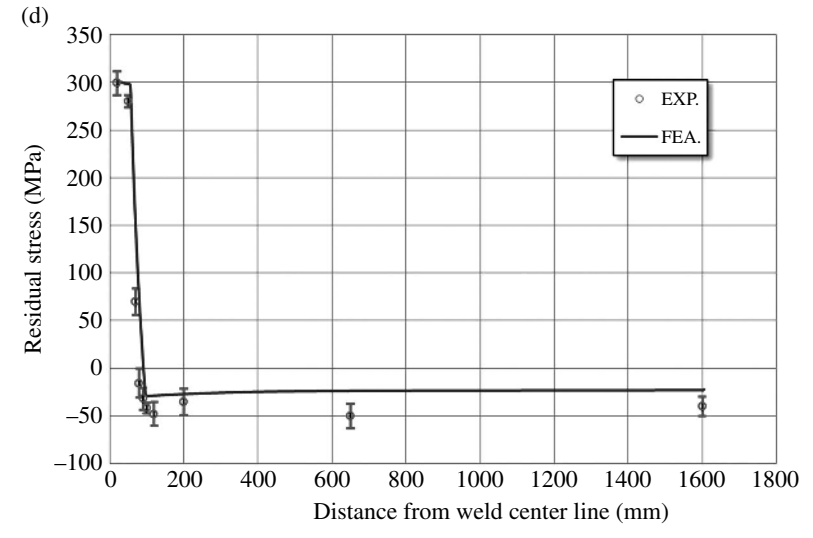


Figure 1.28 (Continued)

where a is the plate length and b is the plate breadth. B_{0ij} indicates the welding induced initial deflection amplitude normalized by the maximum initial deflection, w_{0pl} , which can be determined on the basis of the initial deflection measurements. The subscripts i and j denote the corresponding half-wave numbers in the x and y directions, respectively.

If measured databases for the initial deflection for plating are available, the initial deflection amplitudes of Equation (1.33) can be determined by expanding Equation (1.33) appropriately using a selected number of terms, M and N, depending on the complexity of the initial deflection shape.

For practical design purposes, further idealization may sometimes be necessary. The measurements of the initial deflection for plate elements in plated structures show that a

0003369274.3D 49 24/1/2018 10:48:06 AM

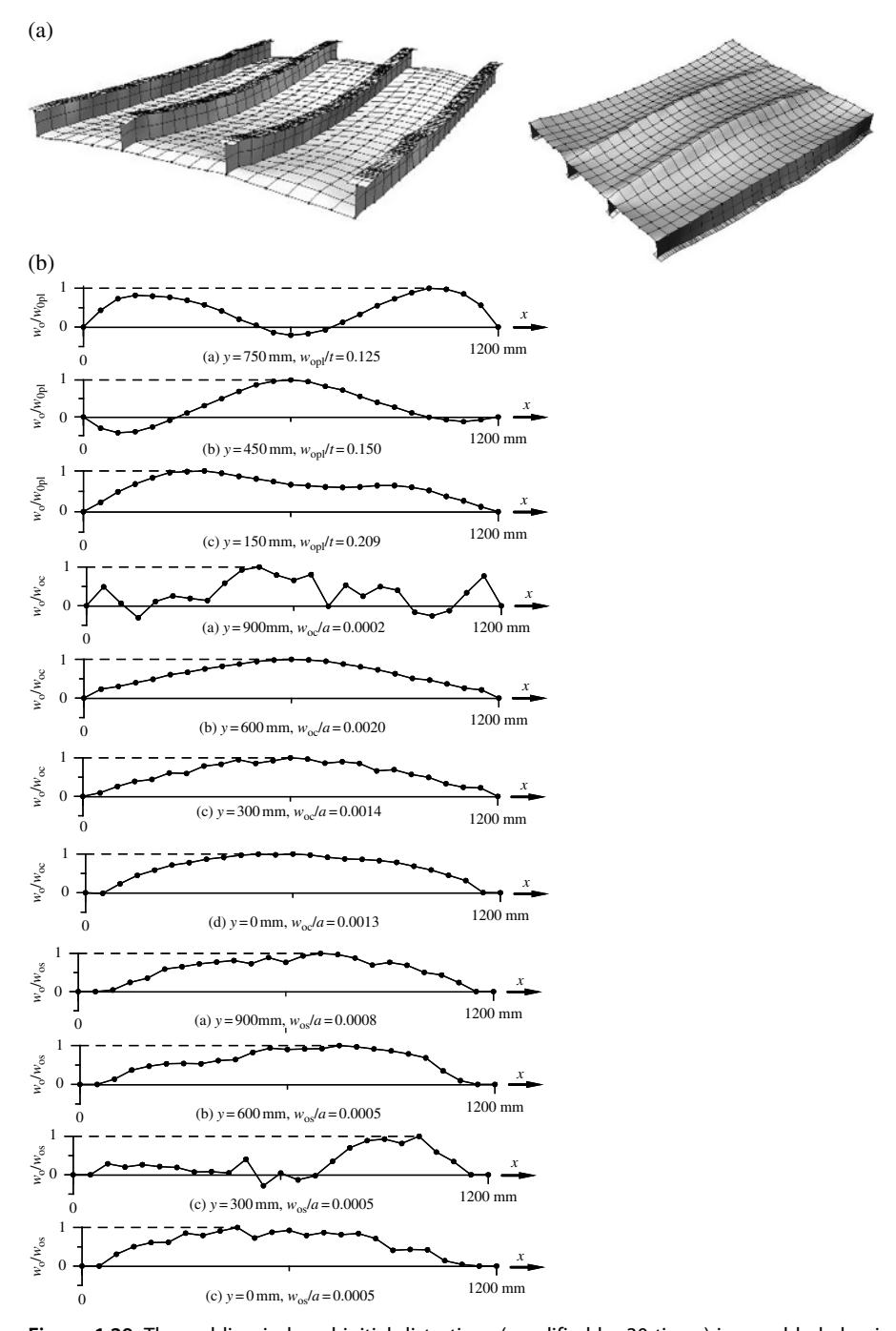


Figure 1.29 The welding induced initial distortions (amplified by 30 times) in a welded aluminum-stiffened plate structure: (a) shape of initial distortions (amplified by 30 times); (b) measurement of initial distortions (w_{0pl} = plate initial deflection; w_{0c} = column-type initial distortion of stiffener; w_{0s} = sideways initial distortion of stiffener); (c) measurement of residual stresses (Paik 2008).

0003369274.3D 50 24/1/2018 10:48:06 AM

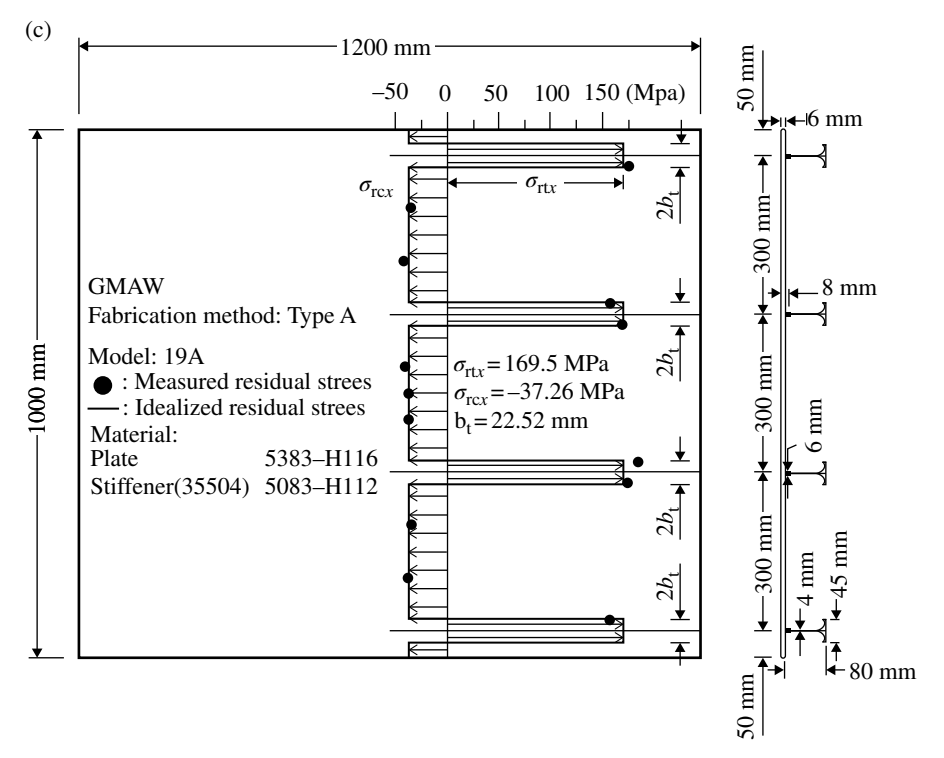
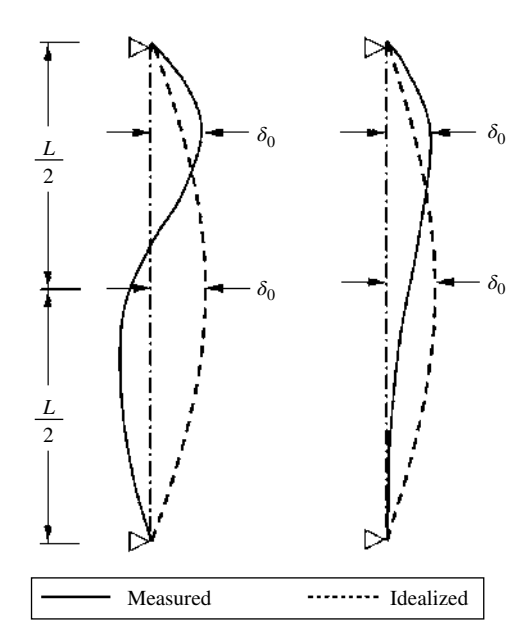


Figure 1.29 (Continued)

Figure 1.30 Idealization of initial deflection shapes for welded one-dimensional members.



0003369274.3D 51 24/1/2018 10:48:07 AM

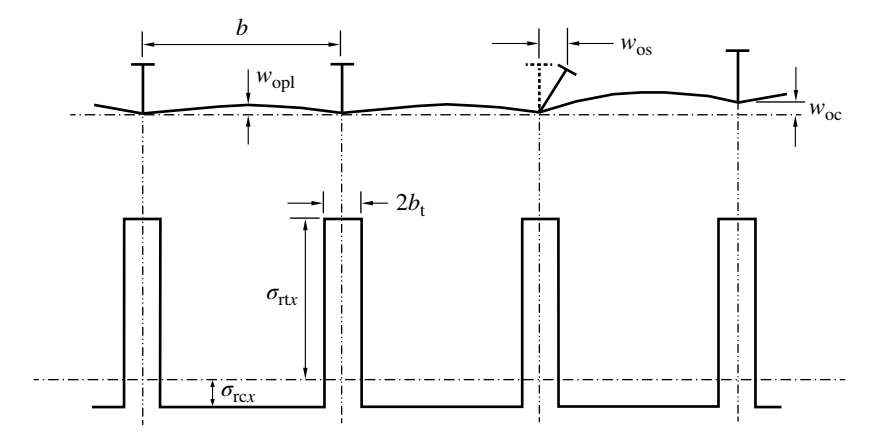


Figure 1.31 Three types of the welding induced initial distortions and residual stresses in a stiffened plate structure.

multiple-wave shape is predominant in the long direction, as shown in Figure 1.32, whereas one half wave is found in the short direction, as shown in Figure 1.31.

For a nearly square plate element, therefore, Equation (1.33) may be simplified by taking M = N = 1. For a long plate element with a multiple-wave shape in the x direction and one half wave in the y direction, Equation (1.33) becomes

$$\frac{w_0}{w_{0pl}} = \sum_{i=1}^{M} B_{0i} \sin \frac{i\pi x}{a} \sin \frac{\pi y}{b}$$
 (1.34)

In practice, M in Equation (1.34) may be taken as an integer that corresponds to about three or more times the a/b ratio greater than 1 (Paik & Pedersen 1996). On this basis, B_{0i} in Equation (1.34) can be determined for the assumed M if the initial deflection measurements are available. The values of coefficients, B_{0i} , for the initial deflection shapes shown in Figure 1.32 are given in Table 1.6, by taking M = 11.

In current industry practice with regard to practical structural design and strength assessment, an average magnitude is assumed for these initial distortions, and their shape is assumed to be the buckling mode, because this shape usually has the most unfavorable consequences for the structure until and after the ULS is reached. The amplitude or maximum magnitude $w_{0\text{pl}}$ of plate initial deflection w_0^{p} is often assumed to be the following:

$$w_0^{\rm p} = w_{\rm 0pl} \sin \frac{m\pi x}{a} \sin \frac{\pi y}{b} \tag{1.35a}$$

$$w_{0pl} = C_1 b \tag{1.35b}$$

$$w_{\rm 0pl} = C_2 \beta^2 t \tag{1.35c}$$

where w_0^p is the plate's initial deflection function, w_{0pl} is the maximum magnitude of plate initial deflection, b is the plate breadth along the short edge or the spacing between the

0003369274.3D 52 24/1/2018 10:48:07 AM

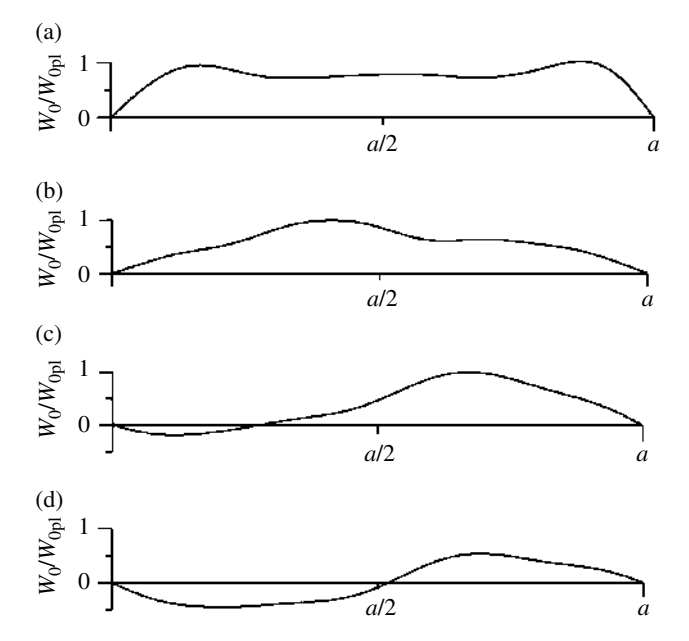


Figure 1.32 Some typical initial deflection patterns in welded plating between stiffeners in the long (plate length) direction (Paik & Pedersen 1996): initial deflection shape (a) 1; (b) 2; (c) 3 and (d) 4.

longitudinal stiffeners, t is the plate thickness, $\beta = (b/t)\sqrt{\sigma_Y/E}$ is the plate slenderness ratio, E is the material's elastic modulus, σ_Y is the yield strength, C_1 and C_2 are constants, and *m* is the buckling half-wave number of the plate.

It is interesting to note that the two alternative formulations, that is, Equations (1.35b) and (1.35c), have different usage backgrounds. Equation (1.35b), supported by some classification societies, states that w_{0pl} is a function only of the plate breadth, whereas Smith et al. (1988) suggested that Equation (1.35c) gives a more precise representation of the plate characteristics because it is a function of the plate slenderness ratio.

In addition, the use of Equation (1.35b) may result in too small initial deflection for very thin plates and too large initial deflection for very thick plates. Equation (1.35c), in contrast, is suitable for both very thin and very thick plates. Nevertheless, the use of Equation (1.35b) remains more popular today in the construction of ships and offshore structures, as long as a moderate plate thickness is considered. This is partly because Equation (1.35b) is more suitable to specify construction tolerances regardless of the slenderness ratio-related characteristics of the plating.

The constants in Equations (1.35b) and (1.35c) may be determined on the basis of statistical analyses of the initial deflection measurements of the welded steel or aluminum plates. The following provides some additional guidance:

 $C_1 = 0.005$ for an average level in steel plates

$$C_1 = \left\{ \begin{array}{l} 0.0032 \;\; \text{for a slight level} \\ 0.0127 \;\; \text{for an average level} \\ 0.0290 \;\; \text{for a severe level} \end{array} \right\} \; \text{in aluminum plates (Paik 2007c)}$$

0003369274.3D 53 24/1/2018 10:48:07 AM

Table 1.6 Initial deflection amplitudes of Equation (1.35a) for various initial deflection shapes indicated in Figure 1.32.

Initial deflection shape	B ₀₁	B ₀₂	B_{03}	B ₀₄	B_{05}	B_{06}	B ₀₇	B_{08}	B ₀₉	B ₀₁₀	B ₀₁₁
1	1.0	-0.0235	0.3837	-0.0259	0.2127	-0.0371	0.0478	-0.0201	0.0010	-0.0090	0.0005
2	0.8807	0.0643	0.0344	-0.1056	0.0183	0.0480	0.0150	-0.0101	0.0082	0.0001	-0.0103
3	0.5500	-0.4966	0.0021	0.0213	-0.0600	-0.0403	0.0228	-0.0089	-0.0010	-0.0057	-0.0007
4	0.0	-0.4966	0.0021	0.0213	-0.0600	-0.0403	0.0228	-0.0089	-0.0010	-0.0057	-0.0007

0003369274.3D 54 24/1/2018 10:48:08 AM

$$C_2 = \left\{ \begin{array}{ll} 0.025 & \text{for a slight level} \\ 0.1 & \text{for an average level} \\ 0.3 & \text{for a severe level} \end{array} \right\} \text{ in steel plates (Smith et al. 1988)}$$

$$C_2 = \begin{cases} 0.018 & \text{for a slight level} \\ 0.096 & \text{for an average level} \\ 0.252 & \text{for a severe level} \end{cases}$$
 in aluminum plates (Paik et al. 2006)

To determine the shape of the buckling mode initial distortions, eigenvalue computations are required. Based on these eigenvalue computations, the buckling modes of the stiffened plate structures can then be decomposed into the three types of initial distortions mentioned previously. Each type of initial distortion should be amplified up to the maximum target value, and the three resulting patterns should then be superimposed to provide a complete picture of the initial distortions. It is worthwhile to discuss here the classical theory of structural mechanics, which gives the buckling half-wave number of a simply supported plate element under longitudinal compression alone. This number is predicted as the minimum integer that satisfies the following condition, as described in Chapter 3 or 4:

$$\frac{a}{b} \le \sqrt{m(m+1)} \tag{1.36a}$$

where *m* is the number of buckling half waves of the plate in the longitudinal direction, whereas the number in the transverse direction is assumed to be unity.

The plate buckling half-wave number can then be determined under any combination of longitudinal compression σ_x and transverse compression σ_y , again as a minimum integer, but satisfying the following condition as described in Chapter 3 or 4:

$$\frac{\left(m^2/a^2 + 1/b^2\right)^2}{m^2/a^2 + c/b^2} \le \frac{\left[\left(m+1\right)^2/a^2 + 1/b^2\right]^2}{\left(m+1\right)^2/a^2 + c/b^2} \tag{1.36b}$$

where $c = \sigma_y / \sigma_x$ is the loading ratio. When c = 0, that is, under longitudinal compression alone, Equation (1.36b) simplifies to Equation (1.36a).

Classification societies or other regulatory bodies specify construction tolerances for strength members as related to the maximum initial deflection with the intention that the initial distortions in the fabricated structure must be less than the corresponding specified values. Some examples of the limit for the maximum plate initial deflection are as follows:

• NORSOK (2004):

$$\frac{w_{0\text{pl}}}{h} \le 0.01$$

• Japanese shipbuilding quality standards (JSQS 1985):

 $w_{0pl} \le 7 \,\mathrm{mm}$ for bottom plate $w_{0pl} \le 6$ mm for deck plate

• Steel box girder bridge quality standards (ECCS 1982):

$$w_{0\text{pl}} \le \min\left(\frac{t}{6} + 2, \frac{t}{3}\right), \quad t \text{ in mm}$$

0003369274.3D 55 24/1/2018 10:48:08 AM Related to this, it is of interest to note that quite often, specifications of quality to be achieved are developed (and used) without specific reference to the loads and load effects at a particular location. In that case, the corresponding specifications suggest what can be generally achieved in an economical way rather than what should be achieved in the context of a particular situation.

1.7.2.2 Column-Type Initial Deflection of a Stiffener

The column-type initial distortion of stiffeners is assumed as follows:

$$w_0^c = w_{0c} \sin \frac{\pi x}{a} \tag{1.37a}$$

$$w_{0c} = C_3 a \tag{1.37b}$$

where w_0^c is the column-type initial distortion of the support members, a is the length of the small stiffeners between two adjacent strong support members, and C_3 is a constant. The constant in Equation (1.37b) may be taken as follows:

 $C_3 = 0.0015$ for an average level in steel plates

$$C_3 = \begin{cases} 0.00016 & \text{for a slight level} \\ 0.0018 & \text{for an average level} \\ 0.0056 & \text{for a severe level} \end{cases}$$
 in aluminum plates (Paik et al. 2006)

1.7.2.3 Sideways Initial Distortion of a Stiffener

The sideways initial distortion of stiffeners is assumed as follows:

$$w_0^{\rm S} = w_{0\rm S} \frac{z}{h_{\rm tot}} \sin\frac{\pi x}{a} \tag{1.38a}$$

$$w_{0s} = C_4 a \tag{1.38b}$$

where w_0^s is the sideways initial distortion of the support member, z is the coordinate in the direction of stiffener web height, h_w is the stiffener web height, a is the length of the small stiffeners between two adjacent strong support members, and C_4 is a constant. The constant in Equation (1.38b) may be taken as follows:

 $C_4 = 0.0015$ for an average level in steel plates

$$C_4 = \begin{cases} 0.00019 & \text{for a slight level} \\ 0.001 & \text{for an average level} \\ 0.0024 & \text{for a severe level} \end{cases}$$
 in aluminum plates (Paik et al. 2006)

1.7.3 Welding Residual Stress Modeling

For practical design purposes, the welding residual stress distributions of a plate element between support members for which welding has been carried out along all four edges may be idealized to be composed of tensile and compressive stress blocks, such as those shown in Figure 1.33. Among them, Figure 1.33c is a typical idealization of the welding residual stress distribution in a plate element.

0003369274.3D 56 24/1/2018 10:48:08 AM

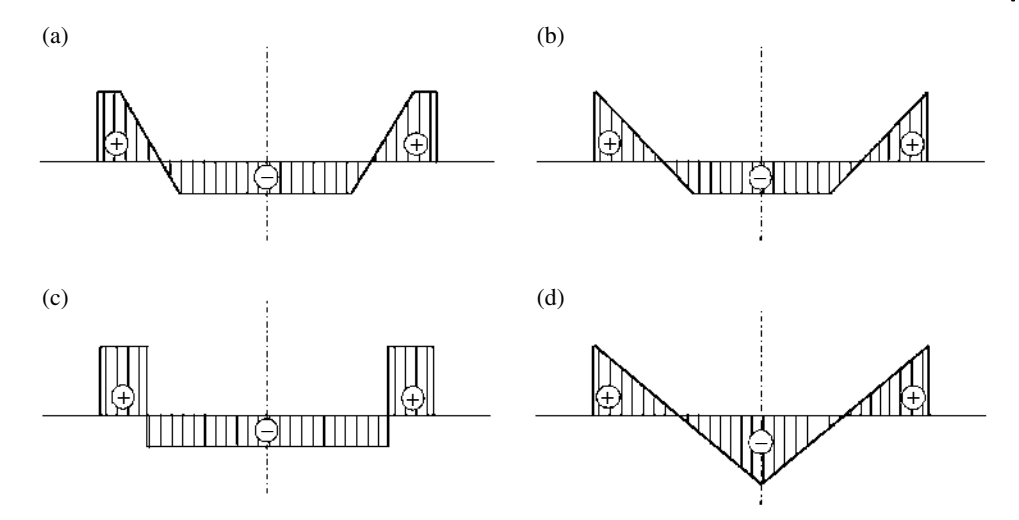


Figure 1.33 Idealized distributions of the welding induced residual stresses in a stiffened plate structure.

Welding residual stresses develop in both longitudinal and transverse directions if the support members are attached by welding in these two directions as shown in Figure 1.34. The breadth of the HAZ is denoted by b_t in the y direction or a_t in the x direction in which the residual stress in the HAZ is approximately equal to the tensile yield stress because the molten metal can expand freely, as a liquid, whereas after welding it quickly reverts to a solid and the shrinkage that occurs during cooling involves "plastic flow."

Along the welding line, tensile residual stresses usually develop with magnitude $\sigma_{\rm rtx}$ in the x direction and $\sigma_{\rm rty}$ in the y direction, with the welding being normally performed in

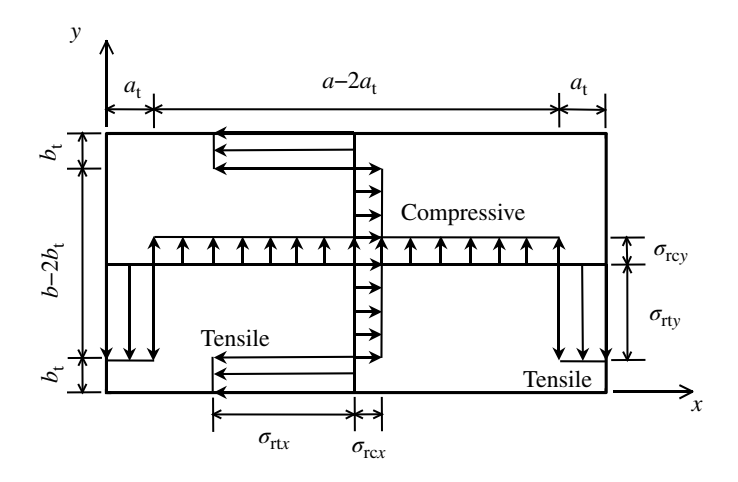


Figure 1.34 Typical idealization of the welding induced residual stress distribution inside the metal plate element in the x and y directions.

0003369274.3D 57 24/1/2018 10:48:08 AM

both x and y directions. To obtain equilibrium, corresponding compressive residual stresses with magnitude σ_{rcx} in the x direction and σ_{rcy} in the y direction develop in the middle part of the plate element.

As the tensile residual stress blocks are equivalent to the HAZ, their breadths can be estimated from the equilibrium between the tensile and compressive residual stresses as follows:

$$2b_{t} = \frac{\sigma_{rcx}}{\sigma_{rcx} - \sigma_{rtx}}b, \quad 2a_{t} = \frac{\sigma_{rcy}}{\sigma_{rcy} - \sigma_{rty}}a$$
(1.39)

where b_t and a_t are the breadths of the tensile residual stress block, σ_{rcx} and σ_{rcy} are the compressive residual stresses in the x or y directions, and $\sigma_{\text{rt}x}$ and $\sigma_{\text{rt}y}$ are the tensile residual stresses in the *x* or *y* directions.

One can then define the residual stress distributions in the x and y directions as follows:

$$\sigma_{rx} = \begin{cases} \sigma_{rtx} & \text{for } 0 \le y < b_t \\ \sigma_{rcx} & \text{for } b_t \le y < b - b_t \\ \sigma_{rtx} & \text{for } b - b_t \le y \le b \end{cases}$$

$$\sigma_{ry} = \begin{cases} \sigma_{rty} & \text{for } 0 \le x < a_t \\ \sigma_{rcy} & \text{for } a_t \le x < a - a_t \\ \sigma_{rty} & \text{for } a - a_t \le x \le a \end{cases}$$

$$(1.40a)$$

$$\sigma_{\text{ry}} = \begin{cases} \sigma_{\text{rty}} & \text{for } 0 \le x < a_{\text{t}} \\ \sigma_{\text{rcy}} & \text{for } a_{\text{t}} \le x < a - a_{\text{t}} \\ \sigma_{\text{rty}} & \text{for } a - a_{\text{t}} \le x \le a \end{cases}$$

$$(1.40b)$$

Smith et al. (1988) suggested the following formula to define the compressive residual stress σ_{rcx} in the x direction of a steel plate:

$$\sigma_{rcx} = \begin{cases} -0.05\sigma_Y & \text{for a slight level} \\ -0.15\sigma_Y & \text{for an average level} \\ -0.3\sigma_Y & \text{for a severe level} \end{cases}$$
 (1.41a)

The counterpart of the compressive residual stress σ_{rcy} in the y direction may be assumed to be as follows:

$$\sigma_{\text{rcy}} = k \frac{b}{a} \sigma_{\text{rcx}} \tag{1.41b}$$

where *k* is a correction factor, which may take a value smaller than 1.0. When the residual stress is considered in the x direction alone, k = 0.

Paik and Yi (2016) suggested an advanced method to predict the welding induced residual stresses in a steel plate element. Based on the experimental and numerical investigations for steel plates with $a/b \ge 1$, they proposed the empirical formulations to predict the breadths of the HAZ as functions of the plate's slenderness ratio and the weld bead length (leg length) as follows:

$$b_{t} = c_{1}L_{w} + c_{2} \tag{1.42a}$$

$$a_{t} = d_{1}L_{w} + d_{2} \tag{1.42b}$$

$$c_1 = -0.4562\beta_x^2 + 4.1994\beta_x + 2.6354, c_2 = 1.1352\beta_x^2 - 4.3185\beta_x - 11.1750, \\ d_1 = -0.0399\beta_y^2 + 2.0087\beta_y + 8.7880, d_2 = 0.1042\beta_y^2 - 4.8575\beta_y - 17.7950,$$

0003369274.3D 58 24/1/2018 10:48:09 AM

 $\beta_x = (b/t)\sqrt{\sigma_Y/E}$, $\beta_y = (a/t)\sqrt{\sigma_Y/E}$, and L_w is the weld bead length (mm), which is usually in the range 4-8 mm (4-5 mm for design requirement and 6 mm in average) for relatively thin plates in shipbuilding industry practice with one pass welding.

Once the breadths of the HAZ are determined from Equation (1.42), depending on the welding conditions and the plate's slenderness ratio, the welding induced compressive residual stresses can then be predicted from Equation (1.39) as follows:

$$\sigma_{\text{rcx}} = \frac{2b_{\text{t}}}{2b_{\text{t}} - b} \sigma_{\text{rtx}} \tag{1.43a}$$

$$\sigma_{\text{rcy}} = \frac{2a_{\text{t}}}{2a_{\text{t}} - a} \sigma_{\text{rty}} \tag{1.43b}$$

where $\sigma_{\text{rt}x} = \sigma_{\text{rt}y} = \sigma_{\text{Y}}$ can be taken for steel.

Modeling of Softening Phenomenon

As previously noted, it is recognized that the strength of aluminum alloys in the softened zone may be recovered by natural aging over a period of time (Lancaster 2003). However, the ultimate strength of welded aluminum alloy-plated structures may be reduced by softening phenomenon as far as the material strength is not recovered.

The breadths of the softened zones approximately equal those of the HAZ in a welded aluminum structure. Paik et al. (2006) proposed the breadths of the softened zones with the nomenclature defined in Figure 1.27 as follows:

$$b'_{p} = b'_{s} = \begin{cases} 11.3 \text{ mm for a slight level} \\ 23.1 \text{ mm for an average level} \\ 29.9 \text{ mm for a severe level} \end{cases}$$
 (1.44)

The yield strength in the HAZ may be obtained as follows, depending on the type of aluminum alloy, following Paik et al. (2006):

a) Yield stress of the HAZ material for aluminum alloy 5083-H116

$$\frac{\sigma_{\text{YHAZ}}}{\sigma_{\text{Y}}} = \begin{cases}
0.906 & \text{for a slight level} \\
0.777 & \text{for an average level} \\
0.437 & \text{for a severe level}
\end{cases} \text{ with } \sigma_{\text{Y}} = 215 \text{ N/mm}^2 \qquad (1.45a)$$

b) Yield stress of the HAZ material for aluminum alloy 5383-H116

$$\frac{\sigma_{\text{YHAZ}}}{\sigma_{\text{Y}}} = \begin{cases}
0.820 & \text{for a slight level} \\
0.774 & \text{for an average level} \\
0.640 & \text{for a severe level}
\end{cases} \text{ with } \sigma_{\text{Y}} = 220 \text{ N/mm}^2 \qquad (1.45\text{b})$$

c) Yield stress of the HAZ material for aluminum alloy 5383-H112

$$\frac{\sigma_{YHAZ}}{\sigma_{Y}} = 0.891$$
 for an average level with $\sigma_{Y} = 190 \text{ N/mm}^2$ (1.45c)

0003369274.3D 59 24/1/2018 10:48:09 AM d) Yield stress of the HAZ material for aluminum alloy 6082-T6

$$\frac{\sigma_{\text{YHAZ}}}{\sigma_{\text{Y}}} = 0.703 \text{ for an average level with } \sigma_{\text{Y}} = 240 \text{N/mm}^2$$
 (1.45d)

where σ_{YHAZ} is the yield strength in the softened zone and σ_{Y} is the yield strength in the base material.

The compressive residual stresses at the plate part and the stiffener web can then be determined from Equation (1.43) using Equations (1.44) and (1.45). Empirical formulations are also given regardless of the type of aluminum alloys as follows (Paik et al. 2006):

$$\sigma_{\text{rcx}} = \begin{cases} -0.110\sigma_{\text{Yp}} & \text{for a slight level} \\ -0.161\sigma_{\text{Yp}} & \text{for an average level} \\ -0.216\sigma_{\text{Yp}} & \text{for a severe level} \end{cases}$$
in the plate part (1.46a)

$$\sigma_{rcx} = \begin{cases} -0.110\sigma_{Yp} & \text{for a slight level} \\ -0.161\sigma_{Yp} & \text{for an average level} \\ -0.216\sigma_{Yp} & \text{for a severe level} \end{cases} \text{ in the plate part}$$

$$\sigma_{rcx} = \begin{cases} -0.078\sigma_{Ys} & \text{for a slight level} \\ -0.137\sigma_{Ys} & \text{for an average level} \\ -0.195\sigma_{Ys} & \text{for a severe level} \end{cases} \text{ in the stiffener web}$$

$$(1.46b)$$

where σ_{Yp} and σ_{Ys} are the yield strengths of the plate part and the stiffener web, respectively.

Age Related Structural Degradation

In aging structures, defects related to corrosion and fatigue cracks are significant, especially in a marine environment (Paik & Thayamballi 2007, Rizzo et al. 2007, Paik & Melchers 2008). In a number of damage cases for aging marine and land-based structures that have been reported, it is possible that corrosion damage and fatigue cracks may have existed in the primary and other strength members. In any event, fatigue and corrosion are the two most important factors that affect structural performance over time.

It is therefore important for the structural designer and operator to have a complete understanding of the location and extent of structural damage formed during the structure's operation and how it can affect the structural capacity. One reason is that this knowledge is necessary to facilitate repair decisions, and another could be to support a structural life extension decision later in the structure's life. The structural capacity associated with Equation (1.17) needs to be determined by dealing with the age related degradation as a parameter of influence.

1.8.1 **Corrosion Damage**

Due to corrosion damage, the structural capacity can be decreased and/or leakages can take place in oil/watertight boundaries, with the latter possibly leading to undesirable pollution, cargo mixing, or gas accumulation in enclosed spaces. The corrosion process varies over time, and the amount of corrosion damage is normally defined by a corrosion rate with units of, say, millimeters per year, representing the depth of corrosion

0003369274.3D 60 24/1/2018 10:48:09 AM

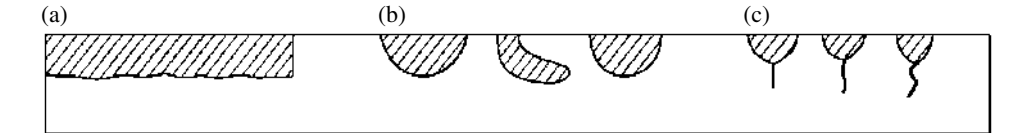


Figure 1.35 Typical types of corrosion damage: (a) general corrosion; (b) localized corrosion; (c) fatigue cracks from localized corrosion.

diminution per year. The corrosion rate itself can be a function of time in some cases, due to effects such as increased structural flexibility as the corrosion process proceeds.

Figure 1.35 shows some of the more typical types of corrosion-related damage that affect the strength of structures. "General" corrosion (also called "uniform" corrosion) uniformly reduces the thickness of structural members, as shown in Figure 1.35a, whereas localized corrosion (e.g., pitting or grooving) causes degradation in local regions, as shown in Figure 1.35b. Fatigue cracks may sometimes arise from localized corrosion, as shown in Figure 1.35c.

The corrosion damage to a structure is influenced by many factors, including the corrosion protection system and various operational parameters (Afanasieff 1975, Schumacher 1979, Melchers & Ahammed 1994, Paik & Thayamballi 2007). Generally used corrosion protection systems include coatings (paint) and anodes. The operational parameters include maintenance, repair, the use of heating coils, humidity conditions, water and sludge accumulation, microbial contamination, and the composition of inert gas. For ships and offshore structures, the percentage of time in ballast, the frequency of tank cleaning, and temperature profiles are also influential parameters. For the past several decades, several studies have been undertaken to understand the effects of many of these factors and their interactions.

To predict tolerance to likely corrosion damage, it is necessary to estimate the corrosion rates for various structural members grouped by type, location, and other parameters. To generalize this further, there are four aspects related to corrosion that one must ideally define for structural members:

- Where is corrosion likely to occur?
- When does it start?
- What is its extent?
- What are the likely corrosion rates as a function of time?

The first question would normally be answered using historical databases of some form, for example, the results of previous surveys. As to when corrosion starts, this again is information that should come from prior surveys for the particular structure. Lacking specific databases, assumptions for the time the corrosion will begin can of course be made, depending on the use of a protection system, the characteristics of the coatings, and the anode residence time.

For the residual strength and similar performance assessment of corroded structures, one must clarify how corrosion develops and proceeds in structural members, the spatial extents of member degradation, and the likely effects of such corrosion on structural performance measures such as strength and leakage characteristics. These considerations are complicated by the sheer number of factors that can potentially affect corrosion,

0003369274.3D 61 24/1/2018 10:48:09 AM

including the type of protection, the type of cargo, temperature, and humidity. In addition, a probabilistic treatment is essential to account for the various uncertainties associated with corrosion.

The extent of corrosion presumably increases with time, but our ability to predict its spatial progress remains meager. The only real alternative is then to pessimistically assume an extent of corrosion than is actually likely, such as what one would do in the case of nominal design corrosion values. To put this in another way, one can assess the structural performance based on premised extents of corrosion when specific information on the extent of corrosion is lacking or unavailable.

Where coatings are present, the progress of corrosion would normally depend greatly on the degradation of such coatings. For this reason, most classification societies usually recommend maintenance of the corrosion protection system over time, and most owners carry out such maintenance, so the particular maintenance philosophy used also has a significant effect on structural reliability considering corrosion effects in the long term.

Figure 1.36 represents a plausible schematic of the corrosion process for a coated area in a structure. It is assumed in Figure 1.36 that there is no corrosion as long as the coating is effective and also during a short transition time after the coating breaks down. Therefore, the corrosion model accounts for three factors: (i) durability of coating (coating life), (ii) transition, and (iii) progress of corrosion.

The curve that shows the corrosion progression, indicated by a solid line in Figure 1.36, is a little convex, but it may in some cases be a concave curve in dynamically loaded structures, as indicated by the dotted line where flexing continually exposes additional fresh surface area to the effects of corrosion. However, one may take a linear approximation between them for practical assessment.

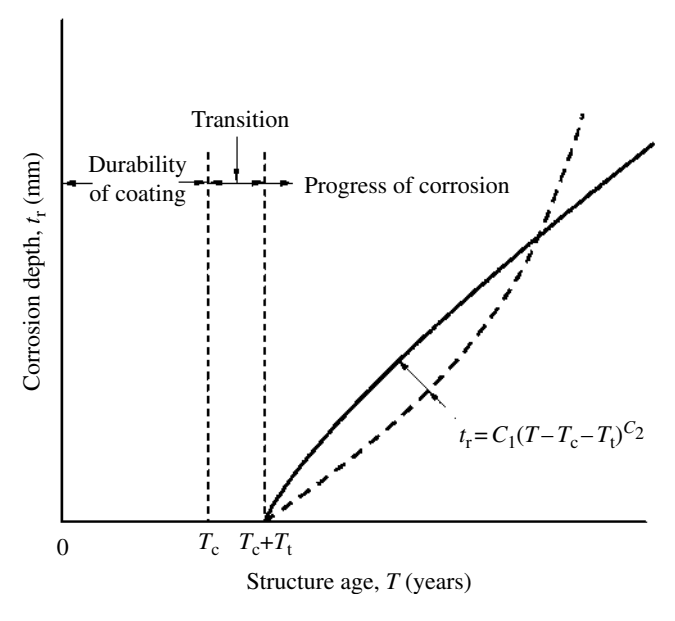


Figure 1.36 A schematic of the corrosion process for structures.

0003369274.3D 62 24/1/2018 10:48:09 AM

The life (or durability) of a coating essentially corresponds to the time when the corrosion begins after the contribution of a structure, or the application of a coating in a previously bare case, or the repair of a coating area to a good, intact standard. The life of a coating typically depends on the type of coating system used and the relevant maintenance, among other factors (Melchers & Jiang 2006). The coating life to a predefined state of breakdown is often assumed to follow a lognormal distribution, given by

$$f(T_{c}) = \frac{1}{\sqrt{2\pi}\sigma_{c}} \exp\left[-\frac{(\ln T_{c} - \mu_{c})^{2}}{2\sigma_{c}^{2}}\right]$$
(1.47)

where μ_c is the mean value of $\ln T_c$ in years, σ_c is the standard deviation of $\ln T_c$, and T_c is the coating life in years.

The coating systems are sometimes classified by their target life. For example, IMO (1995) uses three groups (coating systems I, II, and III) for ships and offshore structures, for which the corresponding target durability is 5, 10, and 15 years, respectively. However, this particular classification is by no means universal. TSCF (2000) defines the requirements for 10-, 15-, and 25-year coating systems for ballast tanks in oil tankers. Generally, however, a 5-year coating life may be considered to represent an undesirable situation, whereas 10 years or longer would represent a relatively more desirable state of affairs. The selection of a target life to be achieved is primarily economical. Any given mean or median coating life is uncertain, and the coefficient of variation of the coating life is sometimes taken as $\sigma_c/\mu_c = 0.4$ for $\ln T_c$ (ClassNK 1995).

After the effectiveness of a coating is lost, some transition time, that is, the duration between the loss of coating effectiveness and the time the corrosion begins, is considered to exist before the corrosion "initiates" over a sufficiently large and easily measured area. The transition time is sometimes considered to be an exponentially distributed random variable. As an example, the mean value of the transition time for transverse bulkhead structures of bulk carriers was shown to be 3 years for deep-tank bulkheads, 2 years for watertight bulkheads, and 1.5 years for stool regions (Yamamoto & Ikegami 1998). When the transition time is assumed to be zero, that is, $T_t = 0$, it is implied that the corrosion will begin immediately after the effectiveness of the coating is lost.

As illustrated in Figure 1.36, the wear of plate thickness due to corrosion may be generally expressed as a function of the time after the corrosion starts (years), namely,

$$d_{c} = C_{1} T_{c}^{C_{2}} \tag{1.48}$$

where d_c is the corrosion depth (or wear of plate thickness due to corrosion; mm); T_e is the exposure time after breakdown of the coating (years), which is taken as $T_e = T - T_c - T_t$; T is the age of the structure (years); T_c is the life of the coating (years); T_t is the duration of transition (years), which may be pessimistically taken as $T_t = 0$; and C_1 and C_2 are coefficients.

The coefficient C_2 in Equation (1.48) determines the trend of corrosion progress, whereas the coefficient C_1 is in part indicative of the annual corrosion rate that can be obtained by differentiating Equation (1.48) with respect to time. As may be surmised from Equation (1.48), the two coefficients closely interact, and they can be determined simultaneously based on the carefully collected statistical corrosion data of existing structures. However, this approach is not straightforward to apply in most cases, mainly because of differences in the database collection sites typically visited over the life of the structure.

0003369274.3D 63 24/1/2018 10:48:09 AM That is, it is normally difficult to track corrosion at a particular site based on the typically available gauging data. This is part of the reason for the relatively large scatter of corrosion data in many studies.

An easier alternative is to determine the coefficient C_1 at a constant value of the coefficient C_2 . This is mathematically a simpler model, but it does not negate any of the short-comings due to the usual methods of data collection in surveys. It does, however, make possible the postulation of different modes of corrosion behavior over time depending on the value adopted for C_2 in an easy-to-understand way.

For corrosion of ships and offshore structures, studies have indicated that the coefficient C_2 can sometimes fall within the range of 0.3–1.5 (Yamamoto & Ikegami 1998, Melchers 1999b). This implies a behavior wherein the corrosion rates apparently decrease or stabilize over time. While such behavior is plausible for statically loaded structures, for dynamically loaded structures in which the corrosion scale is continually being lost and new material is being exposed to corrosion because of structural flexing, such values of C_2 may not always be appropriate or safe (Melchers & Paik 2009). For practical design purposes, $C_2 = 1$ is often adopted.

Figure 1.37 shows a schematic of the time-variant corrosion progress, which indicates that the probabilistic characteristics of the corrosion progress differ over time. Figure 1.38a shows evidence of this for time-variant corrosion progress in the ballast tank structures of bulk carriers (Paik & Kim 2012).

Paik and Kim (2012) derived a mathematical model to predict the time-variant corrosion wastage of the ballast tank structures of bulk carriers by accounting for the effects of the varying probabilistic characteristics with time, where the two-parameter Weibull

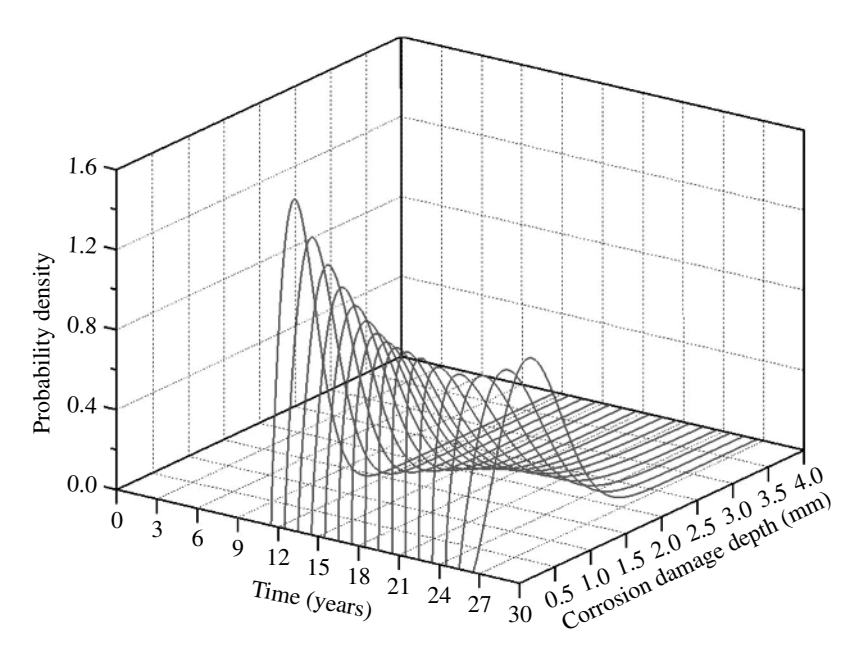


Figure 1.37 A schematic of the probabilistic characteristics of corrosion wastage progress over time (Paik & Kim 2012).

0003369274.3D 64 24/1/2018 10:48:09 AM

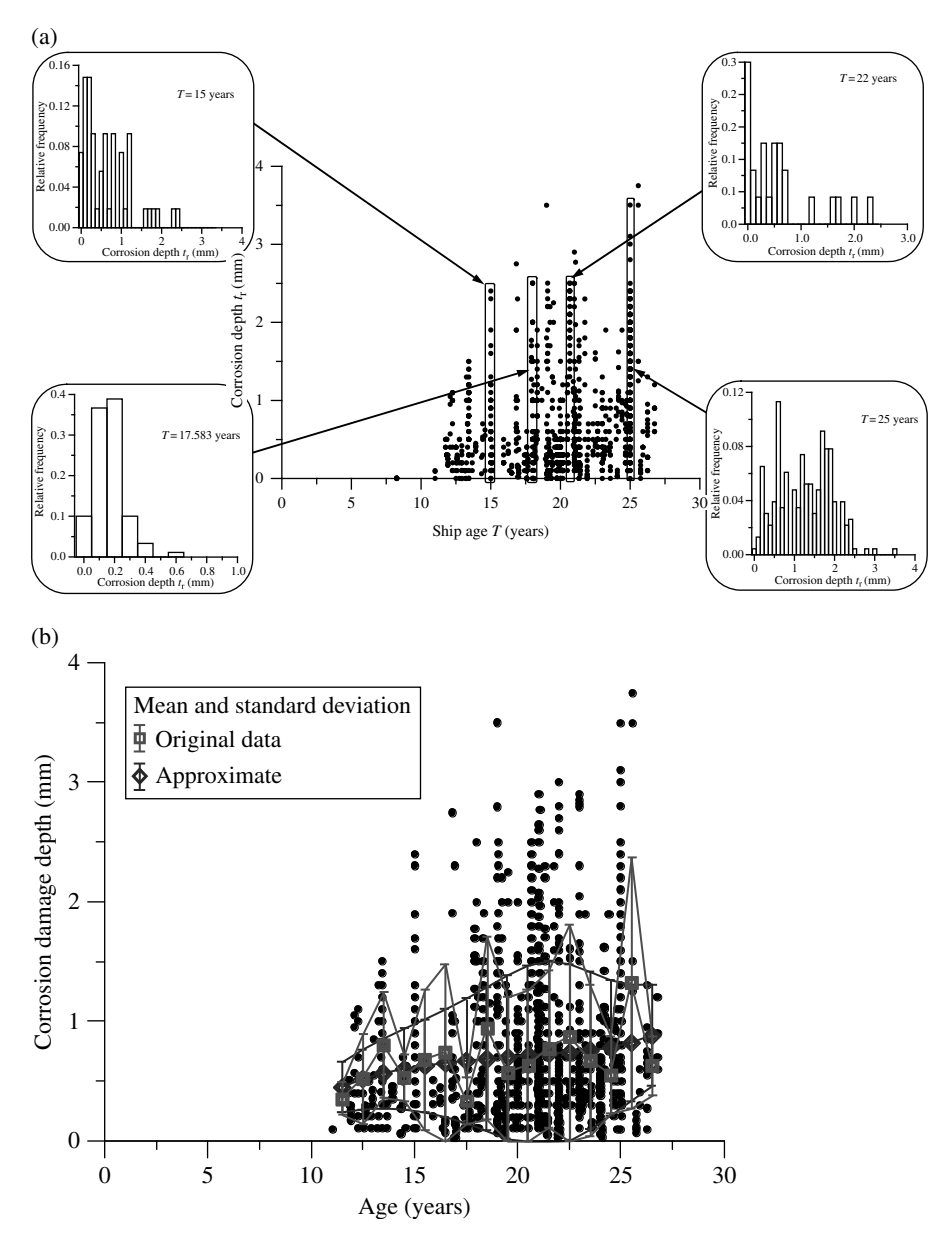


Figure 1.38 Probabilistic characteristics of corrosion wastage progress over time in ballast tank structures of bulk carriers: (a) measurement database; (b) comparison between measurement and prediction (Paik & Kim 2012).

function was realized by the goodness of fit tests to be the best suited to represent the corrosion wastage progress:

$$d_{\rm c} = \frac{\alpha}{\beta} \left(\frac{T_{\rm e}}{\beta} \right)^{\alpha - 1} \exp \left[-\left(\frac{T_{\rm e}}{\beta} \right)^{\alpha} \right] \tag{1.49a}$$

0003369274.3D 65 24/1/2018 10:48:09 AM

where

$$\alpha = 0.0020T_{\rm e}^3 - 0.0994T_{\rm e}^2 + 1.5604T_{\rm e} - 6.0025 \tag{1.49b}$$

$$\beta = 0.0004T_e^3 - 0.0248T_e^2 + 0.4793T_e - 2.3812 \tag{1.49c}$$

Figure 1.38b confirms the applicability of the approximate formula of Equation (1.49) by comparison with the original database of gathered corrosion measurements.

Hairil Mohd and Paik (2013) further applied this method to the time-variant corrosion damage prediction of subsea well tubes, where the two-parameter Weibull function was also found by the goodness of fit tests to be the best suited to represent the corrosion wastage progress. In this case, the coefficients α and β in Equation (1.49a) are now given as follows:

$$\alpha = -0.02287T_{\rm e}^2 + 0.61835T_{\rm e} - 0.94398 \tag{1.50a}$$

$$\beta = 0.001347T_e^2 + 0.004688T_e + 0.292059 \tag{1.50b}$$

Figure 1.39 confirms the validity of Equation (1.50) together with Equation (1.49a) for the time-variant corrosion wastage of subsea well tubes. Hairil Mohd et al. (2014) further

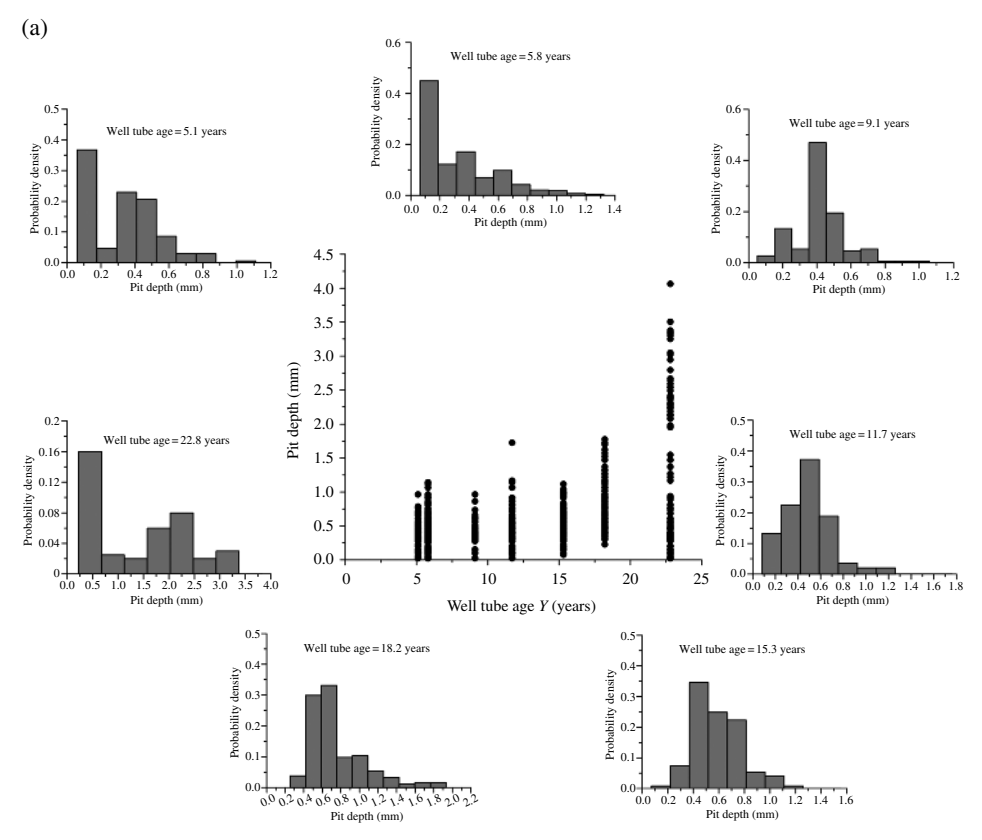
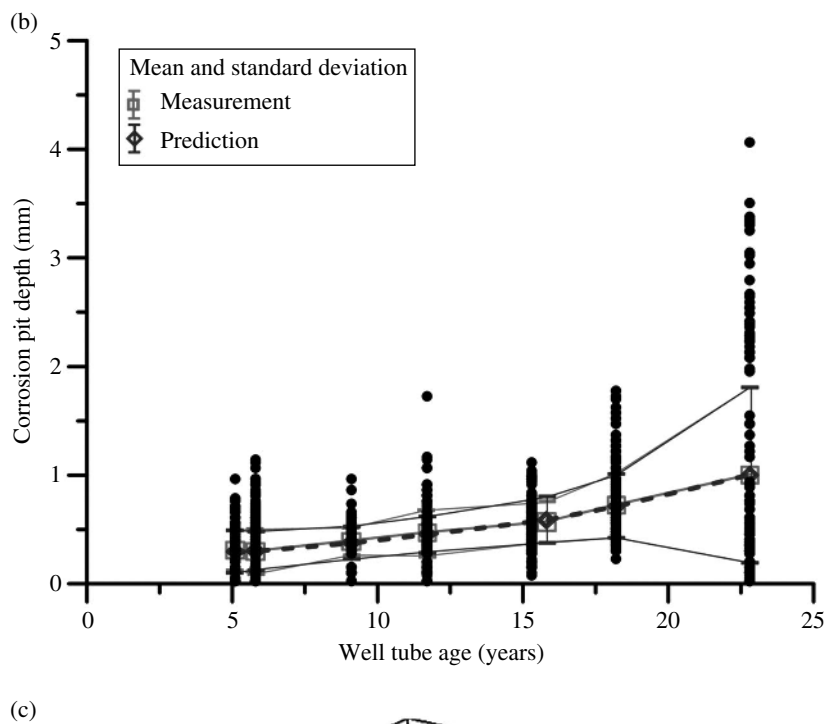


Figure 1.39 Probabilistic characteristics of corrosion wastage progress over time in subsea well tubes: (a) measurement database; (b) comparison between measurement and prediction in mean value; (c) comparison between measurement and prediction in probability (Hairil Mohd & Paik 2013).

0003369274.3D 66 24/1/2018 10:48:10 AM



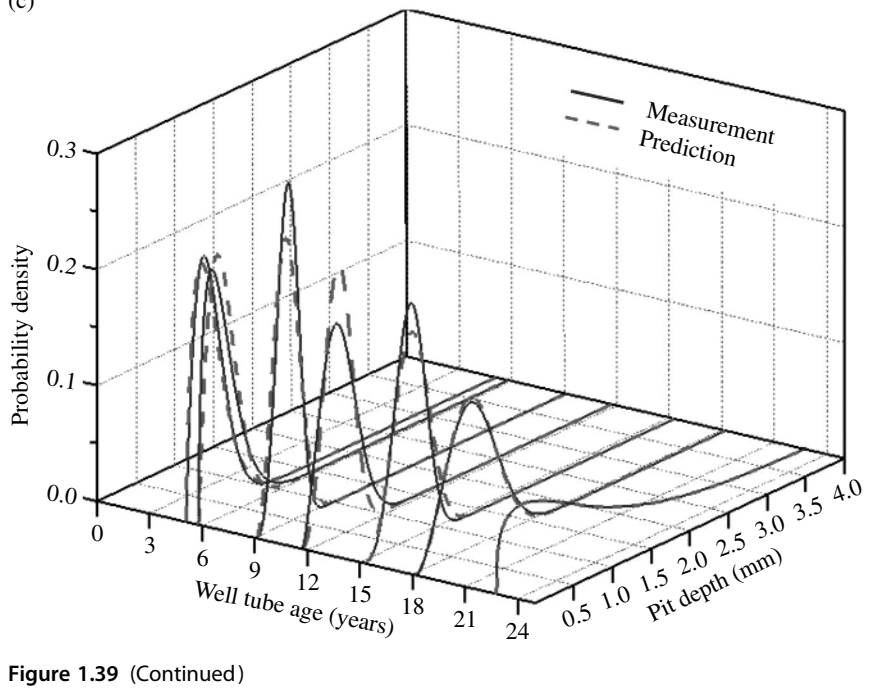


Figure 1.39 (Continued)

0003369274.3D 67 24/1/2018 10:48:10 AM applied this approach to predict the time-variant corrosion wastage progress of subsea gas pipelines as shown in Figure 1.40, where the three-parameter Weibull function was found to be the best suited to represent the corrosion wastage progress as follows:

$$d_{c} = \frac{\alpha}{\beta} \left(\frac{T_{e} - \gamma}{\beta} \right)^{\alpha - 1} \exp \left[-\left(\frac{T_{e} - \gamma}{\beta} \right)^{\alpha - 1} \right]$$
 (1.51a)

where

$$\alpha = 0.003337 T_e^2 - 0.130420 T_e + 2.4557 \tag{1.51b}$$

$$\beta = -0.000997T_{\rm e}^2 + 0.013425T_{\rm e} + 1.58201 \tag{1.51c}$$

$$\gamma = 0.0003455 T_e^2 + 0.062137 T_e - 0.365129 \tag{1.51d}$$

It is obvious that the characteristics of corrosion progress differ depending on the corrosion environment, which can differ at different locations of a structural member, even in the same structure. Paik et al. (2003a) divided the double-hulled oil tanker structures into a total of 34 structural member groups according to the different locations of the corrosion environment, as indicated in Figure 1.41 and Tables 1.7 and 1.8. Paik et al. (2003b) also divided the bulk carrier structures into a total of 23 structural member

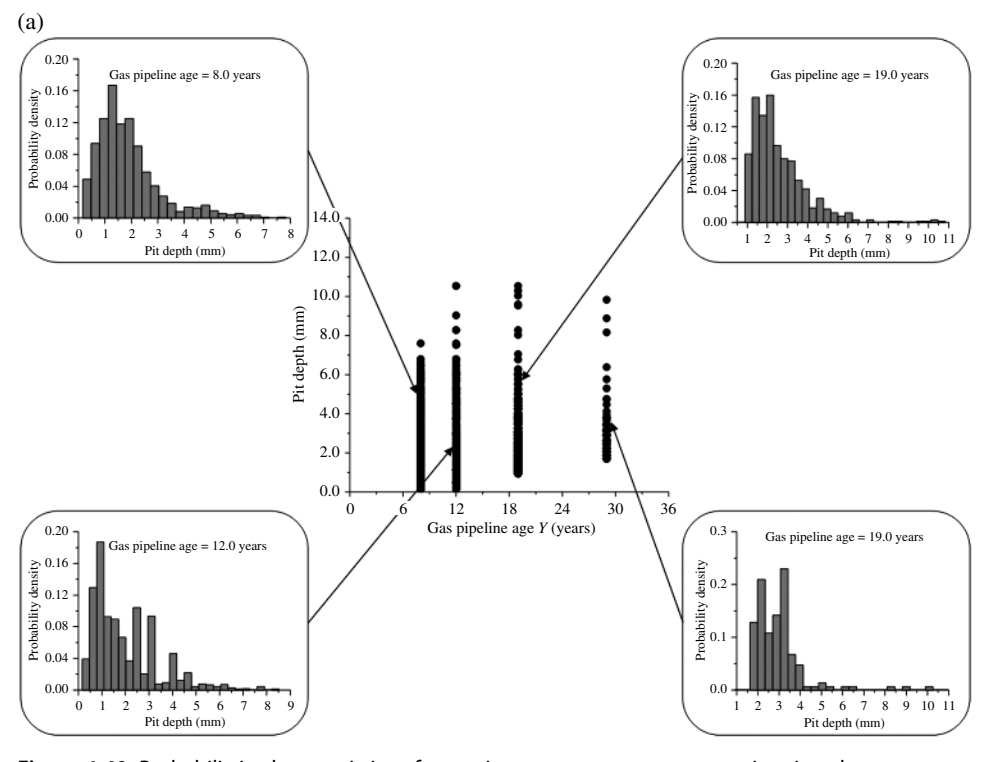
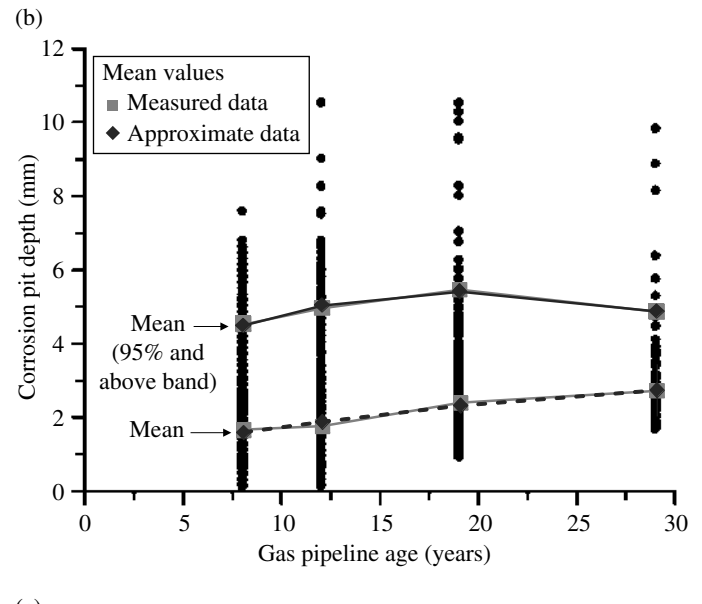


Figure 1.40 Probabilistic characteristics of corrosion wastage progress over time in subsea gas pipelines: (a) measurement database; (b) comparison between measurement and prediction in mean value; (c) comparison between measurement and prediction in probability (Hairil Mohd et al. 2014).

0003369274.3D 68 24/1/2018 10:48:10 AM



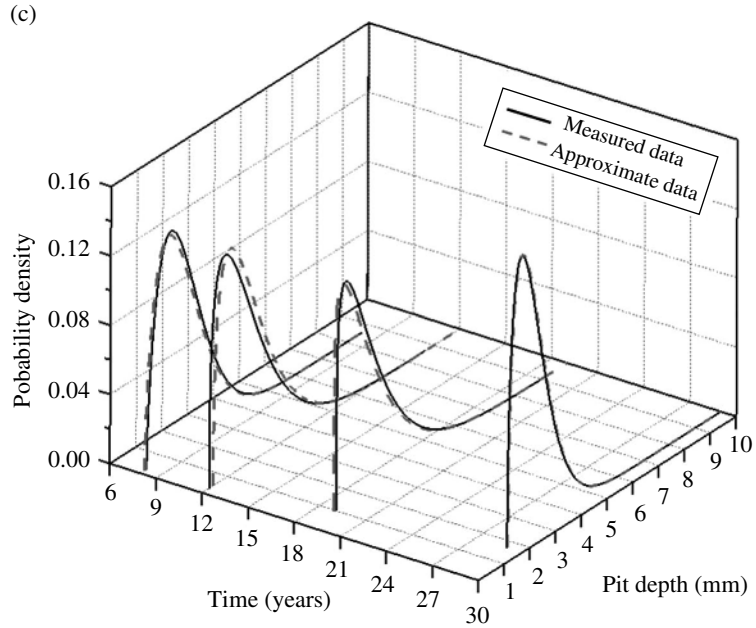


Figure 1.40 (Continued)

groups, as indicated in Figure 1.42 and Table 1.9. Each of the structural member groups has different corrosion characteristics.

1.8.2 Fatigue Cracks

Under repeated loading, fatigue cracks may be initiated in the structure's stress concentration areas. Initial defects or cracks may also form in the structure due to the

0003369274.3D 69 24/1/2018 10:48:11 AM

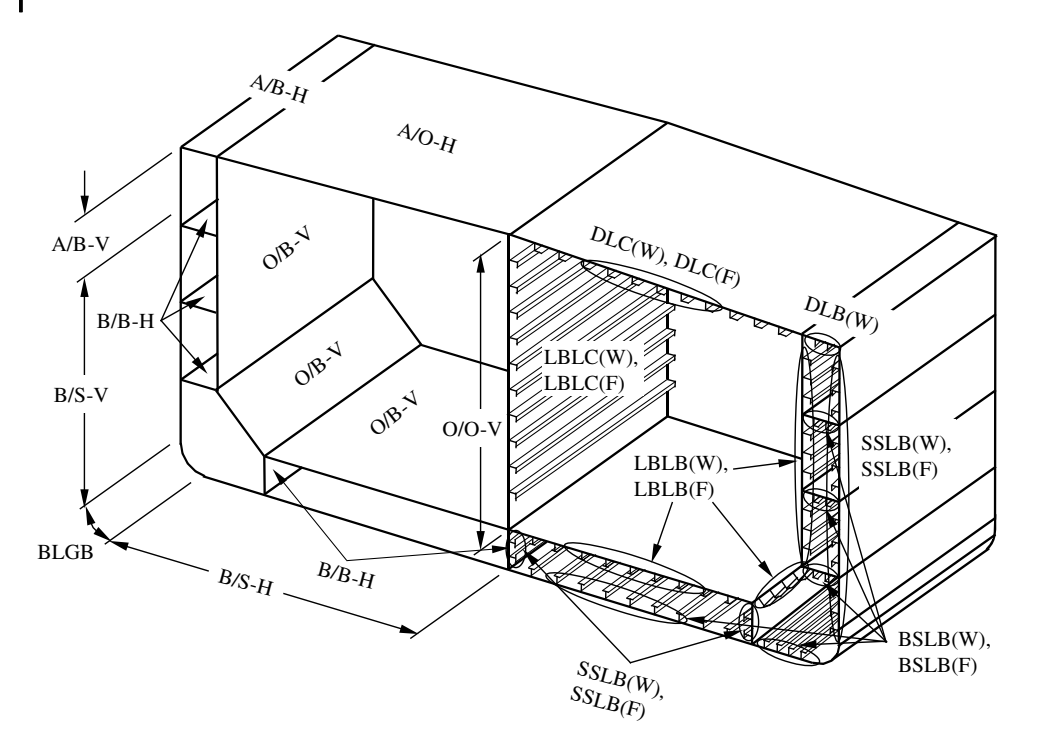


Figure 1.41 The 34 structural member groups (location and category groups) of double-hulled oil tanker structures (Paik et al. 2003a).

Table 1.7 Identification of 14 member location/category groups for the plating of tankers.

ID	Member type	
B/S-H	Bottom shell plating (ballast tank)	
A/B-H	Deck plating (ballast tank)	
A/B-V	Side shell plating above draft line (ballast tank)	
B/S-V	Side shell plating below draft line (ballast tank)	
BLGB	Bilge plating (ballast tank)	
O/B-V	Longitudinal bulkhead plating (ballast tank)	
B/B-H	Stringer plating (ballast tank)	
O/S-H	Bottom shell plating (cargo oil tank)	
A/O-H	Deck plating (cargo oil tank)	
A/O-V	Side shell plating above draft line (cargo oil tank)	
O/S-V	Side shell plating below draft line (cargo oil tank)	
BLGC	Bilge plating (cargo oil tank)	
O/O-V	Longitudinal bulkhead plating (cargo oil tank)	
O/O-H	Stringer plating (cargo oil tank)	

0003369274.3D 70 24/1/2018 10:48:11 AM

Table 1.8 Identification of 20-member location/category groups for the stiffener webs and flanges of tankers.

ID (stiffener web)	Member types	ID (stiffener flange)	Member types
BSLBW	Bottom shell longitudinals in ballast tank—web	BSLBF	Bottom shell longitudinals in ballast tank—flange
SSLBW	Side shell longitudinals in ballast tank—web	SSLBF	Side shell longitudinals in ballast tank—flange
LBLBW	Longitudinal bulkhead longitudinals in ballast tank—web	LBLBF	Longitudinal bulkhead longitudinals in ballast tank—flange
BSLCW	Bottom shell longitudinals in cargo oil tank—web	BSLCF	Bottom shell longitudinals in cargo oil tank—flange
DLCW	Deck longitudinals in cargo oil tank—web	DLCF	Deck longitudinals in cargo oil tank—flange
SSLCW	Side shell longitudinals in cargo oil tank—web	SSLCF	Side shell longitudinals in cargo oil tank—flange
LBLCW	Longitudinal bulkhead longitudinals in cargo oil tank—web	LBLCF	Longitudinal bulkhead longitudinals in cargo oil tank—flange
BGLCW	Bottom girder longitudinals in cargo oil tank—web	BGLCF	Bottom girder longitudinals in cargo oil tank—flange
DGLCW	Deck girder longitudinals in cargo oil tank—web	DGLCF	Deck girder longitudinals in cargo oil tank—flange
DLBW	Deck longitudinals in ballast tank—web		
SSTLCW	Side stringer longitudinals in cargo oil tank—web		

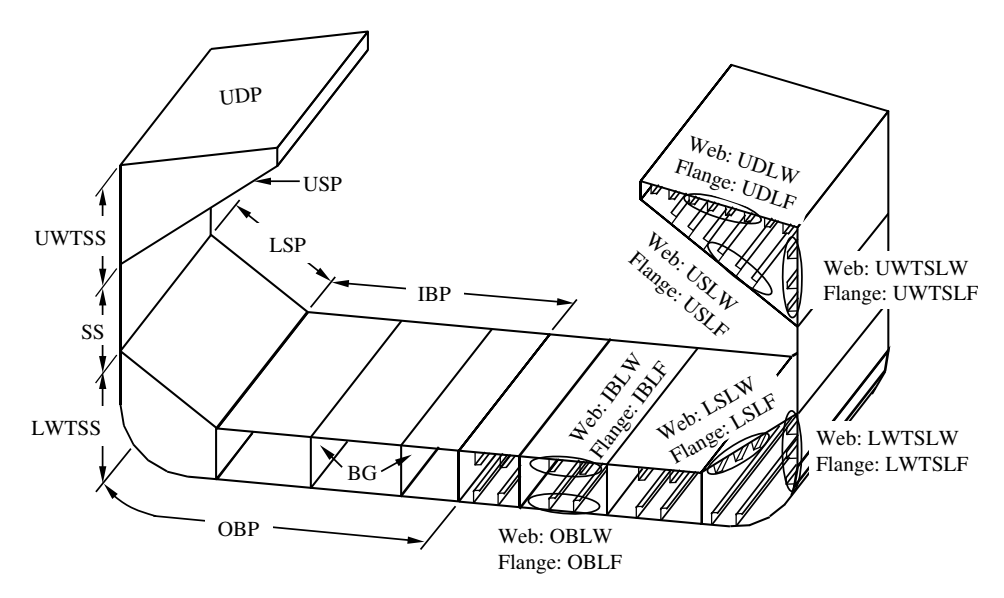


Figure 1.42 The 23 structural member groups (location and category groups) of bulk carrier structures (Paik et al. 2003b).

24/1/2018 10:48:11 AM 0003369274.3D 71

Table 1.9 Identification of the 23-member groups for a bulk carrier structure.

ID	Member type
OBP	Outer bottom plates
IBP	Inner bottom plates
LSP	Lower sloping plates
LWTSS	Lower wing tank side shells
SS	Side shells
UWTSS	Upper wing tank side shells
USP	Upper sloping plates
UDP	Upper deck plates
BG	Bilge girders
OBLW	Outer bottom longitudinals—web
OBLF	Outer bottom longitudinals—flange
IBLW	Inner bottom longitudinals—web
IBLF	Inner bottom longitudinals—flange
UWTSLW	Upper wing tank side longitudinals—web
UWTSLF	Upper wing tank side longitudinals—flange
USLW	Upper sloping longitudinals—web
USLF	Upper sloping longitudinals—flange
UDLW	Upper deck longitudinals—web
UDLF	Upper deck longitudinals—flange
LWTSLW	Lower wing tank side longitudinals—web
LWTSLF	Lower wing tank side longitudinals—flange
LSLW	Lower sloping longitudinals—web
LSLF	Lower sloping longitudinals—flange

fabrication procedures applied. In addition to their fatigue propagation under repeated cyclic loading, cracks, as they grow, may also propagate under monotonically increasing extreme loads, a circumstance that can eventually lead to the structure's catastrophic failure when given the possibility of rapid and uncontrolled crack extension without arrest or if the crack attains a length that results in significant degradation of the structural capacity.

It is obvious that fatigue cracking damage also varies with time. Figure 1.43 shows a schematic of fatigue-related cracking damage progress as a function of time (age) in structures (Paik & Thayamballi 2007). The fatigue damage progress can be separated into three stages: initiation (stage I), propagation (stage II), and failure (fracture) (stage III) (ISO 2394 1998). For assessment of residual strength in aging structures under extreme loads and under fluctuating loads, it is thus often necessary to account for an existing crack as a parameter of influence (Paik & Melchers 2008).

0003369274.3D 72 24/1/2018 10:48:12 AM

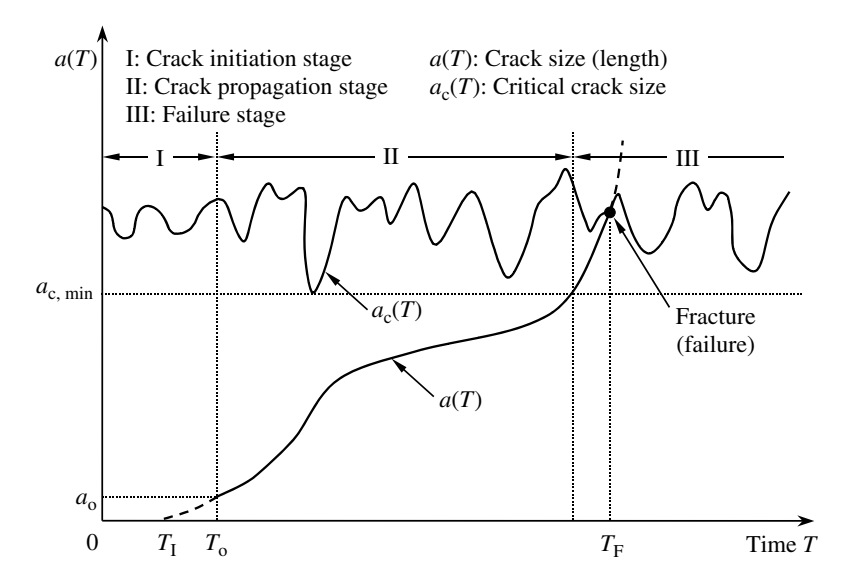


Figure 1.43 A schematic of crack initiation and growth for a structure with time.

1.9 Accident Induced Damage

The ultimate strength of a structure can be reduced as a result of accident induced damage. Potential accidents, such as collision, grounding, impact from dropped objects or mishandled cargo loading/unloading, fire, and explosions, can result in structural damage that reduces structural capacity (ultimate strength) or even leads to total loss of the structure.

Collision and grounding accidents typically result in crushing (folding), yielding, and tearing. Hydrodynamic impact can cause plastic deformation damage. Dropped objects can cause local dents and/or global permanent deformation. Fire or explosions can expose the structural material to elevated temperatures and explosions also being accompanied by blast. Exposure to a fire at high temperatures can cause not only structural damage but also metallurgical changes. For fire safety and the resistance of structures, refer to Lawson (1992), Nethercot (2001), and Franssen and Real (2010).

Ultimate strength of a structure with accident induced damage is often termed residual strength. The structural capacity associated with Equation (1.17) needs to be determined by dealing with the accident induced damage as a parameter of influence.

References

Afanasieff, L. (1975). Corrosion mechanisms, corrosion defense and wastage. Chapter 16 in *Ship structural design concepts*, Edited by Harvey Evans, J., Cornell Maritime Press, Cambridge, MA.

Benjamin, J.R. & Cornell, C.A. (1970). *Probability, statistics, and decision for civil engineers*. McGraw-Hill, New York.

0003369274.3D 73 24/1/2018 10:48:12 AM

- Bodner, S.R. & Symonds, P.S. (1962). Experimental and theoretical investigation of the plastic deformation of cantilever beams subjected to impulsive loading. *Journal of Applied Mechanics*, **29**:719–728.
- Brockenbrough, R.L. & Johnston, B.G. (1981). *USS steel design manual*. United States Steel Corporation, Pittsburgh, PA.
- BS 5950 (1985). The structural use of steelwork in building. Part 8. British Standards Institution, London.
- Callister, W.D. (1997). *Materials science and engineering*. Fourth Edition, John Wiley & Sons, Inc., New York.
- Campbell, J. & Cooper, R.H. (1966). Yield and flow of low-carbon steel at medium strain rates. Proceedings of the Conference on the Physical Basis of Yield and Fracture, Institute of Physics and Physical Society, London, 77–87.
- Cheng, J.J.R., Elwi, A.E., Grodin, G.Y. & Kulak, G.L. (1996). Material testing and residual stress measurements in a stiffened steel plate. In *Strength and stability of stiffened plate components*, **SSC-399**, Ship Structure Committee, Washington, DC.
- ClassNK (1995). Guidance for corrosion protection system of hull structures for water ballast tanks and cargo oil tanks. Second Revision, Nippon Kaiji Kyokai, Tokyo.
- Cowper, G.R. & Symonds, P.S. (1957). *Strain-hardening and strain-rate effects in the impact loading of cantilever beams*, Technical Report, **23**, Division of Applied Mathematics, Brown University, Providence, RI.
- ECCS (1982). European recommendations for the fire safety of steel structures, ECCS Technical Committee, **3**, European Convention for Constructional Steelwork (ECCS), Brussels.
- ENV 1993-1 (1992a). Eurocode 3: design of steel structures, part 1.1 general rules and rules for buildings. British Standards Institution, London.
- ENV 1993-1 (1992b). Eurocode 3: design of steel structures, part 1.2 fire resistance. British Standards Institution, London.
- Franssen, J.M. & Real, P.V. (2010). *Fire design of steel structures*, ECCS Eurocode Design Manuals, Ernst & Sohn, Berlin.
- Galambos, T.V. (1988). Guide to stability design criteria for metal structures. John Wiley & Sons, Inc., New York.
- Hairil Mohd, M., Kim, D.K., Kim, D.W. & Paik, J.K. (2014). A time-variant corrosion wastage model for subsea gas pipelines. *Ships and Offshore Structures*, **9**(2):161–176.
- Hairil Mohd, M. & Paik, J.K. (2013). Investigation of the corrosion progress characteristics of offshore subsea oil well tubes. *Corrosion Science*, **67**:130–141.
- Hsu, S.S. & Jones, N. (2004). Dynamic axial crushing of aluminum alloy 6063-T6 circular tubes. *Latin American Journal of Solids and Structures*, **1**(3):277–296.
- Hughes, O.F. & Paik, J.K. (2013). *Ship structural analysis and design*. The Society of Naval Architects and Marine Engineers, Alexandria, VA.
- IACS (2014). *Aluminum alloys for hull construction and marine structures*. International Association of Classification Societies, London.
- IMO (1995). Resolution A.798(l9). In *Guidelines for the selection, application and maintenance of corrosion prevention systems of dedicated seawater ballast tanks*. International Maritime Organization, London.
- ISO 2394 (1998). *General principles on reliability for structures*. Second Edition, International Organization for Standardization, Geneva, Switzerland.
- Jones, N. (2012). Structural impact. Second Edition, Cambridge University Press, Cambridge.

0003369274.3D 74 24/1/2018 10:48:12 AM

- JSQS (1985). *Japanese shipbuilding quality standards*. The Society of Naval Architects of Japan, Tokyo.
- Kenno, S.Y., Das, S., Kennedy, J., Rogge, R.B. & Gharghouri, M.A. (2010). Distribution of residual stresses in stiffened plates with one or two stiffeners. *Ships and Offshore Structures*, **5**(3):211–225.
- Kenno, S.Y., Das, S., Rogge, R.B. & Gharghouri, M.A. (2017). Changes in residual stresses caused by an interruption in the weld process of ships and offshore structures. *Ships and Offshore Structures*, **12**(3):341–359.
- Lancaster, J. (2003). Handbook of structural welding: processes, materials and methods used in the welding of major structures, pipelines and process plant. Abington Publishing, Cambridge.
- Lawson, R.M. (1992). Fire resistance and protection of structural steelwork. Chapter 7.3 in *Constructional steel design: an international guide*, Edited by Dowling, P.J., Hrading, J.E. & Bjorhovde, R., Elsevier Applied Science, London.
- Lotsberg, I. (2016). *Fatigue design of marine structures*. Cambridge University Press, Cambridge. Masubuchi, K. (1980). *Analysis of welded structures*. Pergamon Press, Oxford.
- Mazzolani, F.M. (1985). Aluminum alloy structures. Pitman Publishing Ltd., London.
- Melchers, R.E. (1999a). Structural reliability analysis and prediction. John Wiley & Sons, Ltd, Chichester.
- Melchers, R.E. (1999b). Corrosion uncertainty modeling for steel structures. *Journal of Constructional Steel Research*, **52**:3–19.
- Melchers, R.E. & Ahammed, M. (1994). *Nonlinear modeling of corrosion of steel in marine environments*, Research Report, **106.09.1994**, Department of Civil, Surveying and Environmental Engineering, The University of Newcastle, Callaghan.
- Melchers, R.E. & Jiang, X. (2006). Estimation of models for durability of epoxy coatings in water ballast tanks. *Ships and Offshore Structures*, **1**(1):61–70.
- Melchers, R.E. & Paik, J.K. (2009). Effect of flexure on rusting of ship's steel plating. *Ships and Offshore Structures*, **5**(1):25–31.
- Modarres, M., Kaminskiy, M.P. & Krivtsov, V. (2016). *Reliability engineering and risk analysis: a practical guide*. Third Edition, CRC Press, New York.
- Nethercot, D.A. (2001). *Limit states design of structural steelwork*. Third Edition Based on Revised BS 5950: Part I, 2000 Amendment, Spon Press, London.
- NORSOK (2004). Design of steel structures. N-004, Rev.2, Standards Norway, Lysaker.
- Nowak, A.A. & Collins, K.R. (2000). Reliability of structures. McGraw-Hill, Boston.
- Nussbaumer, A., Borges, L. & Davaine, L. (2011). Fatigue design of steel and composite structures. In *Eurocode 3: design of steel structures*. ECCS Eurocode Design Manuals, Ernst & Sohn, Berlin.
- Paik, J.K. (2007a). Practical techniques for finite element modeling to simulate structural crashworthiness in ship collisions and grounding (Part I: Theory). *Ships and Offshore Structures*, **2**(1):69–80.
- Paik, J.K. (2007b). Practical techniques for finite element modeling to simulate structural crashworthiness in ship collisions and grounding (Part II: Verification). *Ships and Offshore Structures*, **2**(1):81–85.
- Paik, J.K. (2007c). Characteristics of welding induced initial deflections in welded aluminum plates. *Thin-Walled Structures*, **45**:493–501.
- Paik, J.K. (2008). *Mechanical collapse testing on aluminum stiffened panels for marine applications*, **SSC-451**, Ship Structure Committee, Washington, DC.

0003369274.3D 75 24/1/2018 10:48:12 AM

- Paik, J.K., Andrieu, C. & Cojeen, H.P. (2008). Mechanical collapse testing on aluminum stiffened plate structures for marine applications. *Marine Technology*, **45**(4):228–240.
- Paik, J.K. & Chung, J.Y. (1999). A basic study on static and dynamic crushing behavior of a stiffened tube. Transactions of the Korean Society of Automotive Engineers (KSAE), 7 (1):219–238.
- Paik, J.K. & Frieze, P.A. (2001). Ship structural safety and reliability. *Progress in Structural Engineering and Materials*, **3**:198–210.
- Paik, J.K. & Kim, D.K. (2012). Advanced method for the development of an empirical model to predict time-dependent corrosion wastage. *Corrosion Science*, **63**:51–58.
- Paik, J.K., Kim, K.J., Lee, J.H., Jung, B.G. & Kim, S.J. (2017). Test database of the mechanical properties of mild, high-tensile and stainless steel and aluminum alloy associated with cold temperatures and strain rates. *Ships and Offshore Structures*, **12**(S1):S230–S256.
- Paik, J.K., Kim, B.J., Sohn, J.M., Kim, S.H., Jeong, J.M. & Park, J.S. (2012). On buckling collapse of a fusion-welded aluminum stiffened plate structure: an experimental and numerical study. *Journal of Offshore Mechanics and Arctic Engineering*, **134**:021402.1–021402.8.
- Paik, J.K., Lee, J.M., Hwang, J.S. & Park, Y.I. (2003a). A time-dependent corrosion wastage model for the structures of single- and double-hull tankers and FSOs and FPSOs. *Marine Technology*, **40**(3):201–217.
- Paik, J.K. & Melchers, R.E. (2008). Condition assessment of aged structures. CRC Press, New York.
- Paik, J.K. & Pedersen, P.T. (1996). A simplified method for predicting the ultimate compressive strength of ship panels. *International Shipbuilding Progress*, **43**:139–157.
- Paik, J.K. & Thayamballi, A.K. (2007). *Ship-shaped offshore installations: design, building, and operation*. Cambridge University Press, Cambridge.
- Paik, J.K., Thayamballi, A.K., Park, Y.I. & Hwang, J.S. (2003b). A time-dependent corrosion wastage model for bulk carrier structures. *International Journal of Maritime Engineering*, **145**(A2):61–87.
- Paik, J.K., Thayamballi, A.K. & Lee, J.M. (2004). Effect of initial deflection shape on the ultimate strength behavior of welded steel plates under biaxial compressive loads. *Journal of Ship Research*, **48**(1):45–60.
- Paik, J.K., Thayamballi, A.K., Ryu, J.Y., Jang, J.H., Seo, J.K., Park, S.W., Seo, S.K., Andrieu, C., Cojeen, H.P. & Kim, N.I. (2006). The statistics of weld induced initial imperfections in aluminum stiffened plate structures for marine applications. *International Journal of Maritime Engineering*, 148(Part A1):19–63.
- Paik, J.K. & Yi, M.S. (2016). Experimental and numerical investigations of welding induced distortions and stresses in steel stiffened plate structures. The Korea Ship and Offshore Research Institute, Pusan National University, Busan.
- Ramberg, W. & Osgood, W.R. (1943). *Description of stress-strain curves by three parameters*, Technical Note, **902**, National Advisory Committee on Aeronautics (NACA), Kitty Hawk, NC.
- Rizzo, C.M., Paik, J.K., Brennan, F., Carlsen, C.A., Daley, C., Garbatov, Y., Ivanov, L., Simonsen, B.C., Yamamoto, N. & Zhuang, H.Z. (2007). Current practices and recent advances in condition assessment of aged ships. *Ships and Offshore Structures*, 2 (3):261–271.
- Schijve, J. (2009). Fatigue of structures and materials. Second Edition, Springer, Cham, Switzerland.

0003369274.3D 76 24/1/2018 10:48:12 AM

- Schumacher, M. (1979). Seawater corrosion handbook. Noyes Data Corporation, Park Ridge, NJ.
- Sielski, R.A. (2007). Review of structural design of aluminum ships and crafts. Transactions of the Society of Naval Architects and Marine Engineers, 115:1-30.
- Sielski, R.A. (2008). Research needs in aluminum structure. Ships and Offshore Structures, 3 (1):57-65.
- Smith, C.S., Davidson, P.C., Chapman, J.C. & Dowling, P.J. (1988). Strength and stiffness of ships' plating under in-plane compression and tension. Transactions of the Royal Institution of Naval Architects, 130:277-296.
- Steinhardt, O. (1971). Aluminum constructions in civil engineering. Aluminum, 47:131–139; 254 - 261.
- TSCF (2000). Guidelines for ballast tank coating systems and edge preparation. Tanker Structure Cooperative Forum, Presented at the TSCF Shipbuilders Meeting in Tokyo, Japan, October.
- Ueda, Y. (1999). Computational welding mechanics (a volume of selected papers in the commemoration of the retirement from Osaka University). Joining and Welding Research Institute, Osaka University, Osaka, Japan, March.
- Yamamoto, N. & Ikegami, K. (1998). A study on the degradation of coating and corrosion of ship's hull based on the probabilistic approach. Journal of Offshore Mechanics and Arctic Engineering, **120**:121–128.

0003369274.3D 77 24/1/2018 10:48:12 AM

0003369274.3D 78 24/1/2018 10:48:12 AM